



저작자표시-비영리 2.0 대한민국

이용자는 아래의 조건을 따르는 경우에 한하여 자유롭게

- 이 저작물을 복제, 배포, 전송, 전시, 공연 및 방송할 수 있습니다.
- 이차적 저작물을 작성할 수 있습니다.

다음과 같은 조건을 따라야 합니다:



저작자표시. 귀하는 원저작자를 표시하여야 합니다.



비영리. 귀하는 이 저작물을 영리 목적으로 이용할 수 없습니다.

- 귀하는, 이 저작물의 재이용이나 배포의 경우, 이 저작물에 적용된 이용허락조건을 명확하게 나타내어야 합니다.
- 저작권자로부터 별도의 허가를 받으면 이러한 조건들은 적용되지 않습니다.

저작권법에 따른 이용자의 권리는 위의 내용에 의하여 영향을 받지 않습니다.

이것은 [이용허락규약\(Legal Code\)](#)을 이해하기 쉽게 요약한 것입니다.

[Disclaimer](#)

A DISSERTATION FOR THE DEGREE OF DOCTOR OF PHILOSOPHY

**Bioactive substances derived from subtropical color
foods suppress stemness of breast cancer stem cells**

Ren Liu

Interdisciplinary Graduate Program in Advanced Convergence

Technology and Science

Graduate School

Jeju National University

August, 2021

A DISSERTATION FOR THE DEGREE OF DOCTOR OF PHILOSOPHY

**Bioactive substances derived from subtropical color
foods suppress stemness of breast cancer stem cells**

Ren Liu

Supervised by

Professor Dong-Sun Lee

Interdisciplinary Graduate Program in Advanced Convergence

Technology and Science

Graduate School

Jeju National University

August, 2021

Bioactive substances derived from subtropical color foods suppress stemness of breast cancer stem cells

Ren Liu

(Supervised by Professor Dong-Sun Lee)

A dissertation submitted in partial fulfillment of the requirement for the degree of Doctor of Philosophy in the Interdisciplinary Graduate Program in Advanced Convergence Technology & Science Graduate School

August, 2021

This thesis has been examined and approved by

.....
Chairperson of the supervising committees

Young-Ok Son, Ph.D., Department of Animal Biotechnology, Jeju National University

.....
Young-Jun Park, Ph.D., Department of Pharmacy, Jeju National University

.....
Man-Young Jung, Ph.D., Department of Biology Education, Jeju National University

.....
Hu-Nan Sun, Ph.D., Department of Life Science & Technology, Heilongjiang Bayi Agricultural University

.....
Dong-Sun Lee, Ph.D., Department of Biotechnology, Jeju National University

Interdisciplinary Graduate Program in Advanced Convergence Technology & Science

Graduate School

Jeju National University

CONTECT

LIST OF ABBREVIATIONS.....V

LIST OF FIGURES..... VII

LIST OF TABLE.....X

CHAPTER I.....1

 1.1 Breast cancer stem cells.....2

 1.2 Color foods.....5

 1.3 Breast cancer stem cell and signaling pathway.....8

 1.4 Breast cancer stem cell and cytokines11

CHAPTER II15

 2.1 ABSTRACT16

 2.2 INTRODUCTION16

 2.3 MATERIALS AND METHODS.....18

 2.3.1 Chemical and reagents.....18

 2.3.2 Plant material18

 2.3.3 Isolation of an inhibitor.....18

 2.3.4 4 Culture of human breast cancer cells and mammospheres19

 2.3.5 Cell proliferation assay.....20

 2.3.6 Colony formation assay.....20

 2.3.7 Assessment of CD44⁺/CD24⁻ expression.....20

 2.3.8 Transwell assay.....21

 2.3.9 Real-time quantitative reverse transcription PCR21

 2.3.8 Immunofluorescence (IF).....21

 2.3.10 Western blotting.....22

2.3.11 EMSA.....	22
2.3.12 Statistical analysis.....	23
2.4 RESULTS.....	24
2.4.1 Isolation of a BCSC inhibitor from Beta vulgaris	24
2.4.2 Structure analysis of the purified compound	26
2.4.3 Betavulgarin inhibits breast cancer cell growth and mammosphere formation.....	28
2.4.4 Betavulgarin decreases CD44 ⁺ /CD24 ⁻ -expressing cancer cell numbers	28
2.4.5 Betavulgarin inhibits the nuclear translocation of Stat3 in BCSCs.....	28
2.4.6 Betavulgarin inhibits the mRNA levels of BCSC-specific marker genes and mammosphere growth	29
2.5 DISCUSSION	37
2.6 CONCLUSION.....	39
CHAPTER III.....	40
3.1 ABSTRACT	41
3.2 INTRODUCTION	41
3.3 MATERIALS AND METHODS.....	43
3.3.1 Isolation and identification of a breast CSC inhibitor derived from <i>D. carota</i> L.....	43
3.3.2 Structure analysis of the purified compound	44
3.3.3 Cell line and culture of mammospheres	45
3.3.4 Cell proliferation.....	46
3.3.5 Colony formation assay.....	46
3.3.6 Flow cytometric assay of CD44 ⁺ /CD24 ⁻ expression.....	46
3.3.7 Migration.....	47
2.3.7 Real-time quantitative reverse transcription PCR	47
3.3.8 Western blotting.....	47
3.3.9 EMSA.....	48

3.3.10 Quantification of extracellular human IL-6 and IL-8 cytokines using the cytometric bead array (CBA).....	48
3.3.11 Statistical analysis.....	49
3.4 RESULTS	50
3.4.1 Isolation and identification of a breast CSC inhibitor derived from <i>D. carota</i> L.....	50
3.4.2 6-Methoxymellein suppresses the growth of breast cancer cells and mammospheres	50
3.4.3 6-Methoxymellein reduces the proportion of CD44 ⁺ /CD24 ⁻ -expressing breast cancer cells.....	56
3.4.4 6-Methoxymellein inhibits the protein expression of cancer stem cell-specific markers and inhibits mammosphere growth	56
3.4.5 6-Methoxymellein suppresses the nuclear localization of NF-κB p65 and NF-κB p50 in BCSCs	56
3.4.6 6-Methoxymellein decreases the mRNA and protein levels of secretory IL-6 and IL-8 in mammospheres.....	57
3.5 DISCUSSION	62
3.6 CONCLUSION.....	65
CHAPTER IV	66
4.1 ABSTRACT	67
4.2 INTRODUCTION	67
4.3 MATERIALS AND METHODS.....	70
4.3.1 Chemical and reagents.....	70
4.3.2 Plant material	70
4.3.3 Isolation and purification of a mammosphere inhibitor from <i>Artemisia princeps</i>	70
4.3.4 Structure analysis of the purified compound	71
4.3.5 Culture of human breast cancer cells and mammospheres	72
4.3.6 Cell proliferation assay.....	73
4.3.7 CD44 ⁺ /CD24 ⁻ expression, aldehyde dehydrogenase (ALDH) activity and apoptosis using a flow cytometric assay	73

4.3.8 Real-time quantitative reverse transcription PCR	74
4.3.9 Western blotting.....	74
4.3.10 Electrophoretic mobility shift assay (EMSA).....	75
4.3.11 Quantitative measurement of human IL-6 and IL-8 using the BD™ CBA human inflammatory cytokines assay kit	76
4.3.12 Stat3 and YAP1 knockdown using small interfering RNA (siRNA).....	76
4.3.13 Statistical analysis.....	76
4.4 RESULTS	77
4.4.1 Isolation of breast cancer stem cells (BCSCs) inhibitor from <i>Artemisia princeps</i>	77
4.4.2 5-Desmethylsinensetin inhibits mammosphere formation of breast cancer cells.....	77
4.4.3 5-Desmethylsinensetin decreases CD44 ⁺ /CD24 ⁻ -expressing and ALDH-expressing cancer cells	80
4.4.4 5-Desmethylsinensetin induces apoptosis and inhibits the mRNA levels of cancer stem cell specific marker genes and mammosphere growth	80
4.4.5 5-Desmethylsinensetin decreases the total and nuclear levels of p-Stat3 and Stat3 in BCSCs..	81
4.4.6 5-Desmethylsinensetin reduces the secretion and mRNA levels of IL-6 and IL-8 in mammospheres.....	84
4.4.7 5-Desmethylsinensetin inhibits the nuclear localization of YAP1	84
4.5 DISCUSSION	91
4.6 CONCLUSION.....	94
REFERENCES	96
SUPPLEMENTARY FIGURES	126
LIST OF TABLE.....	153
LIST OF PUBLICATION INCLUDED IN THE THESIS	154
Acknowledgment.....	156

LIST OF ABBREVIATIONS

BCSCs	Breast cancer stem cells
TLC	Thin layer chromatography
HPLC	High-pressure liquid chromatography
Stat3	Signal transducer and activator of transcription 3
SOX2	Sex determining region Y (SRY)-box 2
c-Myc	c-Myelocytomatosis
Oct4	Octamer-binding transcription factor 4
KIF4A	Chromosome-associated kinesin
TNBC	Triple-negative breast cancer
IF	Immunofluorescence
EMSA	Electrophoretic mobility shift assay
MSCs	Mesenchymal stem cells
TILs	Tumor-associated leukocytes
CAFs	Cancer-associated fibroblasts
TME	Tumor microenvironment
IL-6	Interleukin-6
IL-8	Interleukin-8
ALDH1	Aldehyde dehydrogenase 1
DEAB	N,N-diethylaminobenzaldehyde
NF- κ B p65	Nuclear factor- κ B subunit p65
NF- κ B p50	Nuclear factor- κ B subunit p65

LIST OF FIGURES

Figure 1-1. Characteristics of CSCs, cancer cells, and normal cells.

Figure 1-2. Red beetroot

Figure 1-3. Carrot

Figure 1-4. Artemisia

Figure 1-5. Regulation of BCSCs

Figure 1-6. Cytokines secreted by cells in the tumor microenvironment regulate BCSC self-renewal.

Figure 2-1. Isolation of the cancer stem cell (CSC) inhibitor from the beet extracts via mammosphere formation assay:

Figure 2-2. Molecular structure of the CSC inhibitor isolated from beet. Molecular structure of betavulgarin.

Figure 2-3. The effect of betavulgarin on cancer cell growth and mammosphere formation.

Figure 2-4. Effect of betavulgarin on the proportion of CD44⁺/CD24⁻.

Figure 2-5. The effect of Betavulgarin on Stat3 signaling pathway.

Figure 2-6. The effect of betavulgarin on the expression of CSC marker genes and mammosphere growth.

Figure 3-1. Isolation of breast CSC inhibitors from carrot extracts based on mammosphere formation assays.

Figure 3-2. Molecular structure of the CSC inhibitor isolated from carrots. Molecular structure of 6-methoxymellein.

Figure 3-3. The antiproliferation and mammosphere formation inhibitory effect of 6-methoxymellein.

Figure 3-4. 6-Methoxymellein reduces the proportion of CD44⁺/CD24⁻ cells.

Figure 3-5. 6-Methoxymellein suppresses the protein expression of CSC markers and inhibits mammosphere growth.

Figure 3-6. The effect of 6-methoxymellein on the NF-κB signaling pathway.

Figure 3-7. 6-Methoxymellein suppresses the secretion and transcription of IL-6 and IL-8.

Figure 4-1. Isolation of a breast cancer stem cell (BCSC) inhibitor from *Artemisia princeps* using a mammosphere formation assay.

Figure 4-2. Molecular structure of the CSC inhibitor isolated from *Artemisia princeps*. Molecular structure of 5-desmethylninensetin.

Figure 4-3. Effects of 5-desmethylninensetin on cell proliferation and mammosphere formation.

Figure 4-4. 5-Desmethylninensetin reduces the subpopulations of CD44⁺/CD24⁻ and ALDH1⁺ MDA-MB-231 breast cancer cells.

Figure 4-5. 5-Desmethylninensetin induces apoptosis of mammospheres and suppresses the expression of CSC marker genes and mammosphere growth.

Figure 4-6. Effect of 5-desmethylninensetin on the Stat3 signaling pathway.

Figure 4-7. 5-Desmethylsinensetin regulates the secretion and transcription levels of IL-6 and IL-8.

Figure 4-8. 5-Desmethylsinensetin inhibits the YAP1 pathway via Stat3.

Figure 4-9. Proposed model of breast CSC formation mediated through the Stat3-IL6 and Stat3-YAP1 signaling pathways induced by 5-desmethylsinensetin.

LIST OF TABLE

Table 1. Specific Real-time RT-qPCR primer sequences containing *Nanog*, *Sox2*, *Oct4*, *C-myc* and β -actin genes

CHAPTER I

INTRODUCTION

1.1 Breast cancer stem cells

Female breast cancer has now surpassed lung cancer as the leading cause of global cancer incidence in 2020, with an estimated 2.3 million new cases, representing 11.7% of all cancer cases. It is the fifth leading cause of cancer mortality worldwide, with 685,000 deaths. Among women, breast cancer accounts for 1 in 4 cancer cases and for 1 in 6 cancer deaths, ranking first for incidence in the vast majority of countries [1]. According to the intrinsic molecular portraits provided by transcriptome profiling, breast cancer has several major subcategories, such as receptor tyrosine-protein kinase erbB-2 receptor (HER2), progesterone receptor (PR), estrogen receptor (ER) and triple-negative breast cancer (TNBC). Compared to patients with other subtypes, TNBC patients more frequently experience locoregional recurrence, chemoresistance and metastasis. Recently, TNBCs have been divided into luminal androgen receptor (LAR), basal-like 1 (TNBC-BL1), basal-like 2 (TNBC-BL2), immunomodulatory (TNBC-IM), mesenchymal (TNBC-M), mesenchymal stem-like (TNBC-MSL) and unspecified (TNBC-UNS) subtypes.

The standards of therapy for breast cancer are radiation, hormone therapy, surgery and chemotherapeutic drugs, including carboplatin, bevacizumab, cisplatin, epirubicin, cyclophosphamide and docetaxel. The heterogeneity of breast cancer is believed to make it less responsive to chemotherapy.

It has been demonstrated that one of the causes of tumor heterogeneity is cancer cells exhibiting stem cell-like properties, which are named cancer stem cells (CSCs). The discovery of stem cells among cancer cells has had a great impact on cancer biology research and the understanding of cancer stem cell physiology for future anticancer drug development. Breast cancer stem cells (BCSCs) have the ability to self-renew and differentiate within populations of

breast cancer cells. BCSCs have been observed to express cellular markers, such as CD44+/CD24- and ALDH+, in multiple studies. Moreover, multiple signaling pathways and transcription factors are overactivated in BCSCs compared with those in non-BCSCs, including the Wnt, Notch, Hippo, Hedgehog and signal transducer and activator of transcription (Stat) pathways. The Stat pathway plays a critical role in various cellular functions, such as growth, proliferation and the immune response, via various cytokines and growth factors. In addition, CSCs can be regulated by stromal cells, such as mesenchymal stem cells (MSCs), tumor-associated leukocytes (TILs) and cancer-associated fibroblasts (CAFs), in the tumor microenvironment (TME) via extrinsic signals. The most distinguishing characteristic of CSCs compared to cancer and normal cells is stemness; the self-renewal and unlimited ability to proliferate into heterogeneous malignant cells under hypoxic and acidic conditions (Fig. 1-1).

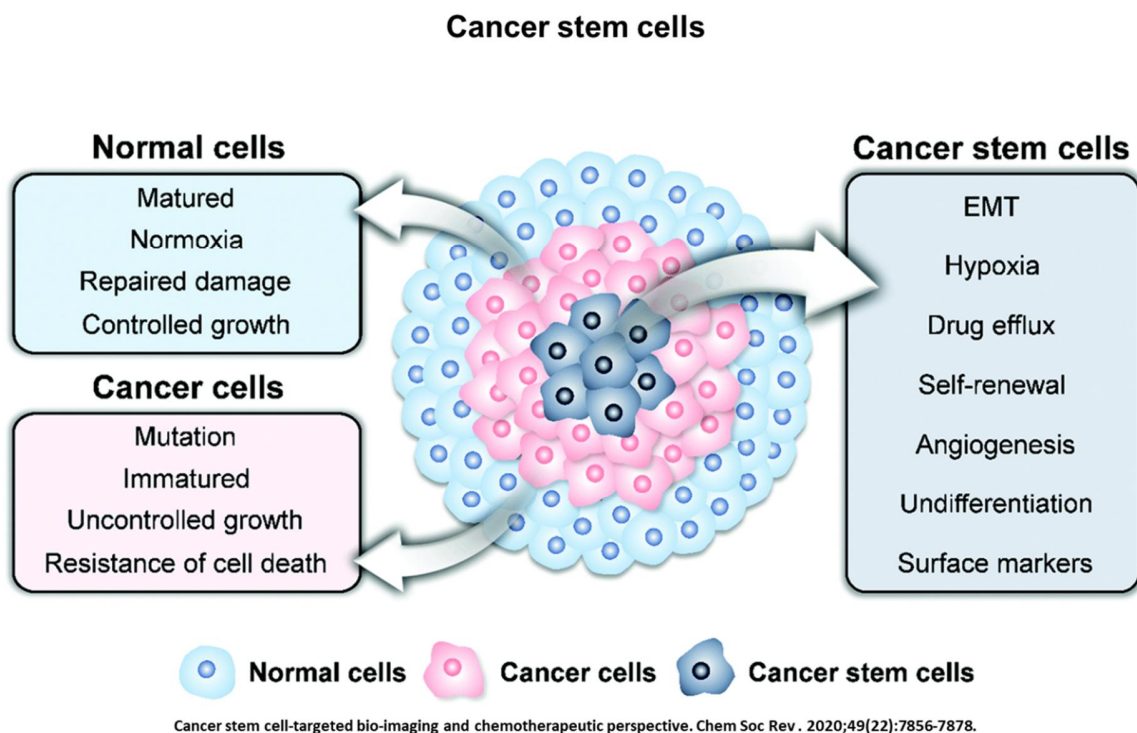


Figure.1-1 Characteristics of CSCs, cancer cells, and normal cells.

The creation of a supportive TME for targeting CSCs has been successfully employed in brain tumors in mice. Breast cancer stem cell functions can be influenced by different cytokines, chemokines and growth factors secreted by various cell types in the TME, such as interleukin-6 (IL-6) and interleukin-8 (IL-8). IL-6 increases the CSC frequency by increasing the CD44⁺/CD24⁻ subpopulation. IL-6 signaling cascade activation results in the generation of cancer stem cells by promoting epithelial–mesenchymal transition (EMT) in breast cancer cells. IL-6-JAK1-Stat3 signaling blockade in endometrial cancer affects the ALDH^{hi}/CD126⁺ stem-like component and reduces the tumor burden. The IL-8 expression level is upregulated in breast cancer compared with that in normal breast tissue. IL-8 promotes invasion and EMT in breast cancer cells. Thus, inhibition of IL-6 and IL-8 may be necessary to achieve therapeutic effects in tumors.

1.2 Color foods

The color of food is often associated with the flavor, safety, and nutritional value of the product. Plant-derived pigments are the result of biochemical pathways within the organism that result in a variety of organic compounds with unique physicochemical properties. These colored compounds are abundant in nature and play important roles in photosynthetic pathways, attract pollinators, and provide protection from predators and solar energy. Plant pigments include a variety of chemical classes, such as flavonoids, porphyrins, carotenoids, anthocyanins, and betalains.



Figure.1-2 Red beetroot

Red beetroot (*Beta vulgaris var. rubra* L.) contains many bioactive compounds, including anthocyanin, betacyanin, folic acid, phenolic compounds, ascorbic acid, flavonoids, vitamin C, and other biologically active components. The most important bioactive phytochemicals in red beetroot are betalains, a class of tyrosine-derived pigments obtained from betalamic acid, whose members are grouped into yellow betaxanthins and red betacyanins. Red dye E162 extract from

beetroot is approved for use in the food industry by the European Food Safety Authority. Betalains have been demonstrated to have strong free radical scavenging, antioxidant, and anti-inflammatory activities. In this report, we isolated a BCSC inhibitor, betavulgarin, based on activity-guided fractionation. Betavulgarin was reported to be a fungus infection response molecule and an antifungal molecule in beetroot.



Figure.1-3 Carrot

Carrot (*D. carota L.*) is the most important root vegetable, is cultivated worldwide, and is rich in natural phytochemicals. Carrot root is widely utilized because of abundant carotenoids, anthocyanins and dietary fiber. Carrots are the main source of carotenoids, and previous studies have demonstrated that carrots may reduce cancer risk and play an important role in a cancer prevention diet. Carrots are traditionally used for the treatment of gastric ulcers, diabetes, muscle pain and cancer in Lebanon. Carrots have been reported to provide numerous biological activities,

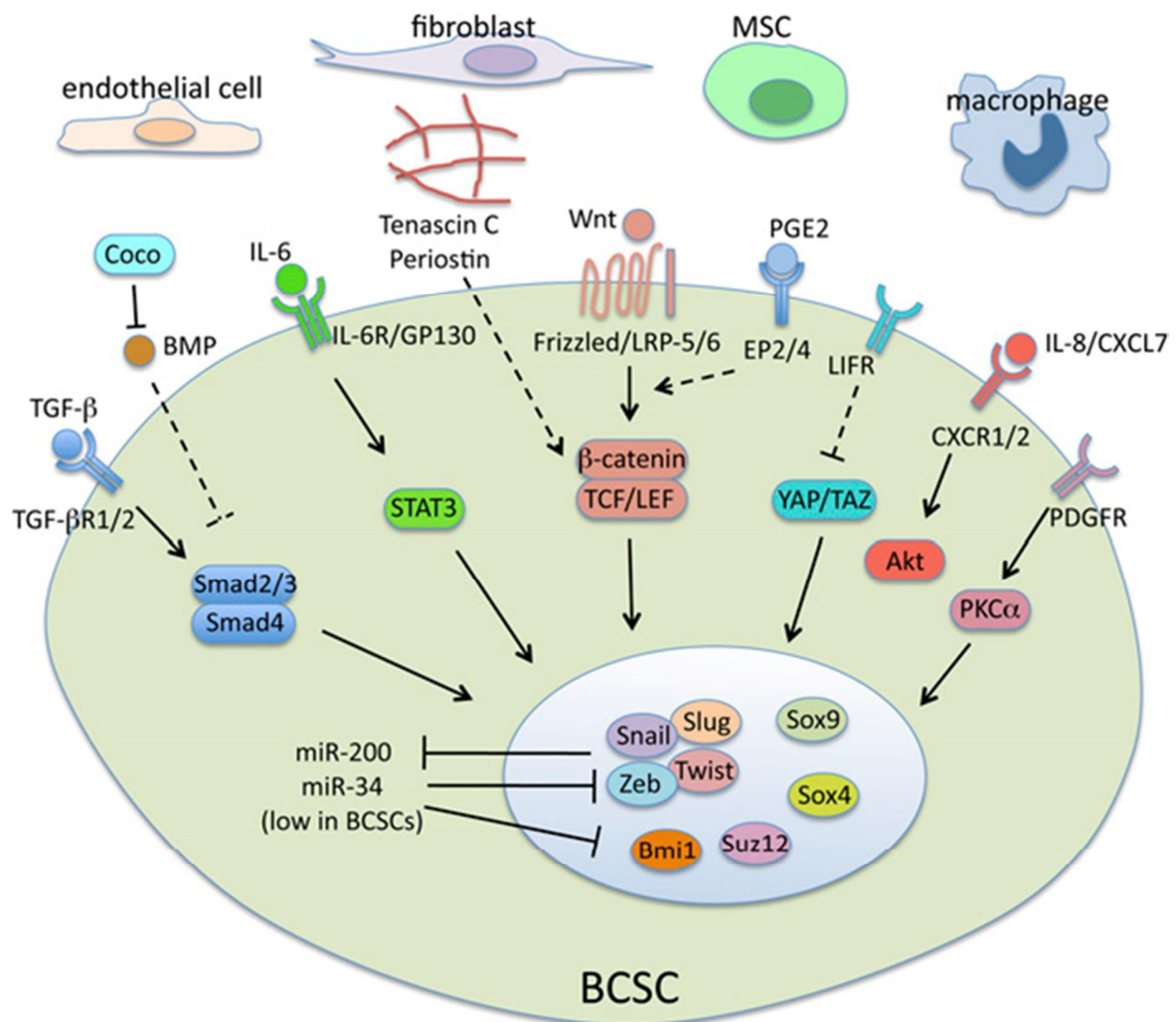
including antibacterial, antifungal, diuretic, antilithic, anticancer, antiinflammatory and antioxidant effects.



Figure.1-4 Artemisia

Artemisia princeps is a species of Artemisia. Artemisia comprises more than 4 hundred important medicinal plants, and most of them have a bitter taste. Increasing attention is being given to phytochemical substances from Artemisia due to their biological and chemical diversity, which are caused by active ingredients and secondary metabolites. *Artemisia princeps* has been found to be rich in phenolic acids, flavonoids, terpenes and other compounds. For instance, isochromanone derivatives isolated from *Artemisia princeps* cultured with endophytic fungi inhibit nitric oxide production in lipopolysaccharide (LPS)-stimulated RAW264.7 cells.

1.3 Breast cancer stem cell and signaling pathway



Concise review: breast cancer stem cells: regulatory networks, stem cell niches, and disease relevance. *Stem Cells Transl Med.* 2014 Aug

Figure.1-5 Regulation of BCSCs

Multiple signaling pathways have been found to play a role in CSCs [2] (Figure. 1-5). Interestingly, some of these pathways are associated with a developmental program called the epithelial-mesenchymal transition (EMT) and regulate the stem cell properties of both normal and cancer stem cells in the breast.

EMT was initially identified as a developmental program that enables polarized epithelial cells to acquire a motile mesenchymal phenotype. This allows stationary epithelial cells to gain the ability to migrate and invade during embryonic morphogenesis. In addition, EMT and its reverse process, the mesenchymal-epithelial transition, are integral steps of cell fate specification during gastrulation and organogenesis [3]. In carcinoma progression, reactivation of the EMT program promotes tumor metastasis by driving tumor cell invasion and enhancing tumor cell survival during the metastatic cascade [4].

The activation of EMT by multiple means, including transforming growth factor β (TGF β) treatment and the expression of various EMT-inducing transcription factors, generates cells that express BCSC markers, such as CD44^{high}CD24^{low}, and form mammospheres [5, 6]. In particular, they highly express a key EMT transcription factor, Slug (also called Snail2), and Slug overexpression greatly increases stem cell activity, as demonstrated by an in vivo gland reconstitution assay [7]. In fact, Slug is a key target of several tumor and metastasis suppressors.

MicroRNAs have emerged as a class of key regulators of CSCs and EMT [8]. Among them, the miR-200 family plays a particularly interesting role in integrating the EMT program and core stem cell pathways [9]. The activation of p53 downregulates Snail and other EMT-inducing transcription factors through the upregulation of the miR-34 family [10, 11]. Interestingly, Snail and ZEB1, conversely, repress miR-34 expression, forming yet another reciprocal negative feedback loop for regulating EMT.

The Sox family includes 20 different transcription factors in mammals that share homologous high-mobility-group DNA-binding domains. Sox proteins play prominent roles in cell fate

regulation during development, including the specification of embryonic and somatic stem and progenitor cells [12].

Multiple developmental signaling pathways have been implicated in regulating BCSCs, including TGF- β , Wnt, and Notch. Treating certain nonmalignant mammary epithelial cells or breast cancer cells with TGF- β efficiently activates EMT programs that are accompanied by the expression of BCSC markers [5, 13, 14].

The role of Wnt signaling in stem cells has been well documented [15, 16]. In adult mammary glands, MaSCs exhibit elevated Wnt signaling [17], and the overexpression of Wnt proteins or activation of canonical Wnt by Axin2 mutation or MMP3 overexpression promotes the expansion of MaSCs [18-20]. In contrast to Wnt, Notch induces the commitment of MaSCs to luminal-specific progenitors [21, 22]. Interestingly, certain aggressive breast cancers, including basal-like breast cancer, are likely to originate from luminal progenitor cells [23, 24]. Therefore, Notch may be particularly important for these breast cancer subtypes [25].

1.4 Breast cancer stem cell and cytokines

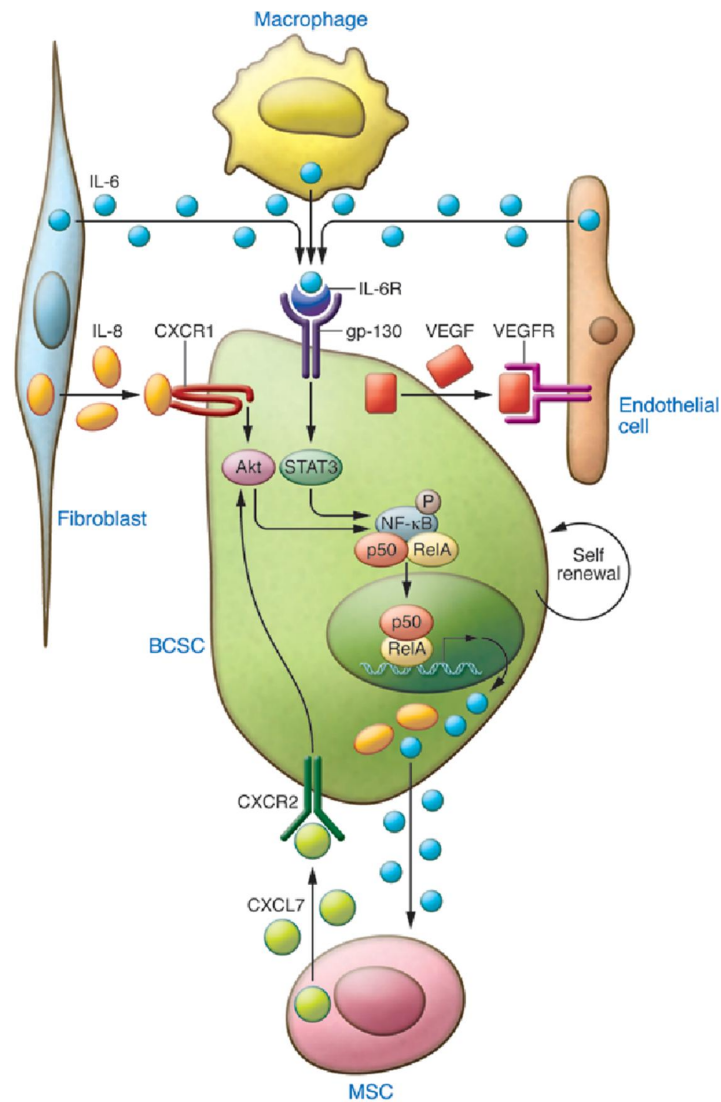


Figure.1-6 Cytokines secreted by cells in the tumor microenvironment regulate BCSC self-renewal.

The link between inflammation and cancer is an old concept that was first proposed by Virchow in 1864, when he observed that inflammatory cells frequently infiltrate tumor stroma [26]. Considerable clinical evidence exists for links between inflammatory states and cancer development, including the association of ulcerative colitis, hepatitis C, and chronic pancreatitis

with cancers of the colon, liver, and pancreas, respectively [26]. Levels of chronic inflammation as assessed by serum C-reactive protein or β -amyloid are correlated with risk of breast cancer recurrence in women after primary therapy [27]. Chronic inflammation, as reflected in expression of these markers, may be mediated by cytokines including IL-1 β , IL-6, and IL-8 [28]. Genetic polymorphisms in these cytokine genes predispose affected individuals to cancer [29]. Cytokines generated by cells within the tumor microenvironment are shown in Figure 1-6. These inflammatory cytokines stimulate CSC self-renewal, which then may promote tumor growth and metastasis [30, 31].

IL-6 and IL-8 have been implicated in both chronic inflammation and in tumor growth [5, 32]. Within the tumor microenvironment, many cell types including mesenchymal cells, macrophages, and immune cells secrete both IL-6 and IL-8 [32]. Furthermore, the serum levels of both of these cytokines have been associated with poor patient outcome in breast cancer [33, 34]. In a variety of preclinical models, IL-6 has been shown to promote tumorigenicity, angiogenesis, and metastasis [30, 35-37]. The clinical relevance of these studies is supported by the demonstrated association between serum IL-6 levels and poor patient outcome in breast cancer patients. IL-6 has been shown to be a direct regulator of BCSC self-renewal, a process mediated by the IL-6 receptor/GP130 complex through activation of STAT3 [38]. Utilizing mouse xenografts, we have recently demonstrated that bone marrow-derived MSCs are recruited to sites of growing breast cancers by gradients of IL-6 [39]. IL-6 is a key component of a positive feedback loop involving these MSCs and BCSCs [39]. Furthermore, Sethi et al. recently demonstrated that IL-6-mediated Jagged1/Notch signaling promotes breast cancer bone metastasis [40]. These studies identify IL-6 and its receptor as attractive therapeutic targets.

Utilizing gene expression profiling, we previously identified the IL-8 receptor CXCR1 as highly expressed on BCSCs and found that IL-8 was able to stimulate their self-renewal [31]. Blocking this receptor in mouse xenografts significantly reduced the number of BCSCs, leading to decreased tumorigenicity and metastasis. The production of inflammatory cytokines including IL-6 and IL-8 is regulated by the NF- κ B signaling pathway [41].

The NF- κ B pathway plays a crucial role in inflammation and carcinogenesis. The NF- κ B family is composed of five related transcription factors: p50, p52, RelA (p65), c-Rel, and RelB [42, 43]. In resting cells, NF- κ B proteins are predominantly found in the cytoplasm, where they are associated with the I κ B family; activation of NF- κ B by diverse signals results in ubiquitin ligase-dependent degradation of I κ B and nuclear translocation of NF- κ B protein complexes. The transcription of a number of cytokines, including IL-6 and IL-8, is activated by NF- κ B [41]. In addition, a positive feedback loop has recently been shown to maintain a chronic inflammatory state in tumor cells. Interestingly, this loop involves the microRNA let7, as well as Lin28, a factor involved in embryonic stem cell self-renewal [38]. This feedback loop is maintained by IL-6 through its activation of STAT3, which in turn activates NF- κ B and its downstream targets Lin28 and let7. The specific role of IL-6 in maintaining this inflammatory loop in BCSCs has been recently demonstrated [38, 44]. NF- κ B may play an important role in normal breast physiology as well as carcinogenesis. In a HER2-neu model of mammary carcinogenesis, suppression of NF- κ B in mammary epithelium reduced the mammary stem cell compartment, resulting in a delayed onset of HER2-neu-induced tumors that displayed reduced angiogenesis and infiltration by macrophages [45]. NF- κ B has also been implicated in the regulation of mouse mammary stem cells during pregnancy. Elevated levels of progesterone during pregnancy induce the production of RANKL by differentiated breast epithelial cells. RANKL in turn stimulates

breast stem cell self-renewal via activation of NF- κ B in these cells [46, 47]. The increased incidence of aggressive breast cancers associated with pregnancy [48] may result from activation of similar pathways in BCSCs [46, 47].

CHAPTER II

Betavulgarin isolated from sugar beet (*Beta vulgaris*)
suppresses breast cancer stem cells through Stat3
signaling

2.1 ABSTRACT

Breast cancer is a major health problem that affects lives worldwide. Breast cancer stem cells (BCSCs) are small subpopulations of cells with capacities for drug resistance, self-renewal, recurrence, metastasis, and differentiation. Herein, powder extracts of beetroot were subjected to silica gel, gel filtration, thin layer chromatography (TLC), and preparatory high-pressure liquid chromatography (HPLC) for isolation of one compound, based on activity-guided purification using tumorsphere formation assays. The purified compound was identified as betavulgarin, using nuclear magnetic resonance spectroscopy and electrospray ionization (ESI) mass spectrometry. Betavulgarin suppressed the proliferation, migration, colony formation, and mammosphere formation of breast cancer cells and reduced the size of the CD44+/CD24- subpopulation and the expression of the self-renewal-related genes, C-Myc, Nanog, and Oct4. This compound decreased the total level and phosphorylated nuclear level of signal transducer and activator of transcription 3 (Stat3) and reduced the mRNA and protein levels of sex determining region Y (SRY)-box 2 (SOX2), in mammospheres. These data suggest that betavulgarin inhibit the Stat3/Sox2 signaling pathway and induces BCSC death, indicating betavulgarin might be an anticancer agent against breast cancer cells and BCSCs.

2.2 INTRODUCTION

Recently, the study of the biological activity of red beetroot (*Beta vulgaris rubra*) has been growing. Beetroot is a healthy vegetable rich in anthocyanin, betacyanin, folic acid, phenolic compounds, ascorbic acid, flavonoids, vitamin C, and other biologically active components [49-51]. Specifically, beetroot contains betalains, which are known for their antioxidant [50, 52, 53], anti-inflammation [53], anticancer [49, 53, 54], and chemopreventive bioactivities[55]. Moreover,

beetroot, as a cost-effective strategy, is considered an effective juice supplement for therapeutic treatment of clinical pathologies related to oxidative stress and inflammation [51].

Breast cancer is a serious health problem diagnosed in women [56]. The treatment options for breast cancer include mastectomy or breast-conserving surgery, hormone therapy, chemotherapy, and radiotherapy. However, patients treated with conventional therapies suffer from breast cancer relapse and metastasis [57]. The existence of cancer stem cells (CSCs) was first identified by Bonnet and Dick [58]. BCSCs are self-renewing and contribute to tumor recurrence; breast cancer stem cells (BCSCs) were first isolated by Al-Hajj [59]. A subpopulation of breast cancer cells exhibit the surface phenotype CD44⁺CD24⁻. Subsequently, this subpopulation can be detected in circulating breast cancer cells from patients and is associated with breast cancer recurrence and distant metastasis [60]. It is essential to target BCSCs in cancer treatment. Stemness proteins and signaling pathways involved in BCSC maintenance include embryonic stemness transcription factors (octamer-binding transcription factor 4 (Oct4), sex determining region Y (SRY)-box 2 (SOX2), c-mycelocytomatosis (c-Myc), and Chromosome-associated kinesin (KIF4A), the canonical and noncanonical wnt pathways, Notch and the hedgehog pathway [57].

The oncogenic transcription factor Signal transducer and activator of transcription 3 (Stat3) is associated with cancer progression, metastasis, chemoresistance, stem cell self-renewal and maintenance, autophagy, and immune evasion [61-63]. In triple-negative breast cancer (TNBC), Stat3 is constitutively activated and highly related to poor survival outcomes [64]. Many studies have also demonstrated that Stat3 phosphorylation and activation upregulate the expression of cMyc and Sox2, which promote the self-renewal of breast cancer cells [65-68].

In this study, we selected Jeju beetroot to target BCSCs, and the active component was isolated based on activity-guided fractionation. Betavulgarin, the isolated active component, inhibited BCSC formation. We demonstrate that betavulgarin suppresses the proliferation of breast cancer and BCSC formation through the regulation of Stat3/Sox2 signaling in BCSCs.

2.3 MATERIALS AND METHODS

2.3.1 Chemical and reagents

Silica gel 60 and TLC plates were purchased from Merck (Darmstadt, Germany), and Sephadex LH-20 was obtained from Pharmacia (Uppsala, Sweden). Cell viability was measured using the EZ-Cytox Cell Viability Assay Kit (DoGenBio, Seoul, Korea). Other compounds were obtained from Sigma-Aldrich (St. Louis, MO, USA).

2.3.2 Plant material

A sample of beet was obtained from verified market sources (Seogwipo, Jeju, Korea). The beets were washed and freeze-dried, and the dried beet was ground. A voucher specimen (No.018_010) was deposited in the Department of Biomaterial, Jeju National University (Jeju-Si, Korea).

2.3.3 Isolation of an inhibitor

The ground samples of beet were extracted with methanol. The isolation method is summarized in Figure 2-1A. The beet powder was solubilized with 10 L of methanol. The

methanol extracts were concentrated and mixed with equal volumes of water, and the methanol part was evaporated. The water-suspended part was extracted with equal volumes of ethyl acetate. The solubilized ethyl acetate-concentrated part was loaded onto a silica gel column (3×35 cm) and eluted with a solvent (chloroform-methanol, 10:1) (Figure S2-1). Five fractions were divided and assayed by evaluating mammosphere formation. The #2 fraction potentially suppressed mammosphere formation. The #2 fraction was loaded onto a Sephadex LH-20 open column (2.5×30 cm) and fractionated into four fractions (Figure S2-2). The four fractions were further fractionated and analyzed by evaluating mammosphere formation. Part #4 showed inhibition of mammosphere formation. Part #4 was isolated using preparatory TLC (glass plate; 20×20 cm) and developed in a TLC chamber. Individual bands were separated, and each fraction was assayed by evaluating mammosphere formation (Figure S2-3). The #1 fraction was loaded onto a Shimadzu HPLC instrument (Shimadzu, Tokyo, Japan). HPLC was performed with an ODS 10×250-mm column (flow rate; 2 ml/min). For elution, the acetonitrile proportion was initially set at 30%, increased to 60% at 20 min and finally increased to 100% at 30 min (Figure S2-4).

2.3.4 4 Culture of human breast cancer cells and mammospheres

MCF-7 (ATCC HTB-22TM) and MDA-MB-231 (ATCC HTB-26TM) breast cancer cell lines were purchased from the American Type Culture Collection (Rockville, MD, USA) and incubated in Dulbecco's modified Eagle's medium (DMEM) supplemented with 10% (V/V) fetal bovine serum (Gibco, ThermoFisher, CA, USA) and 1% penicillin/streptomycin (Gibco, ThermoFisher, CA, USA) in a 5% CO₂ incubator. Breast cancer cells were incubated at 1×10^4 cells per well in an ultralow-attachment 6-well plate with MammoCultTM culture medium (StemCell Technologies, Vancouver, BC, Canada), supplemented with hydrocortisone and

heparin for 7 days. The cancer cells were incubated for 7 days in a 5% CO₂ incubator at 37 °C. Mammosphere formation was quantified using the NICE program [69]. Mammosphere formation was determined by examining the mammosphere formation efficiency (MFE) (%) [70].

2.3.5 Cell proliferation assay

Breast cancer cells were seeded at 1.5×10^4 cells per well in a 96-well plate for 24 h and incubated with betavulgarin (0, 50, 100, 200, 300, 400, or 500 μ M) for 24 h. Then, proliferation was assayed using the EZ-Cytox Kit (DoGenBio, Seoul, Korea) in accordance with the manufacturer's protocol. The optical density at 450 nm (OD₄₅₀) was measured using a VERSA max microplate reader (Molecular Device, San Jose, CA, USA).

2.3.6 Colony formation assay

MDA-MB-231 and MCF-7 cells were cultured at a low density (2×10^3 and 3×10^3 cells/well) in a six-well plate and treated with betavulgarin in DMEM. After 7 days of incubation, the medium was replaced, and the cells were washed with PBS, fixed with 3.7% formaldehyde, and stained for 15 min with 0.05% crystal violet. Images were acquired using a scanner.

2.3.7 Assessment of CD44⁺/CD24⁻ expression

We used a previously described method [71]. After incubation with betavulgarin for 24 h, MDA-MB-231 cells were harvested and dissociated. Next, 1×10^6 cells were labeled with FITC-labeled anti-CD44 and PE-labeled anti-CD24 antibodies (BD), and incubated at 4 °C for 20 min.

Then, the cells were washed two times with $1 \times$ PBS and assayed using a cytometer (Accuri C6, BD, San Jose, CA, USA).

2.3.8 Transwell assay

We followed a previously described method [72]. Migration assays were performed with 12-well hanging inserts (Merck Millipore, Darmstadt, Germany). MDA-MB-231 cells were suspended in 200 μ L of DMEM containing 1% FBS and added to the upper chamber (2×10^5 cells/chamber). The bottom chamber was filled with 750 μ L of DMEM containing 20% FBS. The cells were incubated for 24 h at 37 °C in a 5% CO₂ incubator. The lower surface of the inserts was fixed with 3.7% paraformaldehyde and stained with 0.03% crystal violet. Images were captured with a light microscope.

2.3.9 Real-time quantitative reverse transcription PCR

We used a previously described method [73]. RNA was extracted from MDA-MB-231 cancer cells and mammospheres and purified. Real-time RT-qPCR was performed with a one-step RT-qPCR kit (Enzynomics, Daejeon, Korea). The specific primers are described in Supplementary Table S1.

2.3.8 Immunofluorescence (IF)

Breast cancer cell lines were fixed with 4% paraformaldehyde for 20 min, permeabilized with 0.5% Triton X-100 for 10 min, blocked with 3% bovine serum albumin (BSA) for 30 min,

and stained with an anti-p-stat3 antibody (#9145, Cell Signaling Technology, Danvers, Massachusetts, USA), followed by a secondary anti-rabbit Alexa 488-conjugated antibody (A32723, ThermoFisher, Waltham, MA, USA). The nuclei were stained with DAPI, and pStat3 was visualized with a fluorescence microscope (Lionheart, Biotek, VT, USA).

2.3.10 Western blotting

Proteins derived from MDA-MB-231 mammospheres treated with/without betavulgarin were separated using 10% SDS-PAGE and transferred to a PVDF membrane (Millipore, Billerica, MA, USA). Membranes were blocked in Odyssey blocking buffer in PBS-Tween 20 (0.1%, v/v) at room temperature for 1 h. The blots were incubated at 4 °C overnight in a blocking solution containing the following primary antibodies, anti-p-Stat3 (#9145, Cell Signaling Technology, Denver, CO, USA), anti-p65 (LF-MA30327), anti-stat3 (sc-482), anti-Sox2 (sc-365923), anti-Lamin B (sc-6216), and anti- β -actin (sc-47778) (Santa Cruz Biotechnology, Dallas, TX, USA). After the membranes were washed with PBS-Tween 20 (0.1%, v/v), the membranes were incubated with IRDye 800CW and 680RD-conjugated secondary antibodies, and the band signals were detected using an ODYSSEY CLx instrument (LI-COR, Lincoln, NB, USA).

2.3.11 EMSA

Nuclear extracts were prepared as described previously [74]. An EMSA for Stat3 binding was performed using an IRDye 700-labeled Stat3 DNA (LI-COR). Samples were run on a nondenaturing 5% PAGE gel, and EMSA data were captured with an ODYSSEY CLx instrument (LI-COR).

2.3.12 Statistical analysis

All presented data are the mean \pm standard deviation (SD). Data were analyzed using Student's t-test. A p-value less than 0.05 was considered statistically significant (GraphPad Prism 5 software).

2.4 RESULTS

2.4.1 Isolation of a BCSC inhibitor from *Beta vulgaris*

To screen and purify BCSC inhibitors from *Beta vulgaris rubra*, a mammosphere formation assay using MDA-MB-231 cells was performed, and a BCSC inhibitor was purified using methanol extracts of *Beta vulgaris rubra* generated by ethyl acetate extraction, silica gel filtration, Sephadex LH-20 (GE Healthcare, Uppsala, Sweden) chromatography, preparatory thin-layer chromatography (TLC), and preparatory high-pressure liquid chromatography (HPLC) (Figure 2-1A). The purified compound suppressed BCSC formation (Figure 2-1B) and was analyzed using HPLC (Figure 2-1C). The molecule identified using nuclear magnetic resonance (NMR) data was determined to be betavulgarin (Figure 2-2).

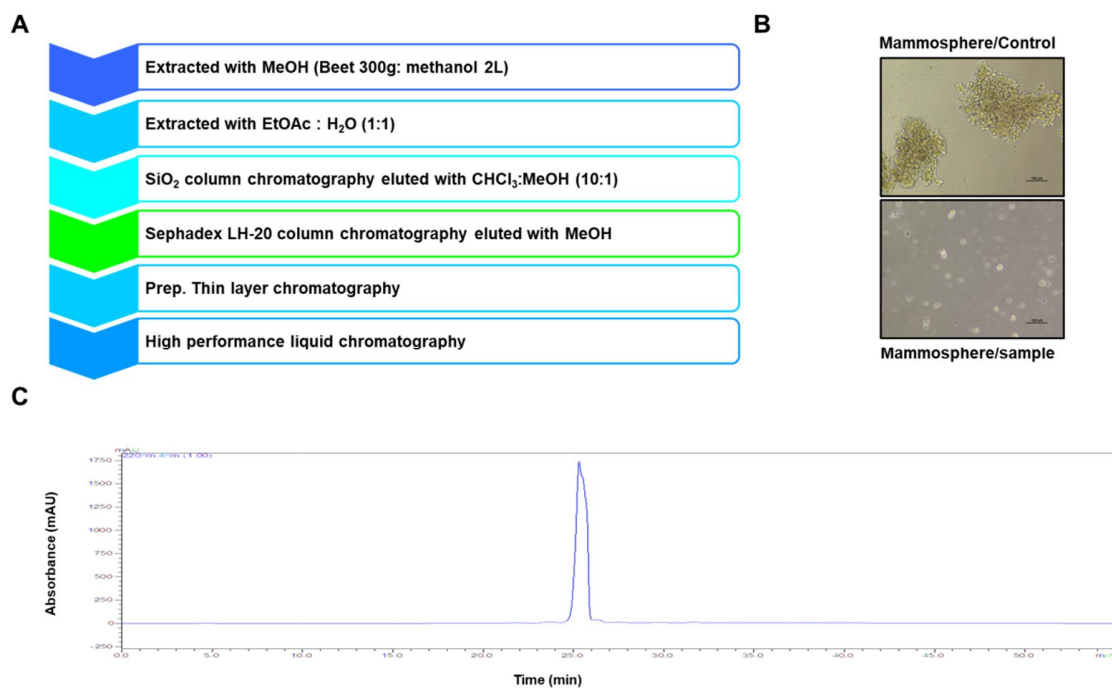
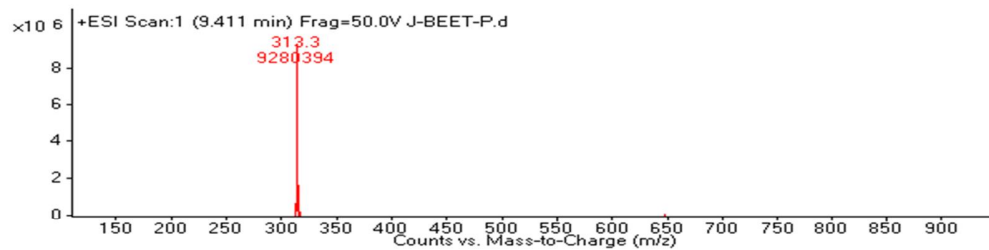


Figure 2-1. Isolation of the cancer stem cell (CSC) inhibitor from the beet extracts via mammosphere formation assay: (A) Isolation procedure of the mammosphere-forming inhibitor; (B) Assay of mammosphere formation inhibition using beet extracts. The mammospheres were incubated with beet extracts or DMSO. MDA-MB-231 cells were treated with beet extracts or DMSO in CSC culture media for seven days. Images were obtained by microscopy at 10× magnification and were representative mammospheres (scale bar = 100 μm); (C) HPLC chromatogram of the inhibitor isolated from the beet extracts.

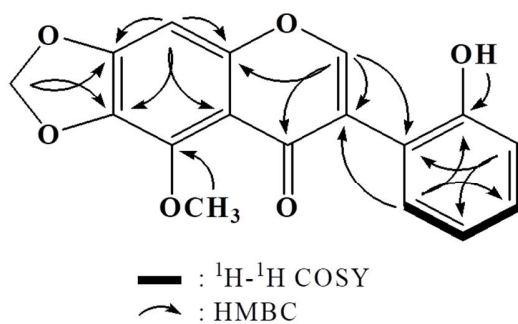
2.4.2 Structure analysis of the purified compound

The chemical structure of the compound was determined by ESI-mass spectrometry and NMR spectroscopy measurements. The molecular weight was estimated to be 312 by ESI-mass spectrometry, which showed a quasi-molecular ion peak at m/z 313.3 $[M + H]^+$ in the positive mode (Figure S2-5). The 1H NMR spectrum measured in $CDCl_3$ exhibited signals due to a hydroxyl proton at δ 9.02, and four aromatic methine protons at δ 7.32, 7.09, 7.07, and 6.93, which could be attributed to a 1,2-disubstituted benzene ring; two aromatic singlet methines at δ 7.90 and 6.70; a dioxymethylene at δ 6.10; and a methoxy group at δ 4.11. In the ^{13}C NMR spectrum, the 17 carbon peaks included a carbonyl carbon at δ 178.7; five oxygenated sp^2 quaternary carbons at δ 156.7, 154.7, 153.8, 141.4, and 135.8; one oxygenated sp^2 methine carbon at δ 153.4; five sp^2 methine carbons at δ 130.4, 130.0, 120.6, 119.4, and 92.9; three sp^2 quaternary carbons at δ 125.7, 120.8, and 112.8; one dioxymethylene carbon at δ 102.4; and one methoxy carbon at δ 61.3 (Figure S2-6). All proton-bearing carbons were assigned by the HMQC spectrum, and the 1H - 1H COSY spectrum revealed a partial structure of 1,2-disubstituted benzene (Figures S2-7 and S2-8). Further structural elucidation was performed with the aid of the HMBC spectrum, which showed long-range correlations from the methine proton at δ 7.90 to the carbons at δ 178.7, 154.7, 125.7, and 120.8; from the methine proton at δ 7.09 to the carbons at δ 156.7 and 125.7; from the methine proton at δ 6.70 to the carbons at δ 154.7, 153.8, 135.8, and 112.8; and from the dioxymethylene protons to the carbons at δ 153.8 and 135.8. Finally, a methyl proton showed a long-range correlation to the carbon at δ 141.4 (Figure S2-9 and S2-10). Therefore, the structure of the isolated compound was identified as that of betavulgarin (Figure 2-2).

A



B



Betavulgarin: $\text{C}_{17}\text{H}_{12}\text{O}_6$, Molecular weight: 312

Figure 2-2. Molecular structure of the CSC inhibitor isolated from beet. Molecular structure of betavulgarin.

2.4.3 Betavulgarin inhibits breast cancer cell growth and mammosphere formation

To ascertain whether betavulgarin has an inhibitory effect on breast cancer growth, we assessed the inhibitory effect of betavulgarin at increased concentrations in MDA-MB-231 and MCF-7 cells. Betavulgarin had an antiproliferative effect on the MDA-MB-231 and MCF-7 cells at $\geq 100 \mu\text{M}$ and $50 \mu\text{M}$, after 24 hrs of treatment (Figure 2-3A, B). To confirm whether betavulgarin can suppress mammosphere formation, it was added to mammospheres derived from MDA-MB-231 or MCF-7 cells. As shown in Figure 2-3C, D, betavulgarin decreased not only the sphere numbers of MDA-MB-231 and MCF-7 cells by 78% and 68%, respectively, but also the sizes of the mammospheres. In addition, betavulgarin inhibited migration and colony formation of MDA-MB-231 and MCF-7 cells (Figure 2-3E, F). We showed that betavulgarin inhibits mammosphere formation, migration, colony formation, and breast cancer growth.

2.4.4 Betavulgarin decreases CD44⁺/CD24⁻-expressing cancer cell numbers

The phenotype indicative of BCSCs was CD44⁺/CD24⁻. The CD44⁺/CD24⁻ cell fraction of MDA-MB-231 cells was examined after betavulgarin treatment. Betavulgarin reduced the CD44⁺/CD24⁻ cell fraction of MDA-MB-231 cells from 90.4% to 57.2% (Figure 2-4).

2.4.5 Betavulgarin inhibits the nuclear translocation of Stat3 in BCSCs

To examine the biochemical mechanism underlying the suppression of mammosphere formation by betavulgarin, we examined the total protein levels of Stat3, p-Stat3, and NF- κ B p65. Our data showed that the levels of Stat3 and p-Stat3 were significantly decreased following betavulgarin treatment (Figure 2-5A). The levels of nuclear Stat3, p-Stat3, and p65 were

determined, and these results showed that the nuclear Stat3 and p-Stat3 levels were significantly reduced by betavulgarin but those of p65 were not (Figure 2-5B). Furthermore, an immunofluorescence (IF) assay assessing pStat3 was performed in MDA-MB-231 cells, and the level of nuclear pStat3 in betavulgarin-treated cancer cells was lower than that in control cells (Figure 2-5C). Moreover, we examined the direct binding of a Stat3 binding probe to Stat3 proteins under betavulgarin treatment, using an electrophoretic mobility shift assay (EMSA) (Figure 2-5D). We examined nuclear Stat3-specific DNA binding using an Infrared Dye (IRDye)-labeled Stat3 probe that bound to Stat3 proteins under betavulgarin treatment. Our data showed that the amounts of nuclear Stat3 proteins bound to the IRDye-labeled Stat3 probe (indicated by arrow) were significantly decreased by betavulgarin treatment (Figure 2-5D, line 3). The specific binding of the Stat3 proteins/probe was confirmed using a self-competitor (Figure 2-5D, line 4) and a mutated Stat3 oligo (Figure 2-5D, line 5). Recently, it was reported that Stat3 protein binds to the promoter region of the SOX2 gene and increases SOX2 transcription. Stat3/SOX2 regulates the self-renewal of lung CSCs [17–20]. After betavulgarin treatment, we checked the Sox2 level because the Stat3 dimer activates the Sox2 gene. Our data showed that betavulgarin decreased the transcript and protein levels of Sox2 (Figure 2-5E). Our data showed that Stat3/Sox2 signaling was important in mammosphere formation.

2.4.6 Betavulgarin inhibits the mRNA levels of BCSC-specific marker genes and mammosphere growth

To examine whether betavulgarin reduced the mRNA levels of BCSC marker genes, we determined the mRNA levels of these genes. Betavulgarin reduced the transcriptional levels of the BCSC marker genes (Figure 2-6A). To check whether betavulgarin decreased mammosphere

growth, we cultured mammospheres with betavulgarin and counted the number of mammosphere cancer cells. Betavulgarin increased cell death and reduced mammosphere growth (Figure 2-6B).

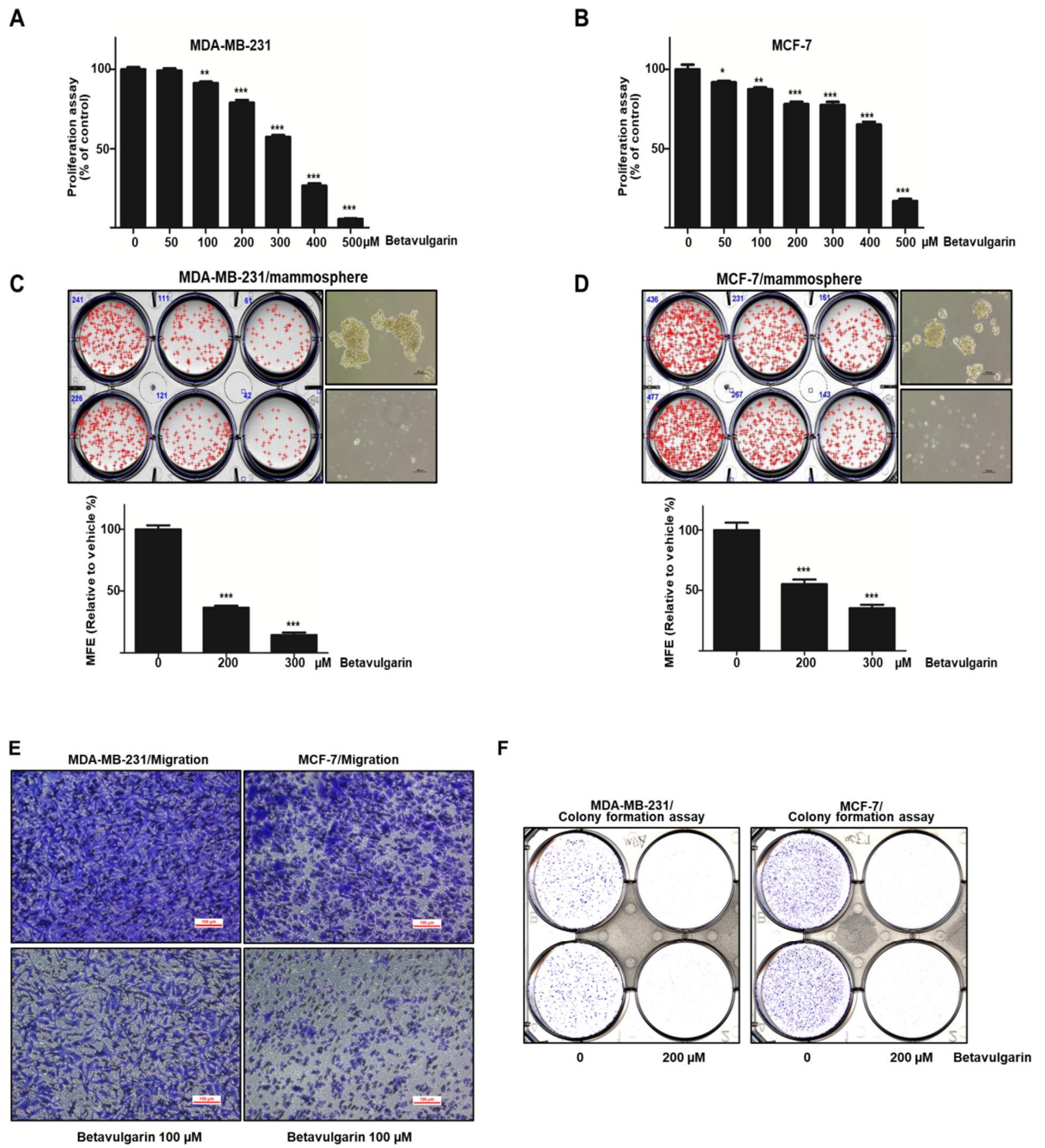


Figure 2-3. The effect of betavulgarin on cancer cell growth and mammosphere formation. **(A)** MDA-MB-231 cells were treated with betavulgarin for 24 h in a culture medium. The cell growth assay using betavulgarin was measured with an EZ-Cytox kit. **(B)** Breast cancer MCF-7 cells were treated with various concentrations of betavulgarin for 24 h in a culture medium. The cell proliferation of the MCF-7 cells was measured with an EZ-Cytox kit. **(C and D)** Betavulgarin inhibits the formation of mammospheres. For the establishment of mammospheres, 1×10^4 MDA-MB-231 cells and 4×10^4 MCF-7 cells were seeded in ultralow 6-well plates using a CSC culture media. The mammospheres were incubated with 200 μ M and 300 μ M of betavulgarin or DMSO for seven days. Images showing representative mammospheres were obtained by microscopy (scale bar: 100 μ m). The mammosphere formation efficiency (MFE) was examined. **(E)** Transwell assays were performed to determine the cell migration of the MDA-MB-231 and MCF-7 cells exposed to betavulgarin (scale bar: 100 μ m). **(F)** Betavulgarin inhibits the colony formation of the MDA-MB-231 and MCF-7 cells. The cancer cells were incubated in 6-well plates and treated with betavulgarin for 7 days. Representative data were collected. The data from triplicate experiments are represented as the mean \pm SD; * p < 0.05; ** p < 0.01; *** p < 0.001.

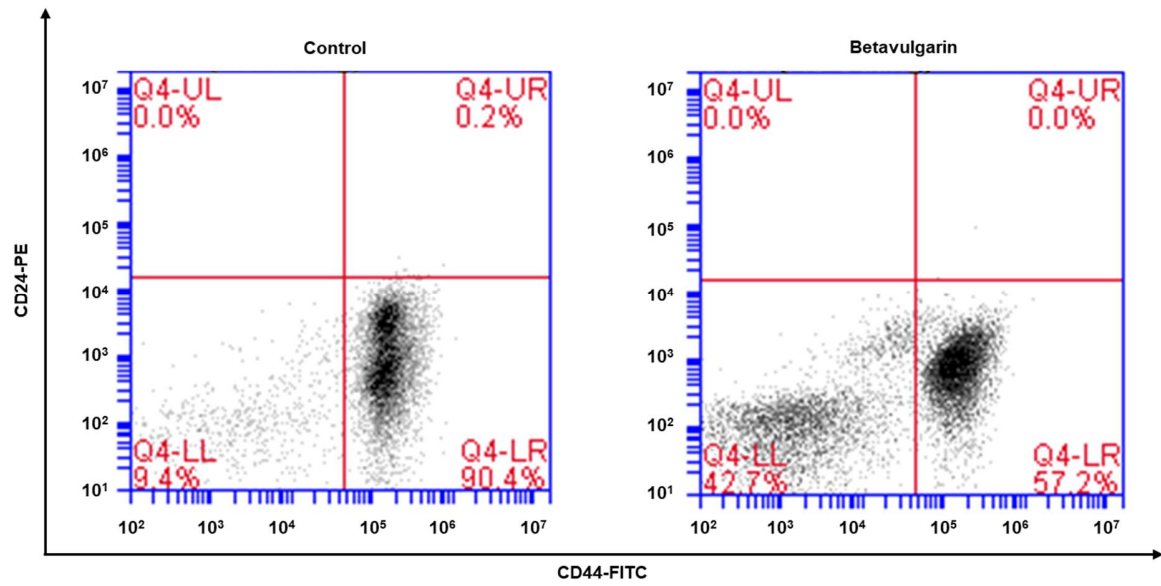


Figure 2-4. Effect of betavulgarin on the proportion of CD44⁺/CD24⁻. The CD44⁺/CD24⁻ cell population of the MDA-MB-231 cells treated with betavulgarin (200 μM) or DMSO for 24h. 1×10⁶ cells was analyzed by flow cytometry. The gating was based on binding of a control antibody (Red Cross).

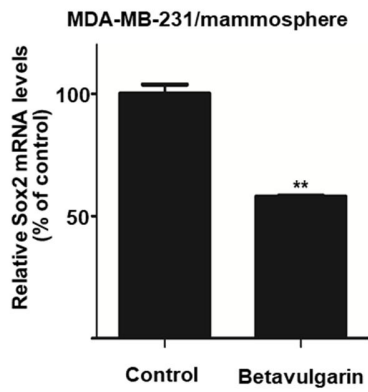
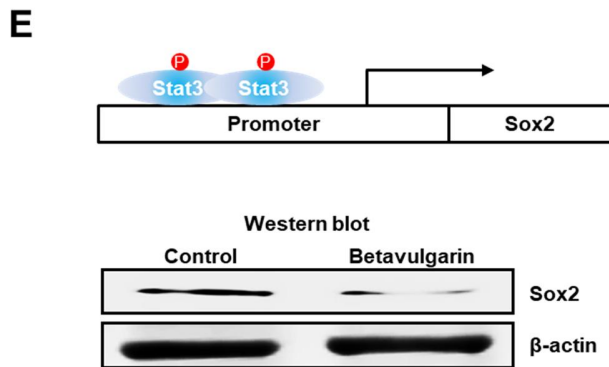
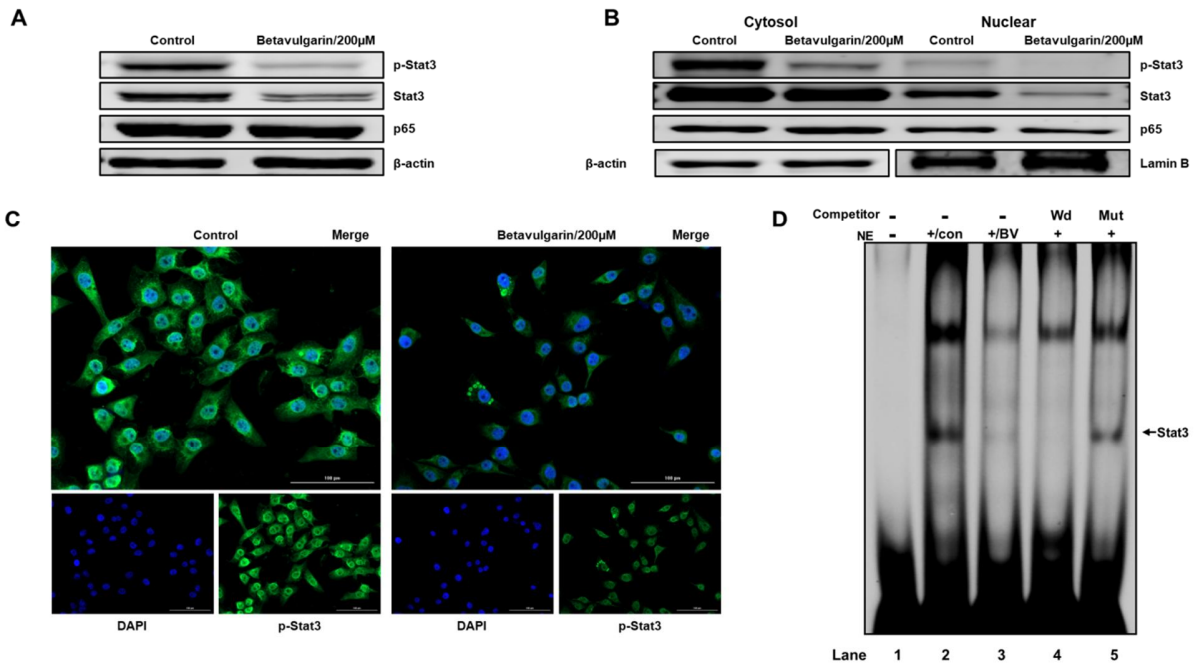


Figure 2-5. The effect of Betavulgarin on Stat3 signaling pathway. **(A)** The levels of p-Stat3, Stat3 and p65 in the total proteins were measured in the MDA-MB-231 derived mammosphere after treatment with betavulgarin for 48 h using western blot analyses. **(B)** The nuclear protein levels of Stat3 and NF- κ B were determined in MDA-MB-231 derived mammospheres treated with betavulgarin (200 μ M) or DMSO, betavulgarin blocks the translocation of Stat3 and decrease the level of p-Stat3 in mammospheres. **(C)** Immunofluorescence (IF) analysis of p-Stat3 (green) expression and localization in the breast cancer cells treated with betavulgarin or DMSO (scale bar: 100 μ m). **(D)** Electrophoresis Mobility Shift Assays (EMSAs) of MDA-MB-231 derived mammosphere nuclear proteins after treatment with betavulgarin. The nuclear extracts were incubated with the Stat3 probe and were separated by 6% native PAGE. Lane 1: Stat3 probe only; lane 2: Untreated nuclear extracts with the Stat3 probe; lane 3: Betavulgarin-treated nuclear proteins with the Stat3 probe; lane 4: Untreated nuclear proteins incubated with the Self-competitor (100x) oligo; lane 5: Untreated nuclear extracts incubated with the mutated-Stat3 (100x) probe. The arrow indicates the DNA/stat3 complex in the mammosphere nuclear lysates. **(E)** Treatment of the tumorsphere for 48 h with betavulgarin (200 μ M) decreased the mRNA and protein levels of the SOX2 gene. The transcript of the SOX2 gene was assayed with specific real-time RT-qPCR primers. The SOX2 protein was assayed with an anti-SOX2 antibody. β -actin was used as an internal control. The data are presented as the mean \pm SD of three independent experiments. $**p < 0.05$; versus the DMSO-treated control group indicated significant differences.

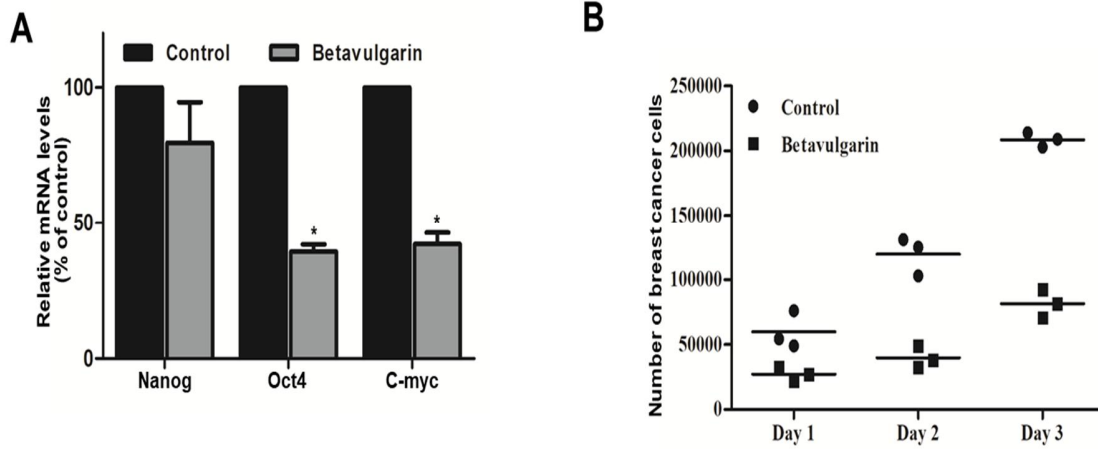


Figure 2-6. The effect of betavulgarin on the expression of CSC marker genes and mammosphere growth: **(A)** Realtime-qPCR analysis of the Nanog, c-Myc and Oct4 gene in the mammospheres after treatment with betavulgarin for 46 hours. **(B)** Mammosphere growth inhibited by betavulgarin. Mammospheres with/without betavulgarin were divided into single cells and plated in 6-well plate in equal numbers. 1, 2 and 3 days later, the cells were counted. The data from triplicate experiments are represented as the mean \pm SD. * $p < 0.05$ versus the DMSO-treated control group indicated significant differences.

2.5 DISCUSSION

Red beetroot (*Beta vulgaris* var. *rubra* L.) contains many bioactive compounds, including anthocyanin, betacyanin, folic acid, phenolic compounds, ascorbic acid, flavonoids, vitamin C, and other biologically active components. The most important bioactive phytochemicals in red beetroot are betalains, a class of tyrosine-derived pigments obtained from betalamic acid, whose members are grouped into yellow betaxanthins and red betacyanins. Red dye E162 extract from beetroot is approved for use in the food industry by the European Food Safety Authority. Betalains have been demonstrated to have strong free radical scavenging, antioxidant [52, 75, 76], and anti-inflammatory activities [77, 78]. In this report, we isolated a BCSC inhibitor, betavulgarin, based on activity-guided fractionation. Betavulgarin was reported to be a fungus infection response molecule and an antifungal molecule in beetroot [79]. For the first time, we report that betavulgarin inhibits BCSCs.

Breast cancer is the most frequent cancer among women [56]. Breast cancer is a systemic disease characterized by early tumor cell dissemination and displays a high degree of intratumor heterogeneity that is important for therapeutic resistance, recurrence, and tumor progression [80, 81]. Recently, a BCSC model was proposed and has received increasing interest in the field. CSCs are characterized by the common features of stem cells, including static behaviors, self-renewal, and differentiation. Achieving efficacious breast cancer treatment is challenging because of the existence of BCSCs. Numerous pathways and factors that could be targeted to inhibit BCSCs were identified. Our results showed that betavulgarin inhibits the proliferation of MDA-MB-231 and MCF-7 cells (Figure 2-3A, B) and the size and number of mammospheres derived from MDA-MB-231 or MCF-7 cells (Figure 2-3C, D). To address changes in the diverse biological properties of breast cancer cells under betavulgarin treatment, cell migration and

colony formation were tested in the context of betavulgarin treatment. Our results showed that betavulgarin inhibits the migration and colony formation of human breast cancer cells (Figure 2-3E, F). Additionally, betavulgarin reduced the size of the CD44⁺/CD24⁻ subpopulation in breast cancer cells (Figure 2-4). It is known that BCSCs are substantially regulated by a multitude of signaling pathways and transcription factors (such as Notch, Hedgehog, Wnt pathways, NF- κ B, and Stat3), and that targeting these pathways represents a potential therapeutic approach [56]. In this regard, we explored the role of betavulgarin in the inhibition of BCSCs. Interestingly, the expression levels of Stat3 and p-Stat3 were downregulated by betavulgarin, as was the nuclear localization of Stat3 (Figure 2-5). It was reported that natural products such as quercetin, apigenin, oroxylin A (flavones), butein (chalcone), piperlongumine, and caffeic acid (hydroxycinnamic acid) act as Stat3 inhibitors [82]. Betavulgarin belongs to isoflavone and might be a small-molecule inhibitor of Stat3 because of a similar structure of flavone. The activation of several transcriptional factors related to embryonic stem cell growth and differentiation, such as sex determining region Y (SRY)-box 2 (SOX2), could explain the enhanced stemness of BCSCs, compared to that of non-BCSCs [57]. One key transcription factor regulating SOX2 expression is Stat3, which directly binds to the promoter of SOX2 [83]. Subsequently, after treatment with betavulgarin, the mRNA transcription and protein expression of SOX2 were assessed, and the results showed that betavulgarin inhibited SOX2 through Stat3 inhibition (Figure 2-5). Betavulgarin reduced the transcriptional levels of the C-Myc, Nanog, and Oct4 genes and decreased mammosphere growth (Figure 2-6). Our data suggest that betavulgarin, which targets Sox2/Stat3 signaling, might be used as an anti-cancer agent.

2.6 CONCLUSION

A BCSC-inhibiting compound from beet extracts was purified using silica gel, gel filtration, TLC, and HPLC. The compound was identified as Betavulgarin, a mammosphere formation inhibitor, was isolated from beetroot and identified by mass and NMR spectroscopy. Betavulgarin inhibited cell proliferation, BCSC formation, and reduced the size of the CD44⁺/CD24⁻ subpopulation and the transcript levels of the C-myc, Nanog, and Oct4 gene. This compound decreased the nuclear localization of Stat3 and reduced the mRNA and protein levels of SOX2 in mammospheres. Our results in this study showed that betavulgarin inhibited the Stat3/Sox2 signaling pathway and induced BCSC death, indicating that betavulgarin might be a potential natural compound that targets breast cancer and BCSCs.

CHAPTER III

6-Methoxymellein isolated from carrot (*Daucus carota* L.)
targets breast cancer stem cells by regulating NF- κ B
signaling

3.1 ABSTRACT

The presence of breast cancer stem cells (BCSCs) induces the aggressive progression and recurrence of breast cancer. These cells are drug resistant, have the capacity to self-renew and differentiate and are involved in recurrence and metastasis, suggesting that targeting BCSCs may improve treatment efficacy. In this report, methanol extracts of carrot root were purified by means of silica gel, Sephadex LH-20, and preparative high-performance liquid chromatography to isolate a compound targeting mammosphere formation. We isolated the compound 6-methoxymellein, which inhibits the proliferation and migration of breast cancer cells, reduces mammosphere growth, decreases the proportion of CD44+/CD24- cells in breast cancer cells and decreases the expression of stemness-associated proteins c-Myc, Sox-2 and Oct4. 6-Methoxymellein reduces the nuclear localization of nuclear factor- κ B (NF- κ B) subunit p65 and p50. Subsequently, 6-methoxymellein decreases the mRNA transcription and secretion of IL-6 and IL-8. Our data suggest that 6-methoxymellein may be an anticancer agent that inhibits BCSCs via NF- κ B/IL-6 and IL-8 regulation.

3.2 INTRODUCTION

Carrot (*Daucus carota* L.) is one of the most important root vegetables cultivated worldwide and has health benefits [84-87]. With increasing health problems, carrots are becoming more popular plants because of their healthy nutrients and benefits for human health [88]. Phytochemicals, which comprise carotenoids, ascorbic acid, polyacetylenes and phenolic compounds, such as β -carotene, lutein, l-ascorbic acid, falcarinol and caffeic acid, contribute to the dietary value of carrots [87]. These compounds have also been shown to be potent inhibitors of inflammation and oxidative stress [89-95]. Breast cancer is a cancer mostly detected in

females and is one of the major causes of female death [56]. It has been increasingly recognized that breast cancer is a malignancy displaying frequent inter- and intratumor heterogeneity [96]. For this reason, histological stratification is used to classify breast cancer based on progesterone receptor, estrogen receptor, and erbB-2 receptor (HER2) expression. Chemotherapy, hormone therapy, immunotherapy, radiotherapy, and surgery are the common modalities for breast cancer [97]. However, breast cancer stem cells (BCSCs) endowed with self-renewal capacity have been demonstrated to contribute to tumor heterogeneity. Multiple independent studies have shown the presence of distinct CSC populations within tumors based on the expression of CSC markers such as CD44⁺/CD24⁻ and aldehyde dehydrogenase (ALDH) [98, 99]. Compared with non-CSCs, CSCs exhibit overactivation of transcription factors and proteins related to signal pathways, such as stemness markers: Sox-2, Oct4, c-Myc; Hedgehog and Wnt pathways [57, 92, 100-103]. c-Myc is important for regulating proliferation and the survival of glioma cancer stem cell [103]. Oct4 is responsible for breast CSC specification and regulated Nanog, Sox2 and Klf4 gene [104]. Sox2 drives cancer stemness and fuels tumor initiation [105]. Many studies show that the tumor microenvironment plays an important role in regulating CSC formation and tumor progression [106, 107].

BCSC formation can be regulated by cytokines and cell types present in the tumor microenvironment, including mesenchymal stem cells, cancer-associated fibroblasts and tumor-infiltrating lymphocytes [108]. Additionally, the tumor microenvironment contains several noncellular components, including cytokines and growth factors. In particular, cytokines contribute to chronic inflammation, which promotes cancer cell survival and cancer disease progression by suppressing immune cell functions [109-111]. For instance, interleukin-6 (IL-6) is sufficient for converting non-CSCs to CSCs in different breast cells [110], and IL-6 regulates

the conversion of non-CSCs into CSCs [111], activating the Notch-3-dependent upregulation of the Notch ligand Jagged-1 in breast cancer cells [30]. Interleukin-8 (IL-8) induces BCSC activity and chemoresistance in triple-negative breast cancer (TNBC) cells [112]. The IL-8 signaling pathway is mediated via an EGFR/HER2-dependent pathway [112]. Nuclear factor- κ B (NF- κ B) subunit p65, a regulator of IL-6 and IL-8, was suggested as a potential target against BCSCs [73, 113].

Herein, we chose a colorful food, *D. carota* L., for isolating mammosphere inhibitors against BCSC. We isolated a compound, 6-methoxymellein that inhibits the mammosphere formation of breast cancer cell lines. We demonstrate that 6-methoxymellein suppresses BCSC formation through the NF- κ B signaling pathway.

3.3 MATERIALS AND METHODS

3.3.1 Isolation and identification of a breast CSC inhibitor derived from *D. carota* L.

We followed a previously described method [73]. The ground carrot sample (1.2 kg) was suspended and extracted with methanol. The purification protocol is described in Figure 3-1. The carrot powder (1.2 kg) was extracted with 12 L of methanol. The methanol extracts were concentrated to 2 L and saturated with H₂O, and the methanol part was evaporated. The water part was extracted with an equal volume of ethyl acetate (v/v = 1:1). The ethyl acetate fraction was recovered and loaded on a silica gel column (3 × 35 cm), and the sample was fractionated with solvent (chloroform-methanol, 10:1) (Figure S3-1). The five fractions were recovered and tested by mammosphere assay. The 1 and 2 fractions suppressed mammosphere formation. Parts 1 and 2 were recovered and loaded on a Sephadex LH-20 column (2.5 × 30 cm) and fractionated

into three parts (Figure S3-2). The three fractions were recovered and tested by mammosphere assay. Fraction 3 suppressed mammosphere formation. Fraction 3 was fractionated using preparatory TLC (glass plate; 20 × 20 cm) and developed in a TLC glass chamber (chloroform-methanol, 100:1). The main band was isolated from the silica gel plate, and the fraction was tested by mammosphere formation assay (Figure S3-3). The major fraction was analyzed using a Shimadzu HPLC LC-20 (Shimadzu, Tokyo, Japan). HPLC was performed using a C₁₈ column (10 × 250 mm, flow rate; 2 mL/min). For isolation, the acetonitrile concentration was initially set at 0%, increased to 60% at 15 min and finally increased to 100% at 40 min (Figure S3-4).

3.3.2 Structure analysis of the purified compound

The molecular structure of the purified compound was analyzed by NMR and mass spectrometry. The molecular weight of the compound was determined to be 208 by ESI-mass spectrometry, which indicated a quasimolecular ion peak at m/z 209.3 [M + H]⁺ in positive mode (Figure S3-9). The ¹H-NMR spectrum in CD₃OD showed signals due to two aromatic methines at δ 6.35, one oxygenated methine at δ 4.66, one methoxy methyl at δ 3.82, a nonequivalent methylene at δ 2.96 and 2.84, and one methyl at δ 1.46. In the ¹³C-NMR spectrum, 11 carbon peaks included one carbonyl carbon at δ 171.7, two oxygenated sp² quaternary carbons at δ 167.7 and 165.7, two sp² methine carbons at δ 107.1 and 100.6, two sp² quaternary carbons at δ 143.4 and 102.6, one oxygenated methine carbon at δ 77.4, one methoxy carbon at δ 56.3, one methylene carbon at δ 35.6, and one methyl carbon at δ 21.0 (Figure S3-5). All proton-bearing carbons were assigned by the heteronuclear multiple-quantum coherence (HMQC) spectrum, and the ¹H-¹H COSY spectrum showed one partial structure (Figures S3-6, S3-7, and S3-9). Further structural elucidation was performed with the aid of the heteronuclear

multiple bond correlation (HMBC) spectrum, which showed long-range correlations from the methine protons at δ 6.35 to the carbon at δ 102.6 and from the methylene protons at δ 2.94/2.84 to the carbons at δ 143.4, 107.1, and 102.6. Finally, the methoxy group was connected by the long-range correlation from the methyl protons at δ 3.82 to the carbon at δ 167.7 (Figures S3-8 and S3-9). The molecular structure of the purified compound was determined to be 6-methoxymellein (Figure 3-2).

3.3.3 Cell line and culture of mammospheres

The growth inhibitory effect of 6-methoxymellein was examined using increasing concentrations in breast cancer cell lines. Treatment with 6-methoxymellein for 24 h induced suppression of proliferation at >0.8 mM (MDA-MB-231) and >0.5 mM (MCF-7) (Figure 3-3A, B). To evaluate whether 6-methoxymellein inhibits mammosphere formation, primary mammospheres were treated with 6-methoxymellein. Compared to the control, 6-methoxymellein decreased the sphere number and decreased the size of the mammospheres (Figure 3-3C, D). In addition, 6-methoxymellein inhibited the formation of colony and cell migration (Figure 3-3E, F). We show that 6-methoxymellein suppresses cell decreased the size of the mammospheres (Figure 3-3C, D). In addition, 6-methoxymellein inhibited the colony formation and migration of breast cancer cells (Figure 3-3E, F). Our data show that 6-methoxymellein suppresses cell migration, growth, colony formation, and mammosphere formation.

3.3.4 Cell proliferation

Breast cancer cells were cultured at 1×10^6 (MDA-MB-231) and 1.5×10^6 (MCF-7) cells in a culture plate for 1 day and incubated with 6-methoxymellein (0, 0.5, 0.8, 1, 2 and 3 mM) for 1 day. Proliferation was determined by using the EZ-Cytox assay kit (DoGenBio, Seoul, Korea). The optical density at 450 nm (OD_{450nm}) was measured by using a plate reader (VERSA max, Molecular Device, San Jose, CA, USA).

3.3.5 Colony formation assay

We used a previously described method for the colony formation assay [113]. Breast cancer cells were cultured in a 6-well plate (1000 cell/well) and cultured with 6-methoxymellein in culture media. After 7 days, the media was removed, washed with 1x PBS, fixed with 3.7% formaldehyde, and stained for 30 min with 0.05% crystal violet. The images were captured by using a scanner.

3.3.6 Flow cytometric assay of CD44⁺/CD24⁻ expression

We followed a previously described method [71]. After treatment of 6-methoxymellein for 24 h, MDA-MB-231 cells were cultured and dissociated into single cells. A total of 1×10^6 cancer cells were labeled with FITC-labeled anti-CD44 and PE- labeled anti-CD24 at 4 °C for 20 min. Then, the cells were washed with 1 × PBS and analyzed using an Accuri C6 flow cytometer (BD, San Jose, CA, USA).

3.3.7 Migration

We followed a previously described method for the migration assay [72]. Migration was examined in 12-well inserts with polycarbonate membranes (Merck, Darmstadt, Germany). MDA-MB-231 and MCF-7 cancer cells were cultured in 200 μ L DMEM containing 1% FBS with DMSO or 6-methoxymellein and cultured in the upper chamber (2×10^5 cells/chamber). The bottom chamber was covered with 750 μ L of DMEM containing 20% FBS. The cells were incubated for 1 day at 37 °C in an incubator (37 °C, 5% CO²). The lower surfaces of the inserts were fixed and stained with 0.03% crystal violet, and images were captured by using a light microscope.

2.3.7 Real-time quantitative reverse transcription PCR

We used a previously described method [73]. Total RNA of MDA-MB-231 mammospheres was isolated. RT-quantitative PCR was performed by using an RNA-direct SYBR qPCR kit (Toyobo, Japan). The specific primers for IL-6, IL-8 and β -actin are described in Table 1.

3.3.8 Western blotting

We used a previously described method for western blotting [73]. Proteins samples (20 μ g/well) of mammospheres treated with 6-methoxymellein were isolated and run on a 10% SDS-PAGE gel. The separated protein gels were transferred to a PVDF membrane (Millipore, Billerica, MA, USA). Membranes were incubated at room temperature for 1 h in Odyssey blocking buffer in PBST (0.1% Tween 20). The membranes were incubated at 4 °C overnight with the following primary antibodies: NF- κ B p65, LF-MA30327, NF- κ B p50, sc-8414; Oct4,

LF-MA30482 (AbFrontier, Seoul, Korea); c-Myc (Cell Signaling Technology, Denver, CO, USA); Sox-2, Lamin B and β -actin (Santa Cruz Biotechnology, Dallas, TX, USA). After the membranes were washed with 1x PBST, they were incubated with IRDye 800CW and 680RD-conjugated secondary antibodies for 1 h, and band densities were examined by using an ODYSSEY CLx (LI-COR, Lincoln, NE, USA).

3.3.9 EMSA

Nuclear proteins were prepared as described previously method [74]. EMSA experiments for NF- κ B binding were performed using an IRDye 700-labeled NF- κ B oligonucleotide. Samples containing the NF- κ B/700 dye oligo complex were run on a native 4% PAGE gel, and the fluorescence of the PAGE gel was scanned and captured by using an ODYSSEY CLx machine (LI-COR).

3.3.10 Quantification of extracellular human IL-6 and IL-8 cytokines using the cytometric bead array (CBA)

Human Inflammatory Cytokine Assay Kit was used. We followed a previously described method [113]. MDA-MB-231 mammospheres were incubated for 5 days and then cultured with 6-methoxymellein for 2 days. The extracellular IL-6 and IL-8 concentrations were analyzed using the BD CBA Human Inflammatory Cytokine Assay Kit. We followed the manufacturer's protocol (BD, San Jose, CA, USA). Fifty microliters of bead assay buffer, equal volumes of cultured media and 50 μ L of PE-labeled capture antibody solution were mixed into each tube. The sample mixes were incubated at room temperature protected from light for 3 h, washed with

1 × washing buffer. The pellet was suspended in reaction buffer and analyzed by flow cytometry Accuri C6 (BD, San Jose, CA, USA).

3.3.11 Statistical analysis

Our results are presented as the mean ± standard deviation (SD). Our results were analyzed using Student's t-test. A p-value less than 0.05 was considered statistically significant (GraphPad Prism 7 Software).

3.4 RESULTS

3.4.1 Isolation and identification of a breast CSC inhibitor derived from *D. carota* L.

Bioassay-guided fractionation was performed to screen and isolate BCSC inhibitor from *Daucus carota* L extracts using a mammosphere formation assay from breast cancer cell lines. The methanol extracts of *D. carota* L. were purified via ethyl acetate extraction (v/v = 1:1), silicon dioxide gel, gel filtration chromatography, and preparatory HPLC (Figure 3-1A). CSC formation was suppressed by the purified compound (Figure 3-1B). The purity of the compound was confirmed using HPLC (Figure 3-1C). NMR and GC-MS data identified the compound as 6-methoxymellein (Figure 3-2).

3.4.2 6-Methoxymellein suppresses the growth of breast cancer cells and mammospheres

The growth inhibitory effect of 6-methoxymellein was examined using increasing concentrations in breast cancer cell lines. Treatment with 6-methoxymellein for 24 h induced suppression of proliferation at >0.8 mM (MDA-MB-231) and >0.5 mM (MCF-7) (Figure 3-3A, B). To evaluate whether 6-methoxymellein inhibits mammosphere formation, primary mammospheres were treated with 6-methoxymellein. Compared to the control, 6-methoxymellein decreased the sphere number and decreased the size of the mammospheres (Figure 3-3C, D). In addition, 6-methoxymellein inhibited the formation of colony and cell migration (Figure 3-3E, F). We show that 6-methoxymellein suppresses cell decreased the size of the mammospheres (Figure 3-3C, D). In addition, 6-methoxymellein inhibited the colony formation and migration of breast cancer cells (Figure 3-3E, F). Our data show that 6-

methoxymellein suppresses cell migration, growth, colony formation, and mammosphere formation.

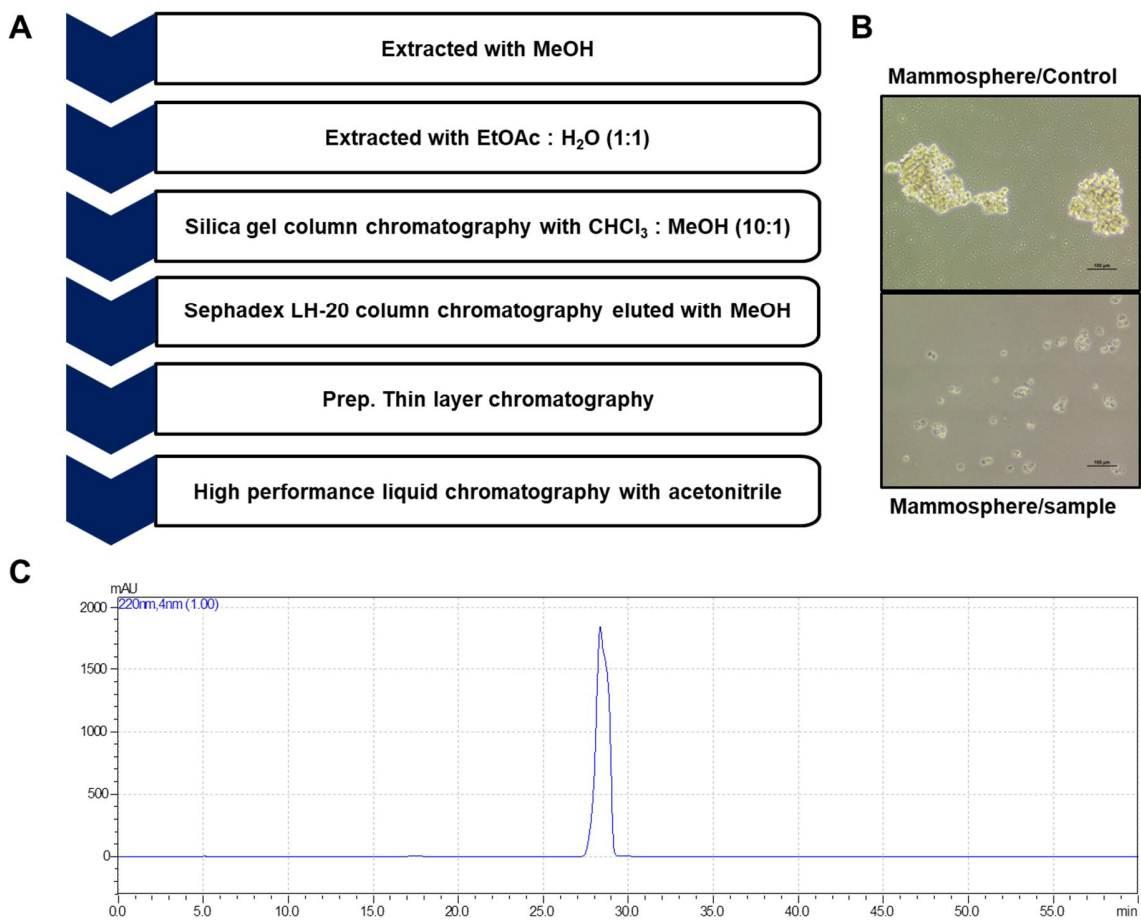


Figure 3-1. Isolation of breast CSC inhibitors from carrot extracts based on mammosphere formation assays. (A) The purification procedure for the mammosphere formation inhibitor. (B) Inhibitory effect of carrot extracts on mammosphere growth. The mammospheres were incubated with carrot extracts or DMSO. The mammospheres were photographed with a microscope at 10x magnification (scale bar = 100 μ m). (C) Purified samples of carrot extracts were analyzed by HPLC chromatogram.

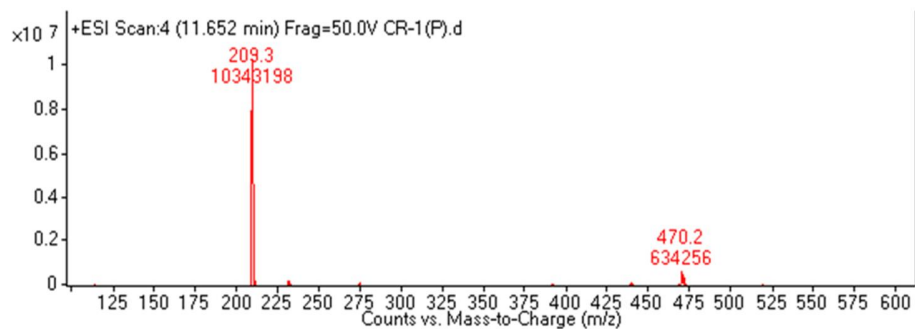
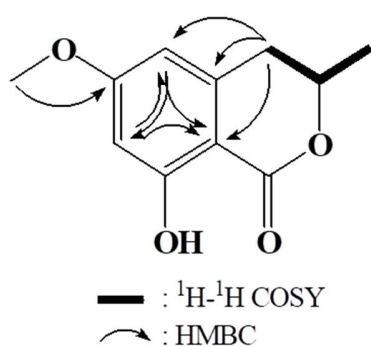
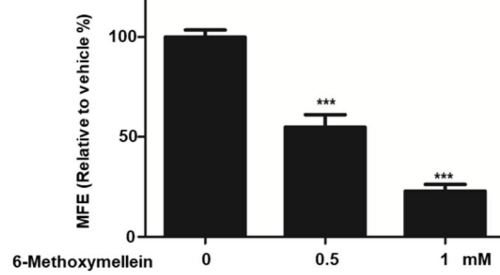
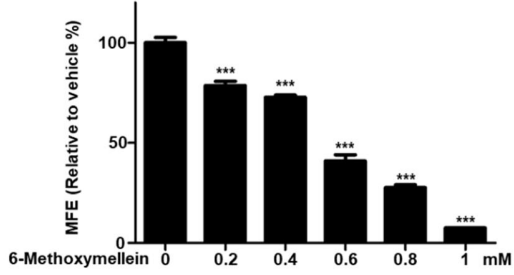
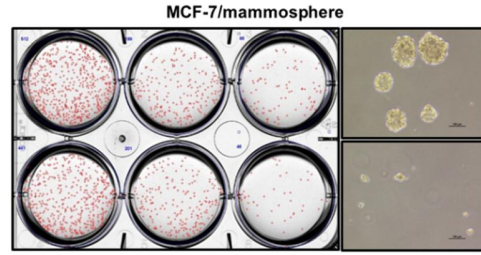
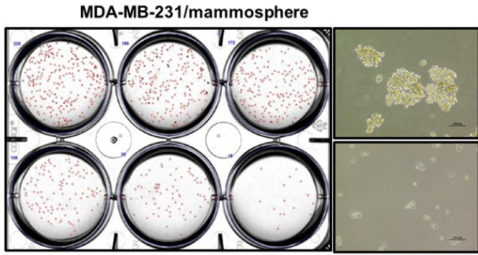
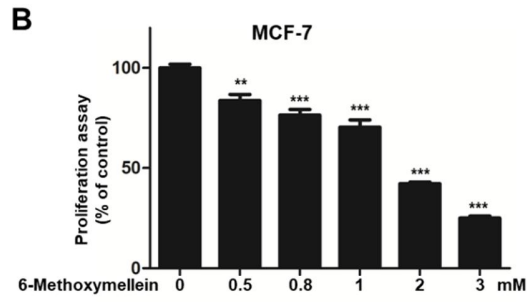
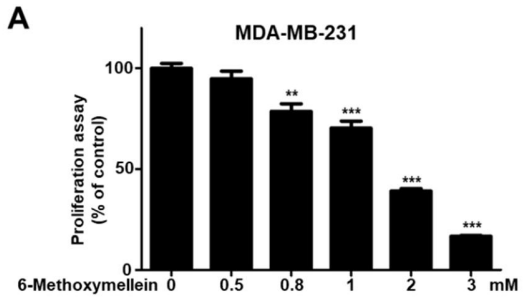
A**B****6-Methoxymellein****C₁₁H₁₂O₄ : 208**

Figure 3-2. Molecular structure of the CSC inhibitor isolated from carrots. Molecular structure of 6-methoxymellein.



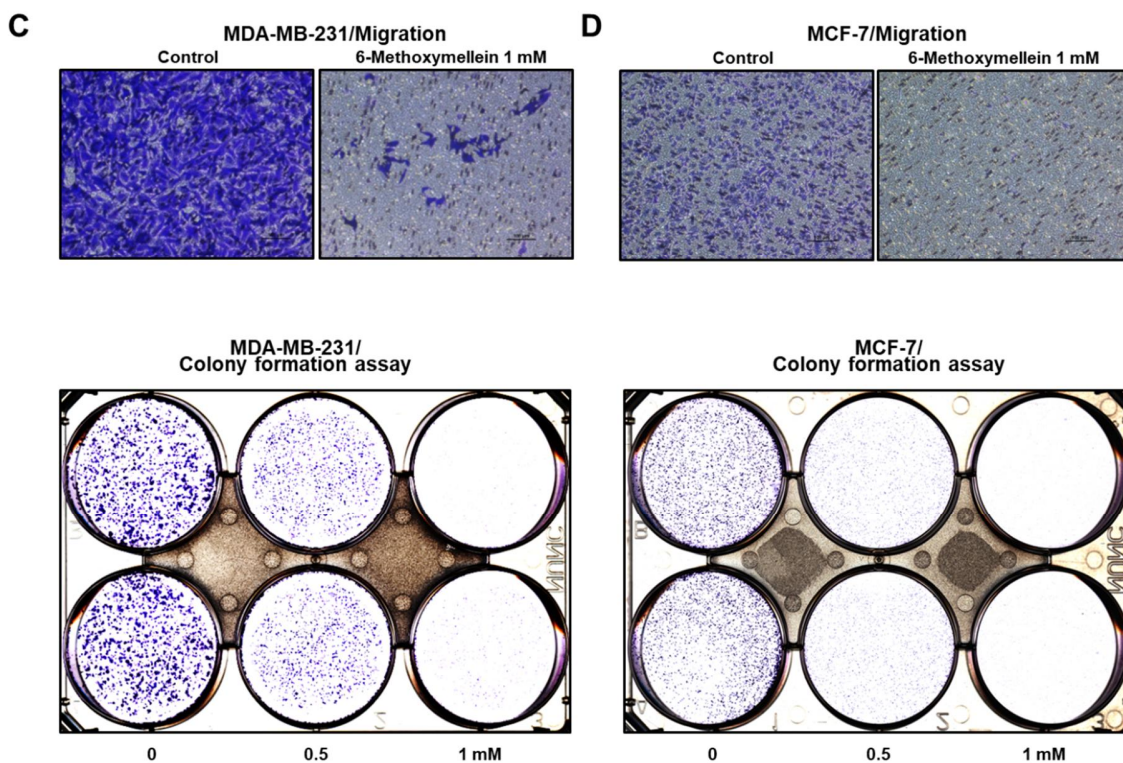


Figure 3-3. The antiproliferation and mammosphere formation inhibitory effect of 6-methoxymellein. (A, B) The antiproliferation ability of 6-methoxymellein was assayed with an EZ-Cytox kit using breast cancer cells treated with various concentrations of 6-methoxymellein. (C, D) To establish the inhibitory effect of 6-methoxymellein on mammosphere formation, breast cancer cells were cultured in 6-well plates (ultralow attachment) with CSC culture media containing increasing concentrations of 6-methoxymellein or DMSO alone after 7 days. The images were captured and are representative mammospheres by microscopy at 10× magnification (scale bar =100 μm). (E, F) The migration ability of MDA-MB-231 and MCF-7 cells was determined by Transwell assay after exposure to 6-methoxymellein (scale bar: 100 μm). 6-Methoxymellein inhibits the colony formation of MDA-MB-231 and MCF-7 cells. Our representative data were collected. Our data from triplicate experiments are represented as the mean ± SD; ** $p < 0.01$; *** $p < 0.001$.

3.4.3 6-Methoxymellein reduces the proportion of CD44⁺/CD24⁻-expressing breast cancer cells

The cell surface marker of breast CSCs is CD44⁺/CD24⁻ of breast cancers. The CD44⁺/CD24⁻ subpopulation of cancer cells was determined under 6-methoxymellein. 6-Methoxymellein decreased the proportion of CD44⁺/CD24⁻ MDA-MB-231 cancer cells from 80.3% to 41.6% (Figure 3-4).

3.4.4 6-Methoxymellein inhibits the protein expression of cancer stem cell-specific markers and inhibits mammosphere growth

Next, we analyzed whether 6-methoxymellein reduces the protein level of CSC marker genes. Indeed, 6-methoxymellein decreased the protein expression levels of cancer stem cell marker genes (Figure 3-5A). To examine whether 6-methoxymellein reduced mammosphere growth, mammospheres were cultured with 6-methoxymellein, and the number of cancer cells of mammospheres was examined. The results indicated that 6-methoxymellein inhibited mammosphere growth (Figure 3-5B)

3.4.5 6-Methoxymellein suppresses the nuclear localization of NF-κB p65 and NF-κB p50 in BCSCs

To determine the cellular mechanism by which 6-methoxymellein reduces mammosphere formation, we examined the total and nuclear protein levels of NF-κB p65 and NF-κB p50. We showed that the nuclear level of NF-κB p65 and NF-κB p50 were significantly reduced after 6-methoxymellein treatment (Figure 3-6A, B). Furthermore, we tested the direct binding of the NF-κB DNA probe to nuclear NF-κB proteins by electrophoretic mobility shift assay (EMSA) under

6-methoxymellein treatment (Figure 3-6C). We indicated that the amount of NF- κ B protein bound to the NF- κ B probe (arrow) was reduced under 6-methoxymellein treatment (Figure 3-6C, #3). The specificity of the NF- κ B/probe complex was analyzed by using a 100X self-competitor oligo (Figure 3-6C, #4) and a 100X mutated NF- κ B competitor (Figure 3-6C, #5).

3.4.6 6-Methoxymellein decreases the mRNA and protein levels of secretory IL-6 and IL-8 in mammospheres

It was investigated whether the activity of NF- κ B is associated with IL-6 and IL-8 secretion [114-116]. To examine whether 6-methoxymellein decreases the level of IL-6 and IL-8 cytokine secretion, we determined the concentrations of secreted IL-6 and IL-8 in mammosphere culture medium using a human inflammatory assay. 6-Methoxymellein reduced the concentrations of the cytokines IL-6 and IL-8 (Figure 3-7A). Subsequently, we checked the levels of IL-6 and IL-8 transcript under 6-methoxymellein, and our data showed that 6-methoxymellein decreased the mRNA expression of IL-6 and IL-8 (Figure 3-7B).

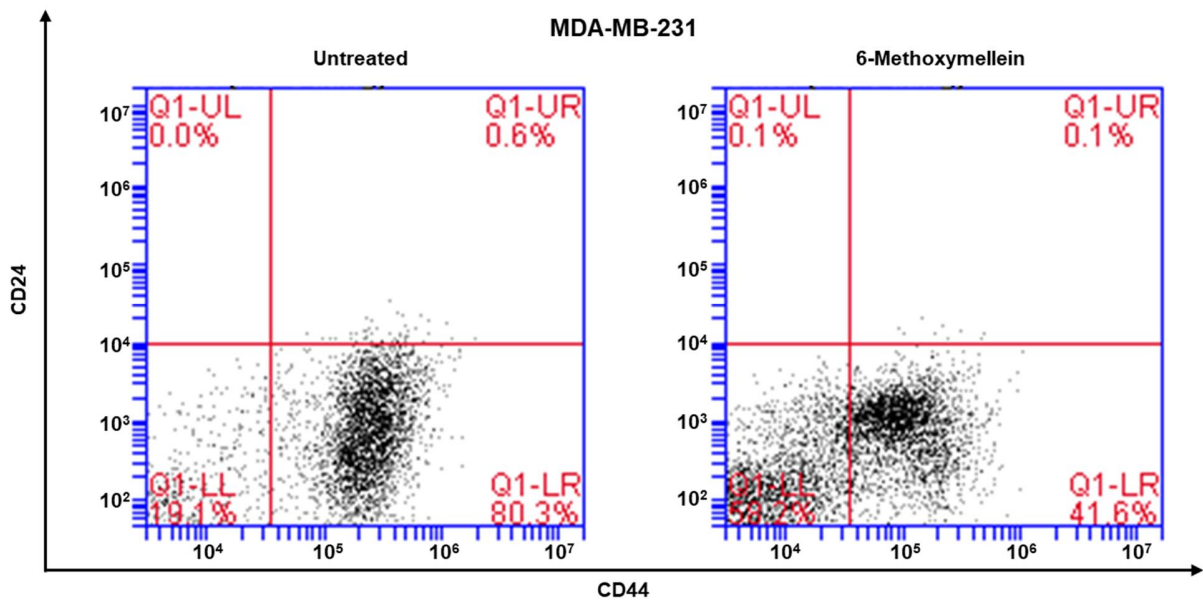


Figure 3-4. 6-Methoxymellein reduces the proportion of CD44⁺/CD24⁻ cells. MDA-MB-231 cells were treated with 6-methoxymellein (1 mM) for 24 hours. The CD44⁺/CD24⁻ cell population was assessed by an Accuri C6 flow cytometer. The red cross was used for binding of a control antibody.

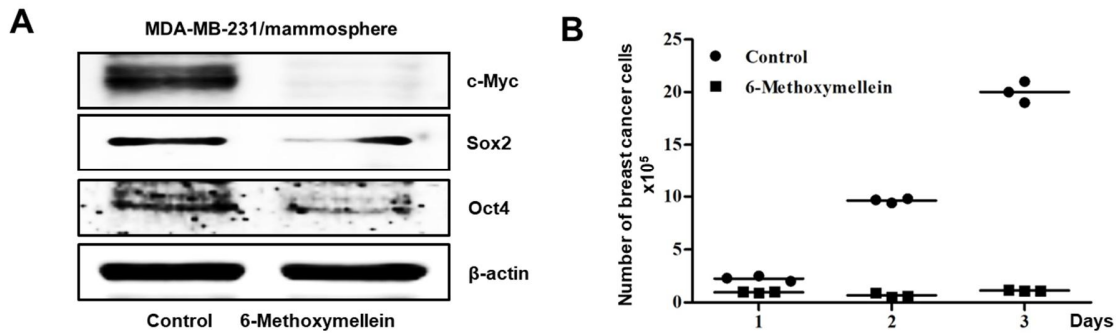


Figure 3-5. 6-Methoxymellein suppresses the protein expression of CSC markers and inhibits mammosphere growth. **(A)** Immunoblot analysis of the c-Myc, Sox2 and Oct4 proteins of mammospheres treated with 6-methoxymellein for 2 days. **(B)** 6-Methoxymellein inhibits mammosphere growth. Mammospheres treated with 6-methoxymellein were split into single cells and plated in 6-cm culture plates. One, 2 and 3 days later, the cells were quantified.

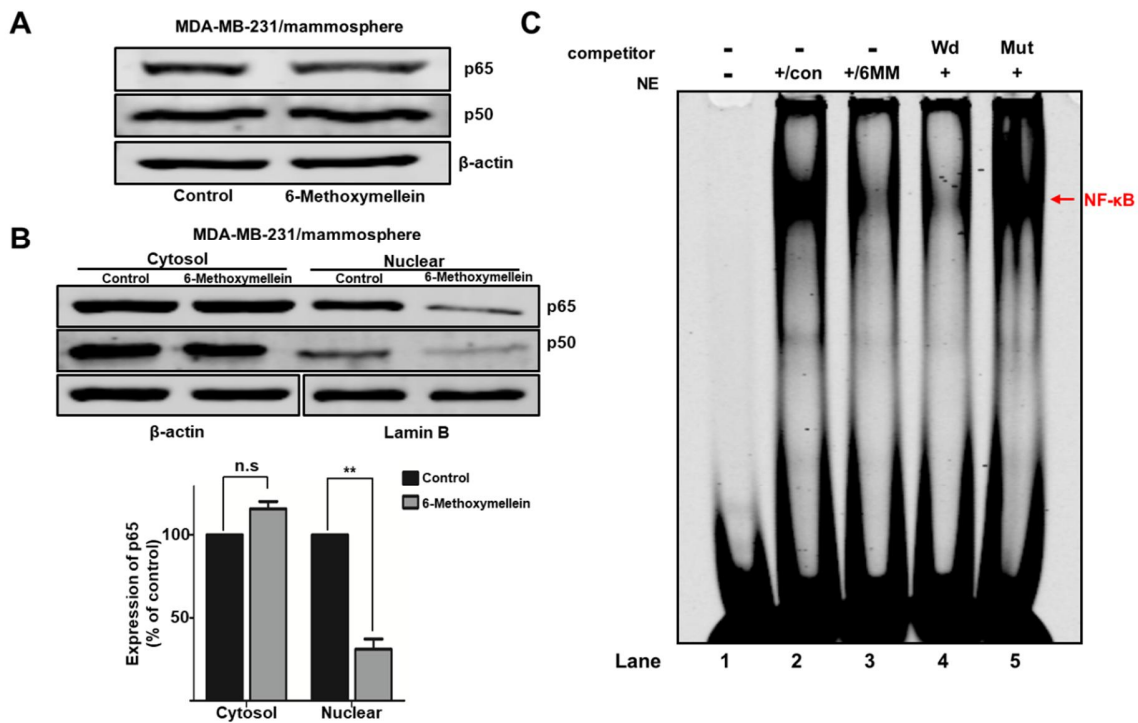


Figure 3-6. The effect of 6-methoxymellein on the NF- κ B signaling pathway. (A) The total protein level of p65 was assayed in mammospheres under 6-methoxymellein for 48 hours using immunoblot analysis. (B) The levels of nuclear p65 were assayed in mammospheres under 6-methoxymellein (1 mM) or DMSO. 6-Methoxymellein blocks the translocation of p65 in mammospheres. (C) EMSAs of nuclear protein in MDA-MB-231 cell-derived mammospheres under 6-methoxymellein. The nuclear extracts were incubated with the NF- κ B probe and run by 4% native PAGE. Lane 1: NF- κ B probe only; lane 2: nuclear extracts with the NF- κ B probe; lane 3: 6-methoxymellein-treated nuclear proteins with the NF- κ B probe; lane 4: untreated nuclear proteins incubated with the self-competitor (200x) oligo; lane 5: untreated nuclear extracts incubated with the mutated-Stat3 (200x) probe. The arrow shows the DNA/NF- κ B protein complex from nuclear lysates of mammospheres. Our data are presented as the mean \pm SD of three independent experiments. ** $p < 0.05$ versus the control group.

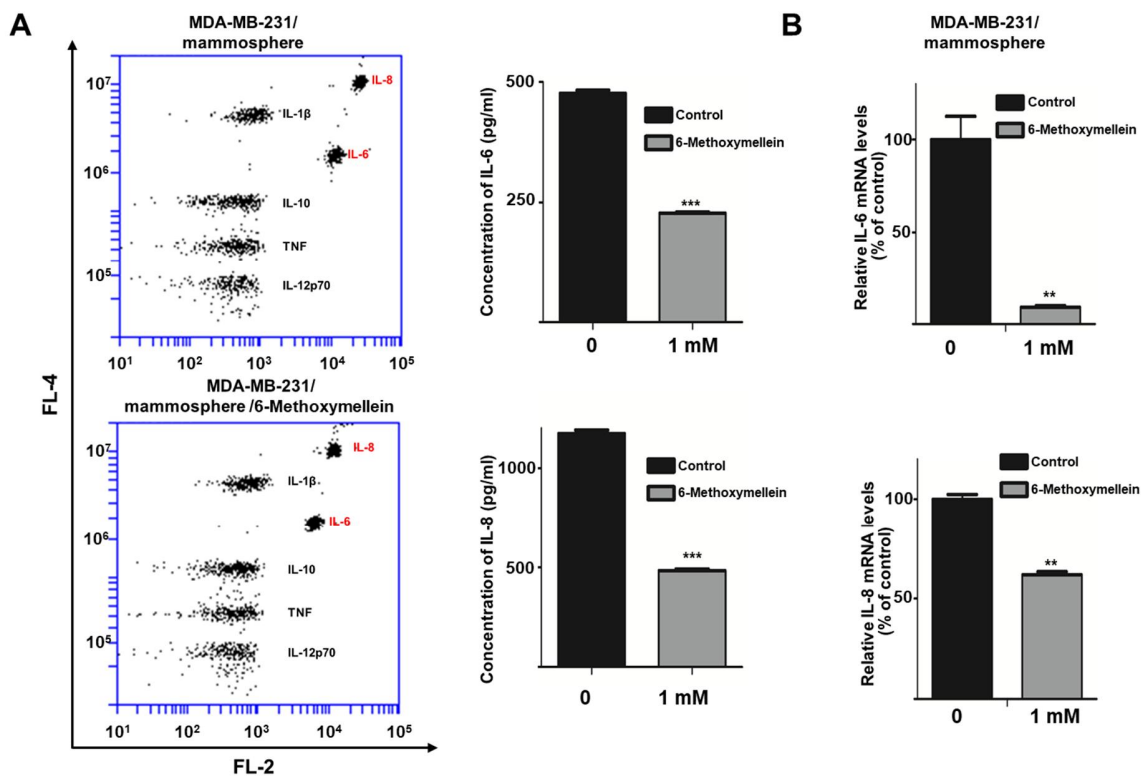


Figure 3-7. 6-Methoxymellein suppresses the secretion and transcription of IL-6 and IL-8. **(A)** The CBA Human Inflammatory Cytokine Assay Kit was used to assay the secretion of cytokines in mammosphere culture media treated with 6-methoxymellein or DMSO. **(B)** Transcript levels of the IL-6 and IL-8 genes were assessed in 6-methoxymellein-treated mammospheres using specific RT-qPCR primers. Our data are represented as the mean \pm SD. $**p < 0.05$ versus the control group.

3.5 DISCUSSION

Carrot (*D. carota* L.) is the most important root vegetable, is cultivated worldwide, and is rich in natural phytochemicals. Carrot root is widely utilized because of abundant carotenoids, anthocyanins and dietary fiber. Carrots are the main source of carotenoids, and previous studies have demonstrated that carrots may reduce cancer risk and play an important role in a cancer prevention diet [117-119]. Carrots are traditionally used for the treatment of gastric ulcers, diabetes, muscle pain and cancer in Lebanon [120]. Carrots have been reported to provide numerous biological activities, including antibacterial, antifungal, diuretic, antilithic, anticancer, antiinflammatory and antioxidant effects [120-124]. In this study, we purified a BCSC inhibitor from carrots (Figure 3-1) and identified as 6-methoxymellein by electrospray ionization (ESI)-MS and NMR spectroscopy (Figure 3-2). 6-Methoxymellein belongs to the mellein family, which is a subgroup of 3,4-dihydroisocoumarins. Previously, mellein was produced by the fungus *Aspergillus ochraceus*. Coumarin and isocoumarin are products of bacteria, fungi, plants, insects, lichens, and marine sponges. These compounds have different biological functions, including antimicrobial, anticancer, antileukemia and antiviral activities [125-127]. 6-Methoxymellein was the first mellein derivative isolated from carrots in 1960 [128]. Subsequently, it was purified from carrot root cultured with *Ceratocystis cimbriata*, *Helminthosporium carbonum*, and *Fusarium oxysporum* [129]. It was supposed that 6-methoxymellein production resulted from a change in plant metabolism induced by the fungi [130], suggesting that 6-methoxymellein induces the active defenses of carrot-based compounds against fungi; thus, 6-methoxymellein was classified as a phytoalexin [130, 131].

Targeting cancer stem cells that contribute to therapy resistance, metastasis, and recurrence is a challenge of breast cancer treatment [132, 133]. Mammosphere formation assays were

performed to identify functional CSCs in vitro [134]. Our results show that 6-methoxymellein suppressed the growth of breast cancer cells, decreased the size and efficiency of mammospheres formation (Figure 3-3C, D), and inhibited cell migration and colony formation (Figure 3-3E, F). In addition, 6-methoxymellein reduced the CD44⁺/CD24⁻ subpopulation in MDA-MB-231 cells (Figure 3-4). To address the effect of 6-methoxymellein on the stemness of mammospheres, we checked the protein levels of c-Myc, Oct4 and Sox-2 in mammospheres under 6-methoxymellein treatment. Our data show that 6-methoxymellein inhibits c-Myc, Oct4 and Sox-2 expression and reduces mammosphere growth (Figure 3-5A, B). It has been reported that the regulatory mechanisms of BCSC formation are extensive and complex. Several pathways, such as the Notch, Wnt, NF- κ B, JAK/STAT and Hedgehog pathways, are involved in the maintenance of stemness [57]. In addition, the tumor microenvironment plays an essential role in supporting and maintaining CSCs [108, 135, 136]. Recently, cytokines were reported to regulate the self-renewal and survival of breast CSCs in the tumor microenvironment [137]. MSCs interact with BCSCs through IL-6 and chemokine (C-X-C motif) ligand 7 cytokine secretion. This signaling is responsible for the self-renewal potential of BCSCs. Subsequently, CXCL7 secreted by MSCs promotes cancer stem cell resistance to anticancer drugs [39]. IL-8 regulates breast cancer stem cell activity by binding to C-X-C motif chemokine receptor 1/2. Targeting CXCR1/2 proteins reduces breast CSC activity and increases their ability to inhibit HER2 [138]. The NF- κ B signaling pathway plays a role in inflammation and tumorigenesis.

The secretion of IL-6 and IL-8 can be regulated by the NF- κ B signaling pathway [139]. 6-Methoxymellein inhibited the localization of NF- κ B p65 and NF- κ B p50 in the nucleus but did not affect the total level of NF- κ B p65 and NF- κ B p50 proteins (Figure 2-6A, B). In addition, the nuclear NF- κ B DNA binding ability was inhibited by 6-methoxymellein (Figure 3-6C).

Subsequently, 6-methoxymellein reduced the mRNA transcription and secretion of IL-6 and IL-8 (Figure 3-7). These data suggest that 6-methoxymellein may be used as an anticancer agent and exerts its effects through the NF- κ B and cytokine signaling pathways.

3.6 CONCLUSION

6-Methoxymellein from carrots identified by mass spectrometry and NMR, acts as a mammosphere formation inhibitor. 6-Methoxymellein inhibits the proliferation, migration, and colony and mammosphere formation of breast cancer cells and decreases the subpopulation of CD44+/CD24- and the expression of c-Myc, Sox-2 and Oct4 proteins. In addition, the compound reduces nuclear NF- κ B p65 and p50 protein expression, subsequently decreasing the transcript expression and secretion of IL-6 and IL-8 by mammospheres. Our data suggest that 6-methoxymellein suppresses the NF- κ B signaling pathway and reduces the expression of c-Myc, Sox-2 and Oct4, may be an inhibitory compound against BCSCs.

CHAPTER IV

5-Desmethylinensetin, a polymethoxylated flavone isolated from *Artemisia princeps*, suppresses the stemness of breast cancer cells via Stat3/IL-6 and Stat3/YAP1 signaling

4.1 ABSTRACT

Breast cancer stem cells are the main causes of recurrence, metastasis, drug resistance, differentiation capacity and self-renewal in breast cancer; therefore, targeting BCSCs will improve the efficacy of breast cancer treatments. In this study, isolation of an inhibitor of *Artemisia princeps* was performed using a silica gel column, a sephadex gel column, and high-performance liquid chromatography. A single compound was purified via activity-based isolation using mammosphere formation assays. The isolated compound was identified as 5-desmethylinensetin using nuclear magnetic resonance and mass spectrometry. 5-Desmethylinensetin suppresses the proliferation and mammosphere formation of breast cancer cells, reduces the subpopulations of CD44⁺/CD24⁻ and ALDH1⁺ cancer cells, and reduces the transcription of the stemness markers Oct4, c-Myc, Nanog and CD44 in BCSCs. 5-desmethylinensetin inhibits the total and nuclear expression of Stat3 and p-Stat3, as well as the translocation of YAP1. Additionally, 5-desmethylinensetin reduces the mRNA and protein levels of IL-6. Our results show that 5-desmethylinensetin exhibits potential anticancer activity against breast cancer stem cells via Stat3-IL-6 and Stat3-YAP1 signaling.

4.2 INTRODUCTION

Breast cancer has surpassed lung cancer as the most commonly diagnosed cancer (11.7%) and the leading cause of cancer death in women [1]. According to the intrinsic molecular portraits provided by transcriptome profiling, breast cancer has several major subcategories, such as receptor tyrosine-protein kinase erbB-2 receptor (HER2), progesterone receptor (PR), estrogen receptor (ER) and triple-negative breast cancer (TNBC). Compared to patients with other subtypes, TNBC patients more frequently experience locoregional recurrence, chemoresistance

and metastasis [140-142]. Recently, TNBCs have been divided into luminal androgen receptor (LAR), basal-like 1 (TNBC-BL1), basal-like 2 (TNBC-BL2), immunomodulatory (TNBC-IM), mesenchymal (TNBC-M), mesenchymal stem-like (TNBC-MSL) and unspecified (TNBC-UNS) subtypes [143, 144]. The standards of therapy for breast cancer are radiation, hormone therapy, surgery and chemotherapeutic drugs, including carboplatin, bevacizumab, cisplatin, epirubicin, cyclophosphamide and docetaxel [57, 145, 146]. The heterogeneity of breast cancer is believed to make it less responsive to chemotherapy. It has been demonstrated that one of the causes of tumor heterogeneity is cancer cells exhibiting stem cell-like properties, which are named cancer stem cells (CSCs) [147]. The discovery of stem cells among cancer cells has had a great impact on cancer biology research and the understanding of cancer stem cell physiology for future anticancer drug development. Breast cancer stem cells (BCSCs) have the ability to self-renew and differentiate within populations of breast cancer cells. BCSCs have been observed to express cellular markers, such as $CD44^+/CD24^-$ and $ALDH^+$, in multiple studies. Moreover, multiple signaling pathways and transcription factors are overactivated in BCSCs compared with those in non-BCSCs, including the Wnt, Notch, Hippo, Hedgehog and signal transducer and activator of transcription (Stat) pathways [146]. The Stat pathway plays a critical role in various cellular functions, such as growth, proliferation and the immune response, via various cytokines and growth factors. In addition, CSCs can be regulated by stromal cells, such as mesenchymal stem cells (MSCs), tumor-associated leukocytes (TILs) and cancer-associated fibroblasts (CAFs), in the tumor microenvironment (TME) via extrinsic signals.

The creation of a supportive TME for targeting CSCs has been successfully employed in brain tumors in mice [148]. Breast cancer stem cell functions can be influenced by different cytokines, chemokines and growth factors secreted by various cell types in the TME, such as interleukin-6

(IL-6) and interleukin-8 (IL-8). IL-6 increases the CSC frequency by increasing the CD44⁺/CD24⁻ subpopulation [149]. IL-6 signaling cascade activation results in the generation of cancer stem cells by promoting epithelial–mesenchymal transition (EMT) in breast cancer cells [150]. IL-6-JAK1-Stat3 signaling blockade in endometrial cancer affects the ALDH^{hi}/CD126⁺ stem-like component and reduces the tumor burden [151]. The IL-8 expression level is upregulated in breast cancer compared with that in normal breast tissue [152]. IL-8 promotes invasion and EMT in breast cancer cells [153, 154]. Thus, inhibition of IL-6 and IL-8 may be necessary to achieve therapeutic effects in tumors.

Artemisia princeps belongs to the Asteraceae family and is used in traditional medicine in Asia, including China, Japan and Korea. *A. princeps* is used for treating circulatory disorders and chronic conditions, such as dymenorrheal disorders, hemorrhoids, cancer, ulcers and digestive disorders [155-158]. Methanol, ethanol or water extracts of *Artemisia princeps* have multiple effects, such as anti-inflammatory [159-161], antioxidant [162-164], antiulcer [165], anticancer [161, 162, 166, 167], chemopreventive [168], antiobesity and antidiabetic effects [169, 170].

In the present study, we isolated a mammosphere inhibitor against BCSCs from *Artemisia princeps* according to activity-based fractionation. The isolated compound was identified as 5-desmethylinensetin, which suppresses mammosphere formation in breast cancer cell lines. This study also investigated whether 5-desmethylinensetin inhibited BCSC formation through the Stat3-IL-6 and Stat3-YAP signaling pathways.

4.3 MATERIALS AND METHODS

4.3.1 Chemical and reagents

Silicon dioxide gel 60 powder, thin layer chromatography silicon dioxide gel 60 F₂₅₄ aluminum sheets and glass plates were purchased from MERK (Darmstadt, Hesse, Germany), and Sephadex LH-20 (LH20100) was purchased from Millipore (Sigma-Aldrich, St. Louis, MO, USA). High-performance liquid chromatography (HPLC) was performed on a Shimadzu application system (Japan). The EZ-Cytox Cell Viability Assay Kit (DoGenBio, Seoul, Korea) was used to determine breast cancer cell viability. The other chemicals and organic solvents used were purchased from Sigma-Aldrich (St. Louis, Missouri, USA).

4.3.2 Plant material

Artemisia princeps was purchased from urban farmers (Seogwipo, Jeju, Korea). The *Artemisia princeps* sample was washed with tap water and freeze-dried, and dried *Artemisia princeps* was ground. A voucher specimen (No. 2018_012) was managed in the Department of Biomaterial, Jeju National University (Jeju-Si, Korea).

4.3.3 Isolation and purification of a mammosphere inhibitor from *Artemisia princeps*

A previously described method was used for the isolation and purification of a mammosphere inhibitor from *Artemisia princeps* [171]. The ground sample of *Artemisia princeps* (1200 g) was extracted using 100% methanol (MeOH 36 L). The purification method is summarized in Figure 4-1A. The powder of *Artemisia princeps* (50 g) was suspended in 1.5 L of

methanol in a 3 L flask (total 24 flasks). The MeOH extracts were concentrated to 6 L and mixed with the same volume of water ($v/v=1:1$), and the methanol in the mixture was evaporated at 50°C. The water-suspended components were extracted with an equal volume of ethyl acetate (EA, $v/v=1:1$). The EA part was collected and concentrated, and the EA-concentrated part was separated on a silicon dioxide gel column (3x 35 cm, 40-63 micron particle size) and eluted with a chloroform-methanol mixture ($\text{CHCl}_3:\text{MeOH}$, 10:1, Figure S4-1). The five fractions were divided based on color and assayed by assessing mammosphere formation. The second fraction potentially inhibited mammosphere formation. The second fraction was purified by a Sephadex LH-20 gel column (2.5x30 cm, 25-100 micron article size) and divided into five parts (Figure S4-2). These five fractions were collected and evaluated by a mammosphere formation assay. Fraction 5 showed an inhibitory effect on mammosphere formation. Fraction 5 was loaded onto a preparatory TLC plate (glass plate; 20x20 cm) and developed in a TLC glass chamber ($\text{CHCl}_3:\text{MeOH}$, 30:1). The major bands were separated on the silicon dioxide gel plate. The fractions were assessed by a mammosphere formation assay (Figure S4-3). The lower fraction was analyzed on an HPLC instrument with an ODS column (10x250-mm, flow rate: 2 ml/min, mobile phase: acetonitrile-water), and the acetonitrile concentration started at 0%; over 10 min, the acetonitrile concentration was increased to 60% and reached 100% from 30 min to 40 min (Figure S4-4). The major peak was collected and assessed using a mammosphere formation assay, and the powder of the major peak was assayed by structure analysis

4.3.4 Structure analysis of the purified compound

The chemical structure of the isolated compound was determined by mass spectrometry and NMR measurements. The molecular weight was determined to be 358 by the ESI-mass measurement, which showed quasimolecular ion peaks at m/z 359.3 $[\text{M}+\text{H}]^+$ and 381.3 $[\text{M}+\text{Na}]^+$

in positive mode (see Supplementary Figure S4-5). The ^1H NMR spectrum measured in CDCl_3 exhibited signals from three aromatic methine protons at δ 7.52 (dd, $J=8.4, 1.8$ Hz), 7.33 (d, $J=1.8$ Hz), and 6.97 (d, $J=8.4$ Hz), which were attributed to 1,2,4-trisubstituted benzene; two aromatic singlet methines at δ 6.59 and 6.55; and four methoxy groups at δ 3.98, 3.97, 3.96, and 3.92. In the ^{13}C NMR spectrum, the 19 carbon peaks included a carbonyl carbon at δ 182.6; seven oxygenated sp^2 quaternary carbons at δ 164.0, 158.7, 153.2, 153.1, 152.2, 149.3, and 132.6; five sp^2 methine carbons at δ 120.1, 111.1, 108.7, 104.5, and 90.6; two sp^2 quaternary carbons at δ 123.8 and 106.1; and four methoxy carbons at δ 60.9, 56.3, 56.1, and 56.1 (see Supplementary Figure S4-6). All of the proton-bearing carbons were assigned by the HMQC spectrum (see Supplementary Figure S4-7). Further structural elucidation was performed with the aid of the HMBC spectrum, which showed long-range correlations of the methine proton at δ 6.59 to the carbons at δ 182.6, 164.0, 123.8, and 106.1; of the methine proton at δ 6.55 to the carbons at δ 158.7, 153.2, 132.6, and 106.1; and of the methine protons at δ 7.52 and 6.97 to the carbons at δ 164.0 and 152.2. Finally, four methoxy protons showed long-range correlations to the oxygenated sp^2 quaternary carbons (see Supplementary Figure S3-8 and S3-9). Therefore, the structure of the isolated compound was identified as 5-desmethylinensetin (Figure 4-2).

4.3.5 Culture of human breast cancer cells and mammospheres

Breast cancer cell lines were obtained from the Korea Cell Line Bank (KCLB, Seoul, Korea) and cultured in complete Dulbecco's modified Eagle's medium (DMEM) with 10% fetal bovine serum and 1% penicillin/streptomycin (Gibco, Thermo Fisher Scientific, CA, USA) in an incubator with 5% CO_2 . Breast cancer cell lines were incubated at 2×10^4 (MDA-MA-231) and 4×10^4 (MCF-7) cells per well in a 6-well plate (ultralow attachment) with MammoCultTM culture

medium (StemCell Technologies, Vancouver, BC, Canada) containing hydrocortisone and heparin in an incubator for 7 days. Mammosphere formation was determined and quantified using the NIST's integrated colony enumerator (NICE) program [69]. Mammosphere formation was measured by determining the mammosphere formation efficiency (MFE %) [70].

4.3.6 Cell proliferation assay

Breast cancer cell lines were seeded at 1×10^6 (MDA-MB-231) and 1.5×10^6 (MCF-7) cells per plate in 96-well plates for 24 hours and treated with 5-desmethylsinensetin (0, 5, 10, 20, 30, 40 and 50 μM) for 1 day. Subsequently, proliferation was assessed using the EZ-Cytox kit (DoGenBio, Seoul, Korea) according to the manufacturer's protocol. A microplate reader (VERSA max microplate reader, Molecular Device, San Jose, CA, USA) was used to measure OD_{450} .

4.3.7 CD44⁺/CD24⁻ expression, aldehyde dehydrogenase (ALDH) activity and apoptosis using a flow cytometric assay

A previously described method was used to determine CD44⁺/CD24⁻ expression, aldehyde dehydrogenase (ALDH) activity and apoptosis [113]. After treatment with 5-desmethylsinensetin for 24 hours, MDA-MB-231 breast cancer cells were harvested and dissociated, and 1×10^6 cells were incubated with anti-human CD44 (FITC-conjugated) and anti-human CD24 (PE-conjugated) antibodies (BD) for 30 min at 4 °C. After washing with PBS, the CD44⁺/CD24⁻ cells were examined using a flow cytometer (Accuri C6, BD, San Jose, CA, USA). The AldefluorTM assay kit (StemCell Technologies, Vancouver, BC, Canada) was used to assay ALDH1 activity. Breast cancer cells were treated with 5-desmethylsinensetin (20 μM) for 24 hours and reacted in ALDH

assay buffer at 37 °C for 20 min. ALDH-positive cells were examined by an Accuri C6 cytometer (BD, San Jose, CA, USA). The FITC Annexin V Apoptosis Detection Kit with PI (640914, BioLegend, San Diego) was used to measure apoptosis of mammospheres treated with 5-desmethylsinensetin (20 μM) in accordance with the manufacturer's protocol. Mammospheres were harvested and dissociated with trypsin (0.05% Trypsin-EDTA 1X, Gibco, Thermo Fisher Scientific, CA, USA); 1×10^6 cells were incubated with Annexin V (FITC) and PI in binding buffer at room temperature with protection from light for 30 min, and the cells were measured using a flow cytometer at the Jeju Center of Korea Basic Science Institute (KBSI, core-facility center).

4.3.8 Real-time quantitative reverse transcription PCR

A previously described method was used for RT-qPCR [73]. Total RNA was extracted and purified from MDA-MB-231 cancer cells or mammospheres. A one-step RT-qPCR kit (Enzynomics, Daejeon, Korea) was used to perform real-time quantitative PCR. All of the specific primers were obtained from Bioneer (Daejeon, Korea). The specific primers are described in Table S1. Statistical analysis of the PCR results was performed. The β-actin gene was used as an internal control.

4.3.9 Western blotting

A previously described method was used for western blotting [73]. Proteins derived from mammospheres of MDA-MB-231 cells treated with 5-desmethylsinensetin (20 μM) were separated by SDS-PAGE (8% or 10%) and transferred to polyvinylidene difluoride membranes

(PVDF, Millipore, Billerica, MA, USA). The PVDF membranes were blocked at room temperature for 60 min in PBST (phosphate buffered saline with Tween 20, 0.1%, v/v) containing Odyssey blocking buffer (927-70001, LI-COR, Lincoln, NB, USA). Subsequently, the membranes were incubated at 4 °C overnight in blocking buffer containing the primary antibodies against: p-Stat3 (#9145s, Cell Signaling Technology, Denver, CO, USA); YAP1 (FNab09559, FineTest, Wuhan, China); Stat3 and sc-482; NF- κ B, p65 and sc-8008; Lamin B, sc-6216, β -actin, and sc-47778 (Santa Cruz Biotechnology, Dallas, TX, USA). The primary antibody solutions were removed, and the membranes were incubated with anti-rabbit (IRDye 800CW-conjugated) and anti-mouse (IRDye 680RD-conjugated) secondary antibodies after washing with PBST. ODYSSEY CLx was used to detect the band signals (LI-COR, Lincoln, NB, USA).

4.3.10 Electrophoretic mobility shift assay (EMSA)

Nuclear fractions were extracted as described previously [74]. Nuclear extracts were preincubated with the wild-type or mutant Stat3 oligonucleotide (LI-COR) for 10 min at room temperature (RT). Subsequently, an electrophoretic mobility shift assay for Stat3 binding was performed using an IRDye 700-labeled special Stat3 oligonucleotide (LI-COR) for 20 min at RT. Samples with loading dye were run on a 6% native PAGE gel, and ODYSSEY CLx (LI-COR) was used to capture the EMSA data.

4.3.11 Quantitative measurement of human IL-6 and IL-8 using the BDTM CBA human inflammatory cytokines assay kit

A previously described method was followed for the quantitative measurement of human IL-6 and IL-6 [113], and cultured media from MDA-MB-231 mammospheres was incubated with 5-desmethylsinensetin (20 μ M) or DMSO for 48 hours. The BDTM Cytometric Bead array (CBA) human inflammatory cytokine assay kit was used to determine the IL6 and IL-8 concentrations in the cultured media. The manufacturer's protocol was followed (BD, San Jose, CA, USA). Fifty microliters of mixed beads with an equal volume of mammosphere culture medium and 50 μ L of PE-labeled antibodies were added to each sample tube. The samples were incubated and protected from light for three hours at RT. The samples were washed and centrifuged, and the pellet was resuspended in washing buffer and analyzed using flow cytometry (BD, Accuri C6, San Jose, CA, USA).

4.3.12 Stat3 and YAP1 knockdown using small interfering RNA (siRNA)

MDA-MB-231 cells were transfected with human YAP-specific siRNAs (Bioneer, Daejeon, Korea) to determine the effect of the YAP1 protein on mammosphere formation, and human Stat3-specific siRNA was transfected to evaluate the effect of Stat3 on the expression of the YAP1 protein. Lipofectamine 3000 (Invitrogen, Carlsbad, CA, USA) was used for siRNA transfection in accordance with the manufacturer's protocol. Western blotting was performed to determine the expression levels of Stat3 and YAP1 after specific siRNA transfection.

4.3.13 Statistical analysis

All experimental data are reported as the mean \pm standard deviation (SD). Nonparametric Student's t-test was used to perform statistical analysis. A *p*-value $<$ 0.05 was considered statistically significant (GraphPad Prism 5 Software).

4.4 RESULTS

4.4.1 Isolation of breast cancer stem cells (BCSCs) inhibitor from *Artemisia princeps*.

BCSC Inhibitor from *Artemisia princeps* was screened and isolated using formation assay of mammosphere derived from MDA-MB-231 cell. The dried methanol extracts of *Artemisia princeps* was purified via an ethyl acetate (EA) and water extraction ($v/v=1:1$), subsequently the EA-extracts was purified using silicon dioxide gel chromatography, a Sephadex gel chromatography, preparatory thin layer chromatography (prep-TLC), and high performance liquid chromatography (HPLC) (Figure 4-1A and Figure S4-1~S4-4). The purified compound suppresses the mammospheres formation of MDA-MB-231 (Figure 3-1B). HPLC analysis showed the purified compound. (Figure 4-1C). The purified compound was identified as 5-desmethylinensetin using NMR and ESI-Mass (Figure 4-2 and Figure S4-5~S4-8).

4.4.2 5-Desmethylinensetin inhibits mammosphere formation of breast cancer cells

The antiproliferative effect of 5-desmethylinensetin was examined by treating MDA-MB-231 and MCF-7 cells with increasing concentrations of 5-desmethylinensetin. No inhibition of cell proliferation was observed at concentrations of 5-desmethylinensetin below 50 μ M after 24 hours (Figure 4-3A and B). To examine the inhibitory effect of 5-desmethylinensetin on mammosphere formation, 5-desmethylinensetin was added to primary mammospheres derived from MDA-MB-231 and MCF-7 cells, and mammospheres were captured and scanned after 7 days of treatment. As shown in Figure 3-3A and B, 5-desmethylinensetin reduced the sphere number and size of mammospheres derived from MDA-MB-231 and MCF-7 cells. Our data

show that 5-desmethylsinensetin suppresses breast cancer mammosphere formation and does not inhibit breast cancer proliferation at concentrations below 50 μM .

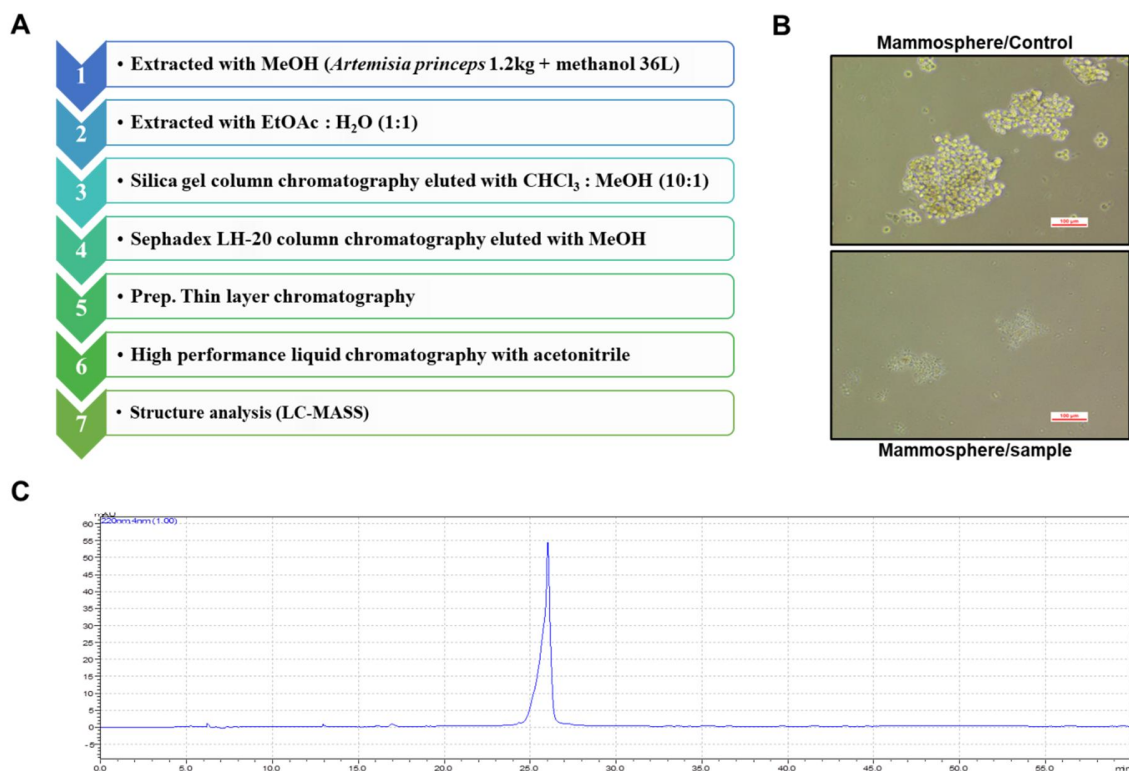


Figure 4-1. Isolation of a breast cancer stem cell (BCSC) inhibitor from *Artemisia princeps* using a mammosphere formation assay. (A) The procedure for the purification of the mammosphere-formation inhibitor from *Artemisia princeps*. (B) Inhibitory effect of extracts from *Artemisia princeps* on mammosphere formation. Mammospheres of MDA-MB-231 cells were incubated with or without *Artemisia princeps* extracts. Images of mammospheres were captured by microscopy at 10× magnification (scale bar = 100 µm). (C) HPLC chromatogram analysis of purified samples of *Artemisia princeps* extracts.

4.4.3 5-Desmethylsinensetin decreases CD44⁺/CD24⁻-expressing and ALDH-expressing cancer cells

The representative markers of BCSCs are CD44⁺/CD24⁻ and ALDH⁺. The CD44⁺/CD24⁻ subpopulation of MDA-MB-231 breast cancer cells was detected after 5-desmethylsinensetin (20 μM) treatment. 5-Desmethylsinensetin decreased the CD44⁺/CD24⁻ subpopulation of MDA-MB-231 cells from 94.1% to 81.0% (Figure 4-4A). MDA-MB-231 cells were treated with or without 5-desmethylsinensetin (20 μM) for 24 hours, and subsequently, the ALDH⁺ subpopulation of MDA-MB-231 cells was investigated using the ALDEFLUOR assay kit. As shown in Figure 4-4B, 5-desmethylsinensetin decreased the ALDH⁺ subpopulation of MDA-MB-231 cells from 17.5% to 8.8%. Our data suggest that 5-desmethylsinensetin reduces the subpopulations of CD44⁺/CD24⁻ and ALDH⁺ MDA-MB-231 cells.

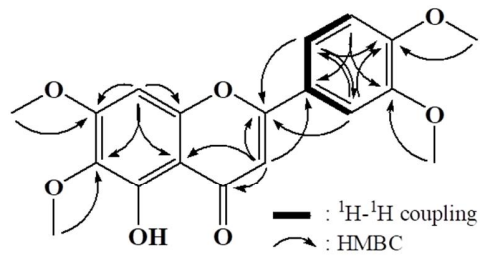
4.4.4 5-Desmethylsinensetin induces apoptosis and inhibits the mRNA levels of cancer stem cell specific marker genes and mammosphere growth

To investigate whether 5-desmethylsinensetin induced BCSC apoptosis, 5-day cultured primary mammospheres derived from MDA-MB-231 cells were treated with or without 5-desmethylsinensetin (20 μM). As shown in Figure 4-5A, 5-desmethylsinensetin induced BCSC apoptosis. Mammospheres derived from MDA-MB-231 cells cultured with or without 5-desmethylsinensetin (20 μM) were divided into single cells and seeded into six-well plates, and the number of cells was counted for 3 days. As shown in Figure 4-5B, 5-desmethylsinensetin inhibited mammosphere growth. The transcription levels of Oct4, c-Myc, Nanog and CD44 were determined using RT-qPCR after 5-desmethylsinensetin (20 μM) treatment. As shown in Figure 5C, 5-desmethylsinensetin decreased the transcription levels of Oct4, c-Myc, Nanog and CD44

in BCSCs. Our data suggest that 5-desmethylsinensetin induces apoptosis and inhibits the growth of BCSCs; moreover, the compound decreases the transcription levels of biomarkers in BCSCs, including Oct4, c-Myc, Nanog and CD44.

4.4.5 5-Desmethylsinensetin decreases the total and nuclear levels of p-Stat3 and Stat3 in BCSCs

The biochemical mechanism of 5-desmethylsinensetin in mammosphere inhibition was investigated by performing western blotting of inflammatory proteins, and we determined the total and nuclear protein levels of p-Stat3, Stat3 and NF- κ B p65. Our data showed that the total and nuclear levels of p-Stat3 and Stat3 were significantly reduced after 5-desmethylsinensetin (20 μ M) treatment (Figure 4-6A and B). In addition, we detected the DNA-binding ability of Stat3 using specific binding probes by an electrophoretic mobility shift assay in the presence of 5-desmethylsinensetin (20 μ M) (Figure 4-6C). Nuclear extracts of mammospheres in the presence of 5-desmethylsinensetin (20 μ M) or DMSO were incubated with an IRDye-labeled Stat3-specific probe (Figure 4-6C lanes 2 and 3), and incubation with wild-type or mutant Stat3-binding oligonucleotides acted as the positive (Figure 4-6C lane 4) and negative controls (Figure 4-6C lane 5), respectively. The IRDye-labeled Stat3 probe alone acted as the blank (Figure 4-6C lane 1). Our data showed that the ability of the IRDye-labeled probe to bind Stat3 proteins in nuclear extracts (indicated by the arrow) was significantly decreased after 5-desmethylsinensetin treatment (Figure 4-6C, line 3).



5-Hydroxy-3', 4', 6, 7-tetramethoxyflavone (5-desmethylinensetin; C₁₉H₁₈O₇; 358)

Figure 4-2. Molecular structure of the CSC inhibitor isolated from *Artemisia princeps*.

Molecular structure of 5-desmethylinensetin.

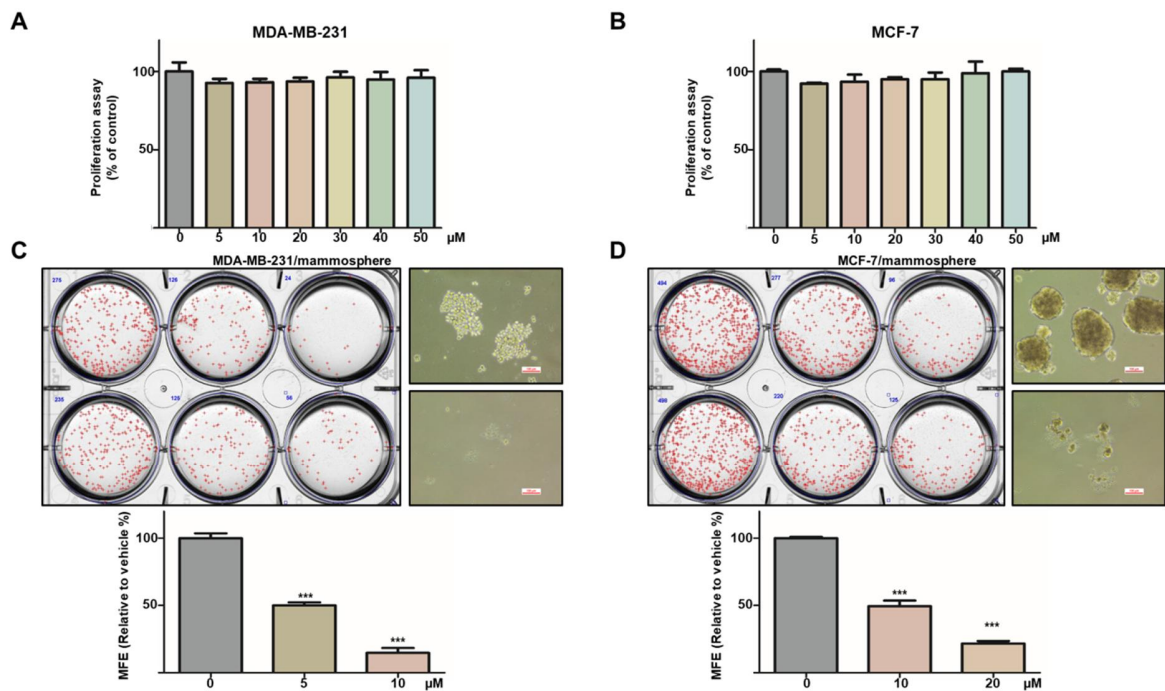


Figure 4-3. Effects of 5-desmethylsinensetin on cell proliferation and mammosphere formation. The antiproliferative ability of 5-desmethylsinensetin was measured with an EZ-Cytox kit using MDA-MB-231 (**A**) and MCF-7 (**B**) cells treated with various concentrations of 5-desmethylsinensetin. (**C** and **D**) To determine the inhibitory effect of 5-desmethylsinensetin on mammosphere formation, MDA-MB-231 (**C**) and MCF-7 (**D**) cells were cultured in ultralow attachment six-well plates with CSC culture media with increasing concentrations of 5-desmethylsinensetin or DMSO. After seven days, mammospheres were captured and calculated. Representative mammosphere images were captured by microscopy at 10 \times magnification (scale bar =100 μ m). Representative data were collected. Data from triplicate experiments are presented as the mean \pm SD; * p < 0.05.

4.4.6 5-Desmethylsinensetin reduces the secretion and mRNA levels of IL-6 and IL-8 in mammospheres

The IL-6/Stat3 and IL-8/Stat3 positive feedback loops promote cancer epithelial-to-mesenchymal transition (EMT), invasion, metastasis, self-renewal and stemness processes [172-174]. To determine whether 5-desmethylsinensetin reduced the secretion of IL-6 and IL-8, the concentrations of IL-6 and IL-8 in mammosphere culture medium were analyzed using a human inflammatory cytokine assay. 5-Desmethylsinensetin decreased the concentrations of IL-6 and IL-8 in the culture medium (Figure 4-7A). Subsequently, the transcription levels of IL-6 and IL-8 were determined after 5-desmethylsinensetin (20 μ M) treatment, and our data showed that 5-desmethylsinensetin reduced transcription of IL-6 and IL-8 (Figure 4-7B).

4.4.7 5-Desmethylsinensetin inhibits the nuclear localization of YAP1

The correlation of expression and coactivation between Stat3 and YAP1 has been reported [175-178]. To determine whether 5-desmethylsinensetin reduced the expression of YAP1, the total and nuclear expression levels of YAP1 in mammospheres were examined. As shown in Figure 4-8A, 5-desmethylsinensetin inhibited the nuclear localization of YAP1. Subsequently, the expression level of the YAP1 protein was decreased after Stat3 knockdown in MDA-MB-231 cells (Figure 4-8B). Additionally, YAP1 knockdown inhibited mammosphere formation and decreased transcription of Sox2 and Oct4 (Figure 4-8C and D). Our data suggest that 5-desmethylsinensetin probably inhibits YAP1 nuclear localization via Stat3 inhibition. A schematic of the inhibition of breast CSC formation through the Stat3-IL6 and Stat3-YAP1 signaling pathways induced by 5-desmethylsinensetin is shown (Figure 4-9).

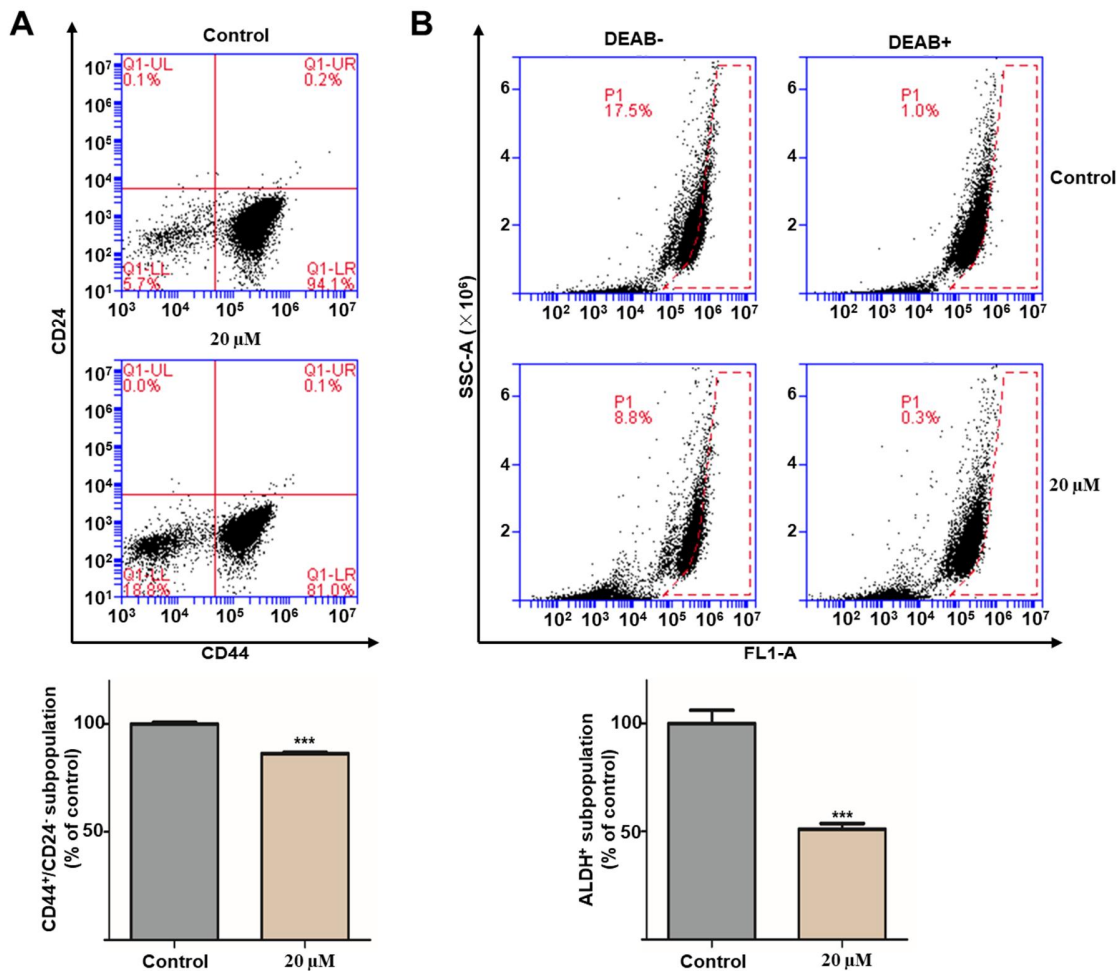


Figure 4-4. 5-Desmethylsinensetin reduces the subpopulations of CD44⁺/CD24⁻ and ALDH1⁺ MDA-MB-231 breast cancer cells. **(A)** MDA-MB-231 cells were treated with 5-desmethylsinensetin (20 μM) or DMSO for 24 hours. The CD44⁺/CD24⁻ cell population of MDA-MB-231 cells was analyzed by flow cytometry. Gating was based on the binding of a control antibody (Red Cross). **(B)** Aldehyde dehydrogenase-positive (ALDH⁺) MDA-MB-231 cells were measured using an ALDEFLUOR assay with or without 5-desmethylsinensetin (20 μM) and the ALDH inhibitor N,N-diethylaminobenzaldehyde (DEAB). Representative data were collected. Data from triplicate experiments are presented as the mean ± SD; **p* < 0.5.

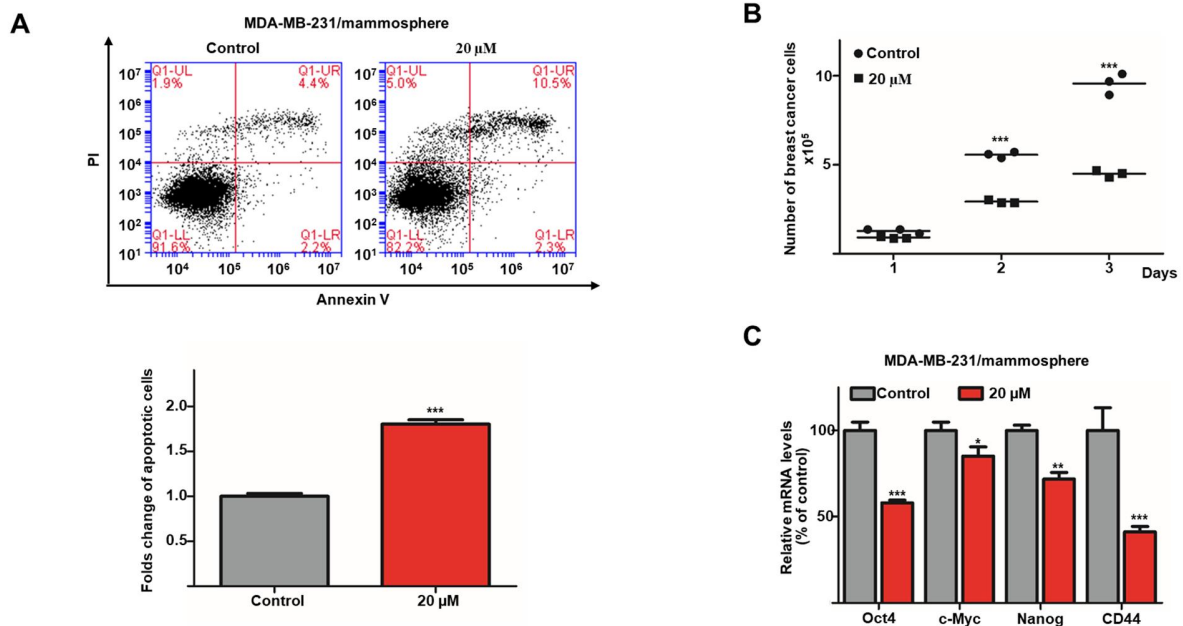


Figure 4-5. 5-Desmethylsinensetin induces apoptosis of mammospheres and suppresses the expression of CSC marker genes and mammosphere growth. (A) MDA-MB-231 mammospheres were cultured for five days and treated with or without 5-desmethylsinensetin (20 μ M) for two days. Mammospheres were divided into single cells, and apoptotic cells were subsequently measured by FACS using an apoptosis assay kit. (B) 5-Desmethylsinensetin inhibited mammosphere growth. Mammospheres with/without 5-desmethylsinensetin (20 μ M) were divided into single cells, and an equal number of cells were plated in 6-well plates. One, 2 and 3 days later, the cells were counted. (C) RT-qPCR analysis of Oct4, c-Myc, Nanog and CD44 in mammospheres after treatment with 5-desmethylsinensetin (20 μ M) for 2 days. Representative data were collected. Data from triplicate experiments are presented as the mean \pm SD; * p < 0.05; ** p < 0.01; *** p < 0.001.

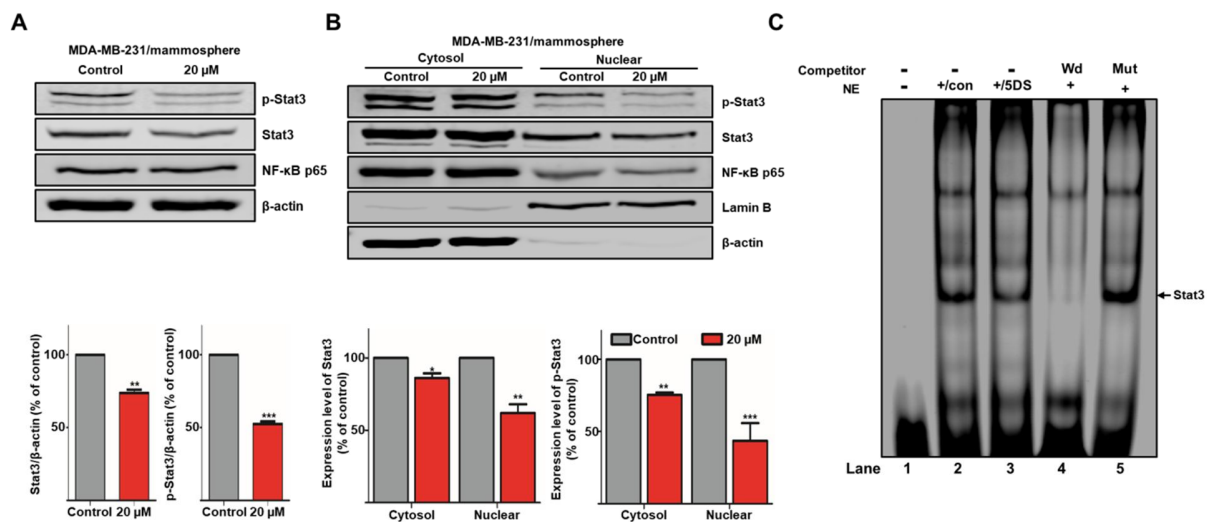


Figure 4-6. Effect of 5-desmethylsinensetin on the Stat3 signaling pathway. **(A)** The levels of p-Stat3, Stat3 and NF-κB p65 in total proteins were measured in MDA-MB-231-derived mammospheres after treatment with 5-desmethylsinensetin (20 μM) for 48 hours using western blot analysis. **(B)** The nuclear protein levels of p-Stat3, Stat3 and NF-κB p65 were determined in MDA-MB-231-derived mammospheres treated with 5-desmethylsinensetin (20 μM) or DMSO, and 5-desmethylsinensetin decreased the levels of p-Stat3 and Stat3, but not NF-κB p65, in mammospheres. **(C)** Electrophoresis mobility shift assays (EMSAs) of nuclear proteins in mammospheres derived from MDA-MB-231 cells after treatment with 5-desmethylsinensetin (20 μM). The nuclear extracts were incubated with the Stat3 probe and separated via 6% native PAGE. Lane 1: Stat3 probe only; lane 2: untreated nuclear extracts with the Stat3 probe; lane 3: 5-desmethylsinensetin (20 μM)-treated nuclear proteins with the Stat3 probe; lane 4: untreated nuclear proteins incubated with the self-competitor (200x) oligo; lane 5: untreated nuclear extracts incubated with the mutated-Stat3 (200x) probe. The arrow indicates the DNA/Stat3 complex in the mammosphere nuclear lysates. Representative data were collected. Data from triplicate experiments are presented as the mean ± SD; **p* < 0.05; ***p* < 0.01; ****p* < 0.001.

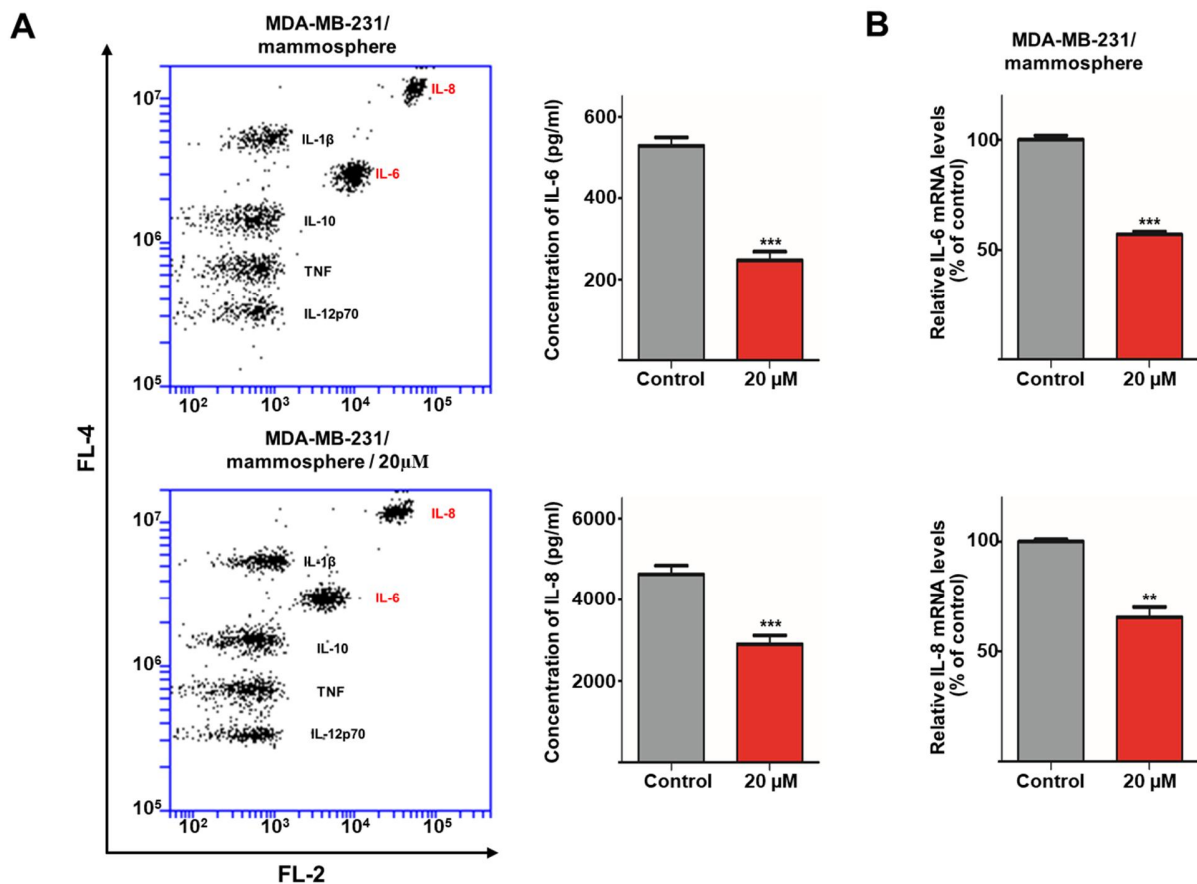


Figure 4-7. 5-Desmethylsinensetin regulates the secretion and transcription levels of IL-6 and IL-8. **(A)** A cytometric bead array (CBA) human inflammatory cytokine assay kit was used to analyze the secretion of cytokines in mammosphere culture media treated with or without 5-desmethylsinensetin (20 μ M). **(B)** The transcriptional levels of IL-6 and IL-8 were determined in 5-desmethylsinensetin (20 μ M)-treated mammospheres using specific primers (SupplementaryTable S1). Representative data were collected. Data from triplicate experiments are represented as the mean \pm SD; ** p < 0.01; *** p < 0.001.

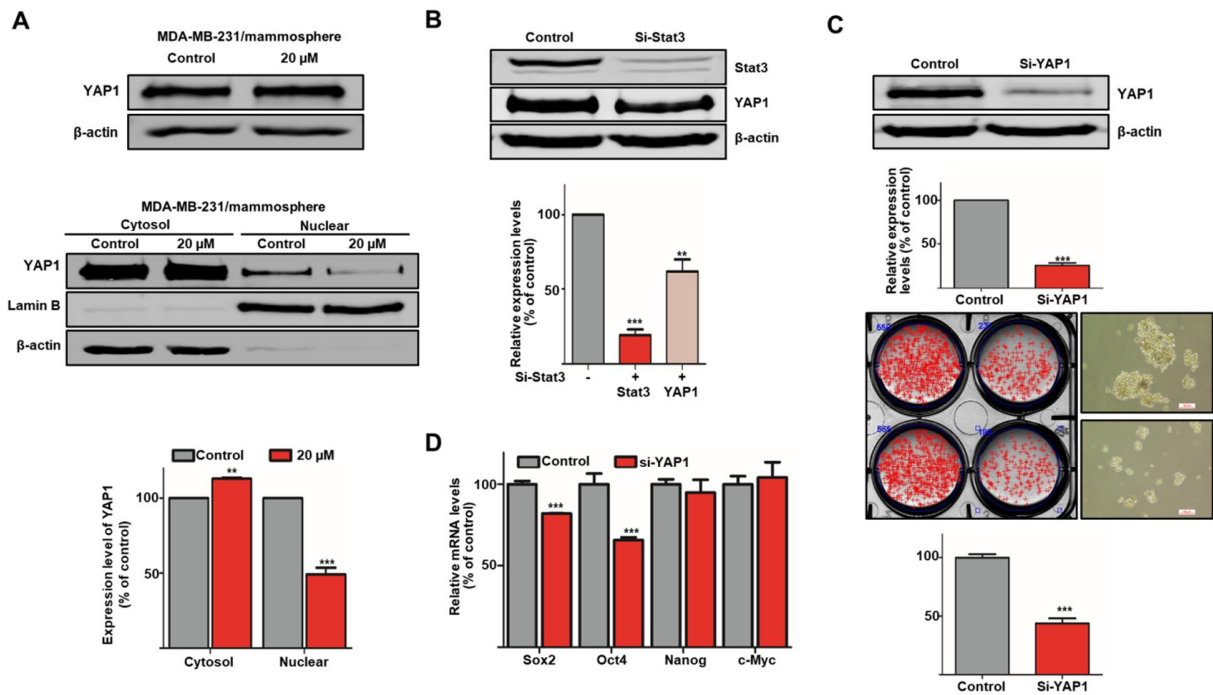


Figure 4-8. 5-Desmethylsinensetin inhibits the YAP1 pathway via Stat3. **(A)** The levels of YAP1 in the total and nuclear proteins were measured in mammospheres after treatment with 5-desmethylsinensetin (20 μ M) for 48 hours. 5-Desmethylsinensetin blocked the nuclear translocation of YAP1. **(B)** The expression levels of Stat3 and YAP1 in MDA-MB-231 cells treated with a specific siRNA against Stat3. Knockdown of Stat3 decreased the expression of YAP1. **(C)** The expression of YAP1 in and mammosphere formation of MDA-MB-231 cells treated with a specific siRNA against YAP1 were evaluated. **(D)** RT-qPCR analysis of cancer stem cell markers in MDA-MB-231 cells treated with a specific siRNA against YAP1. Representative data were collected. Data from triplicate experiments are presented as the mean \pm SD; * p < 0.05; ** p < 0.01; *** p < 0.001.

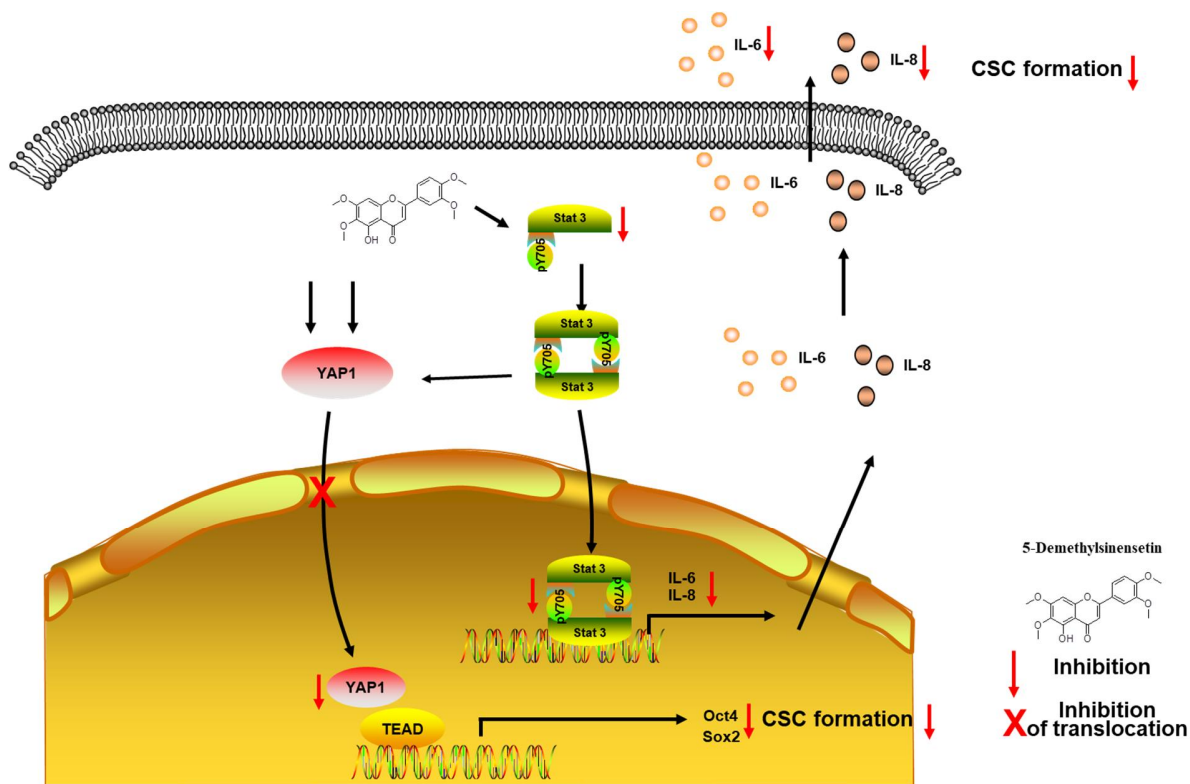


Figure 4-9. Proposed model of breast CSC formation mediated through the Stat3-IL6 and Stat3-YAP1 signaling pathways induced by 5-desmethylsinensetin.

4.5 DISCUSSION

Artemisia princeps is a species of *Artemisia*. *Artemisia* comprises more than 4 hundred important medicinal plants, and most of them have a bitter taste. Increasing attention is being given to phytochemical substances from *Artemisia* due to their biological and chemical diversity, which are caused by active ingredients and secondary metabolites [179]. *Artemisia princeps* has been found to be rich in phenolic acids, flavonoids, terpenes and other compounds. For instance, isochromanone derivatives isolated from *Artemisia princeps* cultured with endophytic fungi inhibit nitric oxide production in lipopolysaccharide (LPS)-stimulated RAW264.7 cells [180].

6-Acetyl-2,2-dimethyl chroman-4-one suppresses the adipogenic differentiation of hBM-MSCs via AMPK activation [181]. Isosecotanaphthalide inhibits TARC and IL-33 production and the activation of ICAM-1-Stat1 induced by TNF- α /IFN- γ in HaCaT cells [181]. Jaceosidin (4',5,7-trihydroxy-3',6-dimethoxyflavone), a flavone found in *Artemisia princeps*, induces G2/M cell cycle arrest by inactivating cdc25c-cdc2 via ATM-Chk1/2 activation in endometrial cancer cells [182] and contributes to the chemopreventive effect on human breast epithelial cells stimulated with 12-O-tetradecanoylphorbol-13-acetate (TPA) by targeting the ERK pathway, which is involved in the regulation of COX-2 and MMP-9 [183].

Eupatilin (5,7-dihydroxy-3',4',6-trimethoxyflavone), a pharmacologically active flavone derived from *Artemisia* plants, inhibits the Raf1/ERK/Cyclin D1 pathway and activates p53-p27^{Kip}/p21^{waf1/Cip1}, which contribute to cell cycle arrest in *ras*-transformed human mammary epithelial cells [184]. Eupatilin also decreases LPS-induced gene expression of iNOS, TNF- α , IL-1 β and COX-2 and attenuates the NF- κ B signaling pathway and downstream inflammatory mediators [185]. Additionally, eupatilin modulates reactive oxygen species (ROS) generation,

cell cyclin arrest, and calcium influx and inhibits the phosphoinositide 3-kinase (PI3K) and mitogen activated protein kinase (MAPK) pathways, which promote cell death in ovarian cancer [186].

Because of the multiple benefits of the many pharmacological compounds from *Artemisia princeps*, we isolated a breast cancer stem cell inhibitor from *Artemisia princeps* via activity-guided fractionation (Figure 4-1). The purified compound was identified as 5-desmethylinensetin (5-hydroxy-3',4',6,7-tetramethoxy flavone) by NMR spectroscopy and ESI-mass measurements (Figure 4-2 and Figure S4-5~S4-9). The antiproliferative ability of 5-desmethylinensetin was demonstrated using MDA-MB-231 and MCF-7 cells. As shown in Figure 4-3A and 4-3B, there was no effect of 5-desmethylinensetin on cell proliferation at a concentration of 50 μ M (at concentrations of 5-desmethylinensetin greater than 50 μ M, the compound precipitated in the medium). However, 5-desmethylinensetin decreased the frequency and size of mammospheres derived from MDA-MB-231 and MCF-7 cells at concentrations of 10 μ M and 20 μ M, respectively (Figure 4-3C and 4-3D). It was confirmed that CD44⁺/CD24⁻ and ALDH1⁺ MDAMB-231 cells exhibited high tumorigenic and metastatic ability compared with CD44⁻/CD24⁺ and ALDH1⁻ cancer cells [187]. The expression of CD44⁺CD24⁻ and ALDH1⁺ is associated with stem-like activity in breast cancer [188]. 5-desmethylinensetin reduced the subpopulations of CD44⁺/CD24⁻ and ALDH1⁺MDA-MB-231 cells (Figure 4-4). Apoptosis and growth of breast cancer stem cells after treatment with 5-desmethylinensetin (20 μ M) were determined. As shown in Figure 4-5A and 4-5B, 5-desmethylinensetin induced apoptosis and decreased the growth of breast cancer stem cells. Subsequently, the transcription levels of Oct4, c-Myc, Nanog and CD44 in breast cancer stem cells were decreased after 5-desmethylinensetin (20 μ M) treatment.

It has been reported that eupatilin decreases the expression of Smoothed (SMO) and GLI1 in cervical cancer cells. Hedgehog signaling is important for tissue regeneration and embryonic development, including proliferation, apoptosis, migration, invasion and stemness [189]. Compared with eupatilin (5,7-dihydroxy-3',4',6-trimethoxyflavone), the C7 position of 5-desmethylinensetin (5-hydroxy-3',4',6,7-tetramethoxyflavone) is a methoxyl group, suggesting that these two compounds may have a similar structure and function. For this reason, the expression of SMO was determined after 5-desmethylinensetin treatment; however, 5-desmethylinensetin did not affect SMO (data not shown). Transcription factors are the main components of the signaling cascades involved in tumorigenesis and are anticancer targets. Activation of Stat3 is required for the growth of CD44⁺/CD24⁻ stem cell-like breast cancer cells in human tumors [81]. The expression of Stat3 and p-Stat3 in the total and nuclear extracts was decreased by 5-desmethylinensetin (Figure 4-6A and 4-6B), but not the expression of NF-κB p65, which is a cofactor of Stat3 [190]. As a transcription factor, the DNA-binding ability of nuclear Stat3 was determined using EMSA, and our data showed that 5-desmethylinensetin inhibited the ability of nuclear Stat3 to bind to particular oligonucleotides (Figure 4-6C). Additionally, the IL-6R-Stat3-miR-34a feedback loop promotes colorectal cancer EMT, invasion and metastasis [172]. IL-6 enhances mitochondrial superoxide production at a level suitable to maintain stem cell-like activity in breast cancer cells [173]. IL-8 knockdown results in the inhibition of migration and invasion and downregulation of p-Stat3. Stat3 knockdown reduces PIM2 expression, which is a regulator of IL-8, and these data suggest that IL-8/Stat3 may be a positive feedback loop in breast cancer cells [191]. In the present study, the mRNA transcription and secretion of IL-6 and IL-8 were inhibited by 5-desmethylinensetin (Figure 4-7A and 4-7B).

Recently, yes-associated protein 1 (YAP1), which is a transcription coactivator involved in the Hippo pathway, has been reported to interact with Stat3 to regulate several intracellular events, such as proliferation, migration and tube formation. YAP overexpression-induced migration and tube formation are reversed by a Stat3 inhibitor (S3I-201) in human retinal microvascular endothelial cells (HRMECs) [175]. 5-desmethylinensetin blocked the nuclear translocation of YAP1 (Figure 4-8A), and the YAP1 expression level was decreased after Stat3 knockdown in MDA-MB-231 cells (Figure 4-8B). YAP1 knockdown inhibited mammosphere formation and the mRNA transcription levels of stemness markers, such as Sox2 and Oct4. Taken together, our results suggest that 5-desmethylinensetin inhibits breast cancer stem cells via the Stat3-IL-6/IL-8 and Stat3-YAP1 pathways.

4.6 CONCLUSION

5-Desmethylinensetin, isolated from *Artemisia princeps* and identified by mass spectrometry and NMR, acts as an inhibitor of mammosphere formation. 5-Desmethylinensetin inhibits mammosphere formation of MDA-MB-231 and MCF-7 breast cancer cells, decreases the subpopulations of ALDH1⁺ and CD44⁺/CD24⁻ MDA-MB-231 cells, induces apoptosis, inhibits the proliferation of MDA-MB-231 mammospheres, and decreases the mRNA levels of Oct4, c-Myc, Nanog and CD44. Additionally, 5-desmethylinensetin decreases the total, cytosolic and nuclear levels of Stat3 and p-Stat3, but not the levels of NF- κ B p65, and then inhibits the DNA binding ability of Stat3, subsequently decreasing the transcription IL-6 and IL-8 in mammospheres as well as their secretion. In addition, 5-desmethylinensetin inhibits the nuclear translocation of YAP1. Knockdown of Stat3 decreases the protein level of YAP1, and subsequent knockdown of YAP1 inhibits mammosphere formation of MDA-MB-231 cells and

the mRNA levels of Sox2 and Oct4. Our results suggest that 5-desmethylsinensetin may be an anticancer agent against breast cancer stem cells.

REFERENCES

- [1]. H. Sung, J. Ferlay, R.L. Siegel, M. Laversanne, I. Soerjomataram, A. Jemal, et al. Global cancer statistics 2020: GLOBOCAN estimates of incidence and mortality worldwide for 36 cancers in 185 countries. *CA Cancer J Clin.* (2021).
- [2]. W. Guo. Concise review: breast cancer stem cells: regulatory networks, stem cell niches, and disease relevance. *Stem Cells Transl Med.* 3 (2014):942-948.
- [3]. J.P. Thiery, H. Acloque, R.Y. Huang, M.A. Nieto. Epithelial-mesenchymal transitions in development and disease. *Cell.* 139 (2009):871-890.
- [4]. J.H. Tsai, J. Yang. Epithelial-mesenchymal plasticity in carcinoma metastasis. *Genes Dev.* 27 (2013):2192-2206.
- [5]. S.A. Mani, W. Guo, M.J. Liao, E.N. Eaton, A. Ayyanan, A.Y. Zhou, et al. The epithelial-mesenchymal transition generates cells with properties of stem cells. *Cell.* 133 (2008):704-715.
- [6]. A.P. Morel, M. Lievre, C. Thomas, G. Hinkal, S. Ansieau, A. Puisieux. Generation of breast cancer stem cells through epithelial-mesenchymal transition. *PLoS One.* 3 (2008):e2888.
- [7]. W. Guo, Z. Keckesova, J.L. Donaher, T. Shibue, V. Tischler, F. Reinhardt, et al. Slug and Sox9 cooperatively determine the mammary stem cell state. *Cell.* 148 (2012):1015-1028.

- [8]. S. Lamouille, D. Subramanyam, R. Blelloch, R. Derynck. Regulation of epithelial-mesenchymal and mesenchymal-epithelial transitions by microRNAs. *Curr Opin Cell Biol.* 25 (2013):200-207.
- [9]. S. Brabletz, T. Brabletz. The ZEB/miR-200 feedback loop--a motor of cellular plasticity in development and cancer? *EMBO Rep.* 11 (2010):670-677.
- [10]. H. Siemens, R. Jackstadt, S. Hunten, M. Kaller, A. Menssen, U. Gotz, et al. miR-34 and SNAIL form a double-negative feedback loop to regulate epithelial-mesenchymal transitions. *Cell Cycle.* 10 (2011):4256-4271.
- [11]. N.H. Kim, H.S. Kim, X.Y. Li, I. Lee, H.S. Choi, S.E. Kang, et al. A p53/miRNA-34 axis regulates Snail1-dependent cancer cell epithelial-mesenchymal transition. *J Cell Biol.* 195 (2011):417-433.
- [12]. A. Sarkar, K. Hochedlinger. The sox family of transcription factors: versatile regulators of stem and progenitor cell fate. *Cell Stem Cell.* 12 (2013):15-30.
- [13]. C. Scheel, E.N. Eaton, S.H. Li, C.L. Chaffer, F. Reinhardt, K.J. Kah, et al. Paracrine and autocrine signals induce and maintain mesenchymal and stem cell states in the breast. *Cell.* 145 (2011):926-940.

- [14]. A. Bruna, W. Greenwood, J. Le Quesne, A. Teschendorff, D. Miranda-Saavedra, O.M. Rueda, et al. TGFbeta induces the formation of tumour-initiating cells in claudinlow breast cancer. *Nat Commun.* 3 (2012):1055.
- [15]. C.M. Alexander, S. Goel, S.A. Fakhraldeen, S. Kim. Wnt signaling in mammary glands: plastic cell fates and combinatorial signaling. *Cold Spring Harb Perspect Biol.* 4 (2012).
- [16]. H. Clevers, R. Nusse. Wnt/beta-catenin signaling and disease. *Cell.* 149 (2012):1192-1205.
- [17]. R. van Amerongen, A.N. Bowman, R. Nusse. Developmental stage and time dictate the fate of Wnt/beta-catenin-responsive stem cells in the mammary gland. *Cell Stem Cell.* 11 (2012):387-400.
- [18]. K. Kessenbrock, G.J. Dijkgraaf, D.A. Lawson, L.E. Littlepage, P. Shahi, U. Pieper, et al. A role for matrix metalloproteinases in regulating mammary stem cell function via the Wnt signaling pathway. *Cell Stem Cell.* 13 (2013):300-313.
- [19]. M. Shackleton, F. Vaillant, K.J. Simpson, J. Stingl, G.K. Smyth, M.L. Asselin-Labat, et al. Generation of a functional mammary gland from a single stem cell. *Nature.* 439 (2006):84-88.
- [20]. Y.A. Zeng, R. Nusse. Wnt proteins are self-renewal factors for mammary stem cells and promote their long-term expansion in culture. *Cell Stem Cell.* 6 (2010):568-577.

- [21]. K.D. Buono, G.W. Robinson, C. Martin, S. Shi, P. Stanley, K. Tanigaki, et al. The canonical Notch/RBP-J signaling pathway controls the balance of cell lineages in mammary epithelium during pregnancy. *Dev Biol.* 293 (2006):565-580.
- [22]. T. Bouras, B. Pal, F. Vaillant, G. Harburg, M.L. Asselin-Labat, S.R. Oakes, et al. Notch signaling regulates mammary stem cell function and luminal cell-fate commitment. *Cell Stem Cell.* 3 (2008):429-441.
- [23]. E. Lim, F. Vaillant, D. Wu, N.C. Forrest, B. Pal, A.H. Hart, et al. Aberrant luminal progenitors as the candidate target population for basal tumor development in BRCA1 mutation carriers. *Nat Med.* 15 (2009):907-913.
- [24]. G. Molyneux, F.C. Geyer, F.A. Magnay, A. McCarthy, H. Kendrick, R. Natrajan, et al. BRCA1 basal-like breast cancers originate from luminal epithelial progenitors and not from basal stem cells. *Cell Stem Cell.* 7 (2010):403-417.
- [25]. H. Harrison, G. Farnie, K.R. Brennan, R.B. Clarke. Breast cancer stem cells: something out of notching? *Cancer Res.* 70 (2010):8973-8976.
- [26]. F. Balkwill, A. Mantovani. Inflammation and cancer: back to Virchow? *Lancet.* 357 (2001):539-545.

- [27]. B.L. Pierce, R. Ballard-Barbash, L. Bernstein, R.N. Baumgartner, M.L. Neuhaus, M.H. Wener, et al. Elevated biomarkers of inflammation are associated with reduced survival among breast cancer patients. *J Clin Oncol.* 27 (2009):3437-3444.
- [28]. L.M. Coussens, Z. Werb. Inflammation and cancer. *Nature.* 420 (2002):860-867.
- [29]. D.S. Michaud, S.E. Daugherty, S.I. Berndt, E.A. Platz, M. Yeager, E.D. Crawford, et al. Genetic polymorphisms of interleukin-1B (IL-1B), IL-6, IL-8, and IL-10 and risk of prostate cancer. *Cancer Res.* 66 (2006):4525-4530.
- [30]. P. Sansone, G. Storci, S. Tavori, T. Guarnieri, C. Giovannini, M. Taffurelli, et al. IL-6 triggers malignant features in mammospheres from human ductal breast carcinoma and normal mammary gland. *J Clin Invest.* 117 (2007):3988-4002.
- [31]. C. Ginestier, S. Liu, M.E. Diebel, H. Korkaya, M. Luo, M. Brown, et al. CXCR1 blockade selectively targets human breast cancer stem cells in vitro and in xenografts. *J Clin Invest.* 120 (2010):485-497.
- [32]. D.J. Waugh, C. Wilson. The interleukin-8 pathway in cancer. *Clin Cancer Res.* 14 (2008):6735-6741.
- [33]. I.H. Benoy, R. Salgado, P. Van Dam, K. Geboers, E. Van Marck, S. Scharpe, et al. Increased serum interleukin-8 in patients with early and metastatic breast cancer correlates with early dissemination and survival. *Clin Cancer Res.* 10 (2004):7157-7162.

- [34]. C. Yao, Y. Lin, M.S. Chua, C.S. Ye, J. Bi, W. Li, et al. Interleukin-8 modulates growth and invasiveness of estrogen receptor-negative breast cancer cells. *Int J Cancer*. 121 (2007):1949-1957.
- [35]. T. Ara, Y.A. Declerck. Interleukin-6 in bone metastasis and cancer progression. *Eur J Cancer*. 46 (2010):1223-1231.
- [36]. D. Conze, L. Weiss, P.S. Regen, A. Bhushan, D. Weaver, P. Johnson, et al. Autocrine production of interleukin 6 causes multidrug resistance in breast cancer cells. *Cancer Res*. 61 (2001):8851-8858.
- [37]. S.P. Gao, K.G. Mark, K. Leslie, W. Pao, N. Motoi, W.L. Gerald, et al. Mutations in the EGFR kinase domain mediate STAT3 activation via IL-6 production in human lung adenocarcinomas. *J Clin Invest*. 117 (2007):3846-3856.
- [38]. D. Iliopoulos, H.A. Hirsch, K. Struhl. An epigenetic switch involving NF-kappaB, Lin28, Let-7 MicroRNA, and IL6 links inflammation to cell transformation. *Cell*. 139 (2009):693-706.
- [39]. S. Liu, C. Ginestier, S.J. Ou, S.G. Clouthier, S.H. Patel, F. Monville, et al. Breast cancer stem cells are regulated by mesenchymal stem cells through cytokine networks. *Cancer Res*. 71 (2011):614-624.

- [40]. N. Sethi, X. Dai, C.G. Winter, Y. Kang. Tumor-derived JAGGED1 promotes osteolytic bone metastasis of breast cancer by engaging notch signaling in bone cells. *Cancer Cell*. 19 (2011):192-205.
- [41]. P.J. Barnes, M. Karin. Nuclear factor-kappaB: a pivotal transcription factor in chronic inflammatory diseases. *N Engl J Med*. 336 (1997):1066-1071.
- [42]. P.N. Moynagh. The NF-kappaB pathway. *J Cell Sci*. 118 (2005):4589-4592.
- [43]. A. Hoffmann, G. Natoli, G. Ghosh. Transcriptional regulation via the NF-kappaB signaling module. *Oncogene*. 25 (2006):6706-6716.
- [44]. D. Iliopoulos, S.A. Jaeger, H.A. Hirsch, M.L. Bulyk, K. Struhl. STAT3 activation of miR-21 and miR-181b-1 via PTEN and CYLD are part of the epigenetic switch linking inflammation to cancer. *Mol Cell*. 39 (2010):493-506.
- [45]. M. Liu, T. Sakamaki, M.C. Casimiro, N.E. Willmarth, A.A. Quong, X. Ju, et al. The canonical NF-kappaB pathway governs mammary tumorigenesis in transgenic mice and tumor stem cell expansion. *Cancer Res*. 70 (2010):10464-10473.
- [46]. P.A. Joshi, H.W. Jackson, A.G. Beristain, M.A. Di Grappa, P.A. Mote, C.L. Clarke, et al. Progesterone induces adult mammary stem cell expansion. *Nature*. 465 (2010):803-807.

- [47]. M.L. Asselin-Labat, F. Vaillant, J.M. Sheridan, B. Pal, D. Wu, E.R. Simpson, et al. Control of mammary stem cell function by steroid hormone signalling. *Nature*. 465 (2010):798-802.
- [48]. J.D. Peck, B.S. Hulka, C. Poole, D.A. Savitz, D. Baird, B.E. Richardson. Steroid hormone levels during pregnancy and incidence of maternal breast cancer. *Cancer Epidemiol Biomarkers Prev*. 11 (2002):361-368.
- [49]. P. Ninfali, D. Angelino. Nutritional and functional potential of Beta vulgaris cicla and rubra. *Fitoterapia*. 89 (2013):188-199.
- [50]. P. Ninfali, A. Chiarabini, D. Angelino. The ORAC/kcal ratio qualifies nutritional and functional properties of fruit juices, nectars, and fruit drinks. *Int J Food Sci Nutr*. 65 (2014):708-712.
- [51]. T.D. Williams, M.P. Martin, J.A. Mintz, R.R. Rogers, C.G. Ballmann. Effect of Acute Beetroot Juice Supplementation on Bench Press Power, Velocity, and Repetition Volume. *J Strength Cond Res*. (2020).
- [52]. I. Belhadj Slimen, T. Najar, M. Abderrabba. Chemical and Antioxidant Properties of Betalains. *J Agric Food Chem*. 65 (2017):675-689.

- [53]. P. Ninfali, E. Antonini, A. Frati, E.S. Scarpa. C-Glycosyl Flavonoids from *Beta vulgaris* Cica and Betalains from *Beta vulgaris rubra*: Antioxidant, Anticancer and Antiinflammatory Activities-A Review. *Phytother Res.* 31 (2017):871-884.
- [54]. E.J. Lee, D. An, C.T. Nguyen, B.S. Patil, J. Kim, K.S. Yoo. Betalain and betaine composition of greenhouse- or field-produced beetroot (*Beta vulgaris* L.) and inhibition of HepG2 cell proliferation. *J Agric Food Chem.* 62 (2014):1324-1331.
- [55]. J.F. Lechner, G.D. Stoner. Red Beetroot and Betalains as Cancer Chemopreventative Agents. *Molecules.* 24 (2019).
- [56]. F. Bray, J. Ferlay, I. Soerjomataram, R.L. Siegel, L.A. Torre, A. Jemal. Global cancer statistics 2018: GLOBOCAN estimates of incidence and mortality worldwide for 36 cancers in 185 countries. *CA Cancer J Clin.* 68 (2018):394-424.
- [57]. X. Bai, J. Ni, J. Beretov, P. Graham, Y. Li. Cancer stem cell in breast cancer therapeutic resistance. *Cancer Treat Rev.* 69 (2018):152-163.
- [58]. D. Bonnet, J.E. Dick. Human acute myeloid leukemia is organized as a hierarchy that originates from a primitive hematopoietic cell. *Nat Med.* 3 (1997):730-737.
- [59]. M. Al-Hajj, M.S. Wicha, A. Benito-Hernandez, S.J. Morrison, M.F. Clarke. Prospective identification of tumorigenic breast cancer cells. *Proc Natl Acad Sci U S A.* 100 (2003):3983-3988.

- [60]. I. Baccelli, A. Schneeweiss, S. Riethdorf, A. Stenzinger, A. Schillert, V. Vogel, et al. Identification of a population of blood circulating tumor cells from breast cancer patients that initiates metastasis in a xenograft assay. *Nat Biotechnol.* 31 (2013):539-544.
- [61]. J. Huynh, A. Chand, D. Gough, M. Ernst. Therapeutically exploiting STAT3 activity in cancer - using tissue repair as a road map. *Nat Rev Cancer.* 19 (2019):82-96.
- [62]. D.E. Johnson, R.A. O'Keefe, J.R. Grandis. Targeting the IL-6/JAK/STAT3 signalling axis in cancer. *Nat Rev Clin Oncol.* 15 (2018):234-248.
- [63]. H. Yu, H. Lee, A. Herrmann, R. Buettner, R. Jove. Revisiting STAT3 signalling in cancer: new and unexpected biological functions. *Nat Rev Cancer.* 14 (2014):736-746.
- [64]. S.R. Sirkisoon, R.L. Carpenter, T. Rimkus, A. Anderson, A. Harrison, A.M. Lange, et al. Interaction between STAT3 and GLI1/tGLI1 oncogenic transcription factors promotes the aggressiveness of triple-negative breast cancers and HER2-enriched breast cancer. *Oncogene.* 37 (2018):2502-2514.
- [65]. D. Zhao, C. Pan, J. Sun, C. Gilbert, K. Drews-Elger, D.J. Azzam, et al. VEGF drives cancer-initiating stem cells through VEGFR-2/Stat3 signaling to upregulate Myc and Sox2. *Oncogene.* 34 (2015):3107-3119.

- [66]. C.C. Wu, X. Jiang, X.Z. Wang, X.J. Liu, X.J. Li, B. Yang, et al. Human Cytomegalovirus Immediate Early 1 Protein Causes Loss of SOX2 from Neural Progenitor Cells by Trapping Unphosphorylated STAT3 in the Nucleus. *J Virol.* 92 (2018).
- [67]. R. Wu, Y. Liu, Y. Zhao, Z. Bi, Y. Yao, Q. Liu, et al. m(6)A methylation controls pluripotency of porcine induced pluripotent stem cells by targeting SOCS3/JAK2/STAT3 pathway in a YTHDF1/YTHDF2-orchestrated manner. *Cell Death Dis.* 10 (2019):171.
- [68]. J. Yin, G. Park, T.H. Kim, J.H. Hong, Y.J. Kim, X. Jin, et al. Pigment Epithelium-Derived Factor (PEDF) Expression Induced by EGFRvIII Promotes Self-renewal and Tumor Progression of Glioma Stem Cells. *PLoS Biol.* 13 (2015):e1002152.
- [69]. M.L. Clarke, R.L. Burton, A.N. Hill, M. Litorja, M.H. Nahm, J. Hwang. Low-cost, high-throughput, automated counting of bacterial colonies. *Cytometry A.* 77 (2010):790-797.
- [70]. H.S. Choi, D.A. Kim, H. Chung, I.H. Park, B.H. Kim, E.S. Oh, et al. Screening of breast cancer stem cell inhibitors using a protein kinase inhibitor library. *Cancer Cell Int.* 17 (2017):25.
- [71]. H.S. Choi, J.H. Kim, S.L. Kim, H.Y. Deng, D. Lee, C.S. Kim, et al. Catechol derived from aronia juice through lactic acid bacteria fermentation inhibits breast cancer stem cell formation via modulation Stat3/IL-6 signaling pathway. *Mol Carcinog.* 57 (2018):1467-1479.

- [72]. X. Zhen, H.N. Sun, R. Liu, H.S. Choi, D.S. Lee. Non-thermal Plasma-activated Medium Induces Apoptosis of Aspc1 Cells Through the ROS-dependent Autophagy Pathway. *In Vivo*. 34 (2020):143-153.
- [73]. H.S. Choi, S.L. Kim, J.H. Kim, H.Y. Deng, B.S. Yun, D.S. Lee. Triterpene Acid (3-O-p-Coumaroyltormentic Acid) Isolated From Aronia Extracts Inhibits Breast Cancer Stem Cell Formation through Downregulation of c-Myc Protein. *Int J Mol Sci*. 19 (2018).
- [74]. H.S. Choi, C.K. Hwang, C.S. Kim, K.Y. Song, P.Y. Law, L.N. Wei, et al. Transcriptional regulation of mouse mu opioid receptor gene: Sp3 isoforms (M1, M2) function as repressors in neuronal cells to regulate the mu opioid receptor gene. *Mol Pharmacol*. 67 (2005):1674-1683.
- [75]. P. Rahimi, S. Abedimanesh, S.A. Mesbah-Namin, A. Ostadrahimi. Betalains, the nature-inspired pigments, in health and diseases. *Crit Rev Food Sci Nutr*. 59 (2019):2949-2978.
- [76]. T. Esatbeyoglu, A.E. Wagner, V.B. Schini-Kerth, G. Rimbach. Betanin--a food colorant with biological activity. *Mol Nutr Food Res*. 59 (2015):36-47.
- [77]. Y. Aratani. Myeloperoxidase: Its role for host defense, inflammation, and neutrophil function. *Arch Biochem Biophys*. 640 (2018):47-52.
- [78]. G. Bauer. HOCl and the control of oncogenesis. *J Inorg Biochem*. 179 (2018):10-23.

- [79]. C.A. Elliger, J.M. Halloin. Phenolics induced in *Beta vulgaris* by *Rhizoctonia solani* infection. *Phytochemistry*. 37 (1994):691-693.
- [80]. Y. Husemann, J.B. Geigl, F. Schubert, P. Musiani, M. Meyer, E. Burghart, et al. Systemic spread is an early step in breast cancer. *Cancer Cell*. 13 (2008):58-68.
- [81]. L.L. Marotta, V. Almendro, A. Marusyk, M. Shipitsin, J. Schemme, S.R. Walker, et al. The JAK2/STAT3 signaling pathway is required for growth of CD44(+)CD24(-) stem cell-like breast cancer cells in human tumors. *J Clin Invest*. 121 (2011):2723-2735.
- [82]. L. Yang, S. Lin, L. Xu, J. Lin, C. Zhao, X. Huang. Novel activators and small-molecule inhibitors of STAT3 in cancer. *Cytokine Growth Factor Rev*. 49 (2019):10-22.
- [83]. K.M. Foshay, G.I. Gallicano. Regulation of Sox2 by STAT3 initiates commitment to the neural precursor cell fate. *Stem Cells Dev*. 17 (2008):269-278.
- [84]. C. Dawid, F. Dunemann, W. Schwab, T. Nothnagel, T. Hofmann. Bioactive C(1)(7)-Polyacetylenes in Carrots (*Daucus carota* L.): Current Knowledge and Future Perspectives. *J Agric Food Chem*. 63 (2015):9211-9222.
- [85]. M. Leja, I. Kaminska, M. Kramer, A. Maksylewicz-Kaul, D. Kammerer, R. Carle, et al. The content of phenolic compounds and radical scavenging activity varies with carrot origin and root color. *Plant Foods Hum Nutr*. 68 (2013):163-170.

- [86]. U. Garba, S. Kaur, S. Gurumayum, P. Rasane. Effect of Hot Water Blanching Time and Drying Temperature on the Thin Layer Drying Kinetics of and Anthocyanin Degradation in Black Carrot (*Daucus carota* L.) Shreds. *Food Technol Biotechnol.* 53 (2015):324-330.
- [87]. T. Ahmad, M. Cawood, Q. Iqbal, A. Arino, A. Batool, R.M.S. Tariq, et al. Phytochemicals in *Daucus carota* and Their Health Benefits-Review Article. *Foods.* 8 (2019).
- [88]. F. Que, X.L. Hou, G.L. Wang, Z.S. Xu, G.F. Tan, T. Li, et al. Advances in research on the carrot, an important root vegetable in the Apiaceae family. *Hortic Res.* 6 (2019):69.
- [89]. S. Aksak Karamese, E. Toktay, D. Unal, J. Selli, M. Karamese, I. Malkoc. The protective effects of beta-carotene against ischemia/reperfusion injury in rat ovarian tissue. *Acta Histochem.* 117 (2015):790-797.
- [90]. S.R. Kim, K. Nakanishi, Y. Itagaki, J.R. Sparrow. Photooxidation of A2-PE, a photoreceptor outer segment fluorophore, and protection by lutein and zeaxanthin. *Exp Eye Res.* 82 (2006):828-839.
- [91]. R.W.S. Chung, P. Leanderson, A.K. Lundberg, L. Jonasson. Lutein exerts anti-inflammatory effects in patients with coronary artery disease. *Atherosclerosis.* 262 (2017):87-93.
- [92]. G. Akolkar, D. da Silva Dias, P. Ayyappan, A.K. Bagchi, D.S. Jassal, V.M.C. Salemi, et al. Vitamin C mitigates oxidative/nitrosative stress and inflammation in doxorubicin-induced cardiomyopathy. *Am J Physiol Heart Circ Physiol.* 313 (2017):H795-H809.

- [93]. F. Zecchinati, M.M. Barranco, M.R. Arana, G.N. Tocchetti, C.J. Dominguez, V.G. Perdomo, et al. Reversion of down-regulation of intestinal multidrug resistance-associated protein 2 in fructose-fed rats by geraniol and vitamin C: Potential role of inflammatory response and oxidative stress. *J Nutr Biochem.* 68 (2019):7-15.
- [94]. A.L. Stefanson, M. Bakovic. Falcarinol Is a Potent Inducer of Heme Oxygenase-1 and Was More Effective than Sulforaphane in Attenuating Intestinal Inflammation at Diet-Achievable Doses. *Oxid Med Cell Longev.* 2018 (2018):3153527.
- [95]. E.M. Fikry, A.M. Gad, A.H. Eid, H.H. Arab. Caffeic acid and ellagic acid ameliorate adjuvant-induced arthritis in rats via targeting inflammatory signals, chitinase-3-like protein-1 and angiogenesis. *Biomed Pharmacother.* 110 (2019):878-886.
- [96]. F. Yang, J. Xu, L. Tang, X. Guan. Breast cancer stem cell: the roles and therapeutic implications. *Cell Mol Life Sci.* 74 (2017):951-966.
- [97]. C.W.S. Tong, M. Wu, W.C.S. Cho, K.K.W. To. Recent Advances in the Treatment of Breast Cancer. *Front Oncol.* 8 (2018):227.
- [98]. S.K. Yeo, J. Wen, S. Chen, J.L. Guan. Autophagy Differentially Regulates Distinct Breast Cancer Stem-like Cells in Murine Models via EGFR/Stat3 and Tgfbeta/Smad Signaling. *Cancer Res.* 76 (2016):3397-3410.

- [99]. S. Liu, Y. Cong, D. Wang, Y. Sun, L. Deng, Y. Liu, et al. Breast cancer stem cells transition between epithelial and mesenchymal states reflective of their normal counterparts. *Stem Cell Reports*. 2 (2014):78-91.
- [100]. M.J. Bak, P. Furmanski, N.L. Shan, H.J. Lee, C. Bao, Y. Lin, et al. Tocopherols inhibit estrogen-induced cancer stemness and OCT4 signaling in breast cancer. *Carcinogenesis*. 39 (2018):1045-1055.
- [101]. J.L. Chew, Y.H. Loh, W. Zhang, X. Chen, W.L. Tam, L.S. Yeap, et al. Reciprocal transcriptional regulation of Pou5f1 and Sox2 via the Oct4/Sox2 complex in embryonic stem cells. *Mol Cell Biol*. 25 (2005):6031-6046.
- [102]. V. Poli, L. Fagnocchi, A. Fasciani, A. Cherubini, S. Mazzoleni, S. Ferrillo, et al. MYC-driven epigenetic reprogramming favors the onset of tumorigenesis by inducing a stem cell-like state. *Nat Commun*. 9 (2018):1024.
- [103]. J. Wang, H. Wang, Z. Li, Q. Wu, J.D. Lathia, R.E. McLendon, et al. c-Myc is required for maintenance of glioma cancer stem cells. *PLoS One*. 3 (2008):e3769.
- [104]. H. Lu, Y. Xie, L. Tran, J. Lan, Y. Yang, N.L. Murugan, et al. Chemotherapy-induced S100A10 recruits KDM6A to facilitate OCT4-mediated breast cancer stemness. *J Clin Invest*. 130 (2020):4607-4623.

- [105]. M.A. Mamun, K. Mannoor, J. Cao, F. Qadri, X. Song. SOX2 in cancer stemness: tumor malignancy and therapeutic potentials. *J Mol Cell Biol.* 12 (2020):85-98.
- [106]. B.C. Prager, Q. Xie, S. Bao, J.N. Rich. Cancer Stem Cells: The Architects of the Tumor Ecosystem. *Cell Stem Cell.* 24 (2019):41-53.
- [107]. F. Bocci, L. Gearhart-Serna, M. Boareto, M. Ribeiro, E. Ben-Jacob, G.R. Devi, et al. Toward understanding cancer stem cell heterogeneity in the tumor microenvironment. *Proc Natl Acad Sci U S A.* 116 (2019):148-157.
- [108]. V. Bhat, A.L. Allan, A. Raouf. Role of the Microenvironment in Regulating Normal and Cancer Stem Cell Activity: Implications for Breast Cancer Progression and Therapy Response. *Cancers (Basel).* 11 (2019).
- [109]. H. Lu, W. Ouyang, C. Huang. Inflammation, a key event in cancer development. *Mol Cancer Res.* 4 (2006):221-233.
- [110]. D. Iliopoulos, H.A. Hirsch, G. Wang, K. Struhl. Inducible formation of breast cancer stem cells and their dynamic equilibrium with non-stem cancer cells via IL6 secretion. *Proc Natl Acad Sci U S A.* 108 (2011):1397-1402.
- [111]. S.Y. Kim, J.W. Kang, X. Song, B.K. Kim, Y.D. Yoo, Y.T. Kwon, et al. Role of the IL-6-JAK1-STAT3-Oct-4 pathway in the conversion of non-stem cancer cells into cancer stem-like cells. *Cell Signal.* 25 (2013):961-969.

- [112]. C. Dominguez, K.K. McCampbell, J.M. David, C. Palena. Neutralization of IL-8 decreases tumor PMN-MDSCs and reduces mesenchymalization of claudin-low triple-negative breast cancer. *JCI Insight*. 2 (2017).
- [113]. X. Zhen, H.S. Choi, J.H. Kim, S.L. Kim, R. Liu, B.S. Yun, et al. Machilin D, a Lignin Derived from *Saururus chinensis*, Suppresses Breast Cancer Stem Cells and Inhibits NF-kappaB Signaling. *Biomolecules*. 10 (2020).
- [114]. J. Nan, Y. Wang, J. Yang, G.R. Stark. IRF9 and unphosphorylated STAT2 cooperate with NF-kappaB to drive IL6 expression. *Proc Natl Acad Sci U S A*. 115 (2018):3906-3911.
- [115]. S. Yoon, S.U. Woo, J.H. Kang, K. Kim, H.J. Shin, H.S. Gwak, et al. NF-kappaB and STAT3 cooperatively induce IL6 in starved cancer cells. *Oncogene*. 31 (2012):3467-3481.
- [116]. Y. Liubomirski, S. Lerrer, T. Meshel, L. Rubinstein-Achiasaf, D. Morein, S. Wiemann, et al. Tumor-Stroma-Inflammation Networks Promote Pro-metastatic Chemokines and Aggressiveness Characteristics in Triple-Negative Breast Cancer. *Front Immunol*. 10 (2019):757.
- [117]. K.D. Sharma, S. Karki, N.S. Thakur, S. Attri. Chemical composition, functional properties and processing of carrot-a review. *J Food Sci Technol*. 49 (2012):22-32.
- [118]. R.G. Zaini, K. Brandt, M.R. Clench, C.L. Le Maitre. Effects of bioactive compounds from carrots (*Daucus carota* L.), polyacetylenes, beta-carotene and lutein on human lymphoid leukaemia cells. *Anticancer Agents Med Chem*. 12 (2012):640-652.

- [119]. C. Sevimli-Gur, B. Cetin, S. Akay, S. Gulce-Iz, O. Yesil-Celiktas. Extracts from black carrot tissue culture as potent anticancer agents. *Plant Foods Hum Nutr.* 68 (2013):293-298.
- [120]. H.E. Daaboul, C.F. Daher, K. Bodman-Smith, R.I. Taleb, W.N. Shebaby, J. Boulos, et al. Antitumor activity of beta-2-himachalen-6-ol in colon cancer is mediated through its inhibition of the PI3K and MAPK pathways. *Chem Biol Interact.* 275 (2017):162-170.
- [121]. M. Staniszewska, J. Kula, M. Wieczorkiewicz, D. Kusewicz. Essential oils of wild and cultivated carrots - the chemical composition and antimicrobial activity. *Journal Of Essential Oil Research.* 17 (2005):579-583.
- [122]. A. Maxia, B. Marongiu, A. Piras, S. Porcedda, E. Tuveri, M.J. Goncalves, et al. Chemical characterization and biological activity of essential oils from *Daucus carota* L. subsp. *carota* growing wild on the Mediterranean coast and on the Atlantic coast. *Fitoterapia.* 80 (2009):57-61.
- [123]. W.N. Shebaby, M. El-Sibai, K.B. Smith, M.C. Karam, M. Mroueh, C.F. Daher. The antioxidant and anticancer effects of wild carrot oil extract. *Phytother Res.* 27 (2013):737-744.
- [124]. W.N. Shebaby, C.F. Daher, M. El-Sibai, K. Bodman-Smith, A. Mansour, M.C. Karam, et al. Antioxidant and hepatoprotective activities of the oil fractions from wild carrot (*Daucus carota* ssp. *carota*). *Pharm Biol.* 53 (2015):1285-1294.
- [125]. A. Saeed. Isocoumarins, miraculous natural products blessed with diverse pharmacological activities. *Eur J Med Chem.* 116 (2016):290-317.

- [126]. J.S. Dickschat. Fungal volatiles - a survey from edible mushrooms to moulds. *Nat Prod Rep.* 34 (2017):310-328.
- [127]. L. Escriva, G. Font, L. Manyes, H. Berrada. Studies on the Presence of Mycotoxins in Biological Samples: An Overview. *Toxins (Basel)*. 9 (2017).
- [128]. P. Condon, J. Kuc. Isolation of a fungitoxic compound from carrot root tissue inoculated with *Cerato-cystis fimbriata*. *Phytopathology*. 50 (1960):267-270.
- [129]. P. Condon, J. Kuc, H. Draudt. Production of 3-methyl-6-methoxy-8-hydroxy-3, 4-dihydroisocoumarin by carrot root tissue. *Phytopathology*. 53 (1963):1244-&.
- [130]. J. Kuc. Resistance of plants to infectious agents. *Annu Rev Microbiol*. 20 (1966):337-370.
- [131]. V. Harding, J. Heale. Isolation and identification of the antifungal compounds accumulating in the induced resistance response of carrot root slices to *Botrytis cinerea*. *Physiological Plant Pathology*. 17 (1980):277-289.
- [132]. S.Q. Geng, A.T. Alexandrou, J.J. Li. Breast cancer stem cells: Multiple capacities in tumor metastasis. *Cancer Lett.* 349 (2014):1-7.
- [133]. S.Y. Park, J.H. Choi, J.S. Nam. Targeting Cancer Stem Cells in Triple-Negative Breast Cancer. *Cancers (Basel)*. 11 (2019).

- [134]. J. Dittmer. Breast cancer stem cells: Features, key drivers and treatment options. *Semin Cancer Biol.* 53 (2018):59-74.
- [135]. K. Kise, Y. Kinugasa-Katayama, N. Takakura. Tumor microenvironment for cancer stem cells. *Adv Drug Deliv Rev.* 99 (2016):197-205.
- [136]. C. Lin, L. Wang, H. Wang, L. Yang, H. Guo, X. Wang. Tanshinone IIA inhibits breast cancer stem cells growth in vitro and in vivo through attenuation of IL-6/STAT3/NF- κ B signaling pathways. *J Cell Biochem.* 114 (2013):2061-2070.
- [137]. W. Chen, Y. Qin, S. Liu. Cytokines, breast cancer stem cells (BCSCs) and chemoresistance. *Clin Transl Med.* 7 (2018):27.
- [138]. J.K. Singh, G. Famie, N.J. Bundred, B.M. Simoes, A. Shergill, G. Landberg, et al. Targeting CXCR1/2 significantly reduces breast cancer stem cell activity and increases the efficacy of inhibiting HER2 via HER2-dependent and -independent mechanisms. *Clin Cancer Res.* 19 (2013):643-656.
- [139]. H. Korkaya, S. Liu, M.S. Wicha. Breast cancer stem cells, cytokine networks, and the tumor microenvironment. *J Clin Invest.* 121 (2011):3804-3809.
- [140]. A. Prat, J.S. Parker, O. Karginova, C. Fan, C. Livasy, J.I. Herschkowitz, et al. Phenotypic and molecular characterization of the claudin-low intrinsic subtype of breast cancer. *Breast Cancer Res.* 12 (2010):R68.

- [141]. R. Liu, P. Shi, Z. Nie, H. Liang, Z. Zhou, W. Chen, et al. Mifepristone Suppresses Basal Triple-Negative Breast Cancer Stem Cells by Down-regulating KLF5 Expression. *Theranostics*. 6 (2016):533-544.
- [142]. J.E. Panoff, J. Hurley, C. Takita, I.M. Reis, W. Zhao, V. Sujoy, et al. Risk of locoregional recurrence by receptor status in breast cancer patients receiving modern systemic therapy and post-mastectomy radiation. *Breast Cancer Res Treat*. 128 (2011):899-906.
- [143]. B.D. Lehmann, B. Jovanovic, X. Chen, M.V. Estrada, K.N. Johnson, Y. Shyr, et al. Refinement of Triple-Negative Breast Cancer Molecular Subtypes: Implications for Neoadjuvant Chemotherapy Selection. *PLoS One*. 11 (2016):e0157368.
- [144]. B.D. Lehmann, J.A. Bauer, X. Chen, M.E. Sanders, A.B. Chakravarthy, Y. Shyr, et al. Identification of human triple-negative breast cancer subtypes and preclinical models for selection of targeted therapies. *J Clin Invest*. 121 (2011):2750-2767.
- [145]. S.J. Isakoff. Triple-negative breast cancer: role of specific chemotherapy agents. *Cancer J*. 16 (2010):53-61.
- [146]. P.R. Dandawate, D. Subramaniam, R.A. Jensen, S. Anant. Targeting cancer stem cells and signaling pathways by phytochemicals: Novel approach for breast cancer therapy. *Semin Cancer Biol*. 40-41 (2016):192-208.

- [147]. N. Cancer Genome Atlas. Comprehensive molecular portraits of human breast tumours. *Nature*. 490 (2012):61-70.
- [148]. C. Calabrese, H. Poppleton, M. Kocak, T.L. Hogg, C. Fuller, B. Hamner, et al. A perivascular niche for brain tumor stem cells. *Cancer Cell*. 11 (2007):69-82.
- [149]. D. Wang, J. Xu, B. Liu, X. He, L. Zhou, X. Hu, et al. IL6 blockade potentiates the anti-tumor effects of gamma-secretase inhibitors in Notch3-expressing breast cancer. *Cell Death Differ*. 25 (2018):330-339.
- [150]. N.J. Sullivan, A.K. Sasser, A.E. Axel, F. Vesuna, V. Raman, N. Ramirez, et al. Interleukin-6 induces an epithelial-mesenchymal transition phenotype in human breast cancer cells. *Oncogene*. 28 (2009):2940-2947.
- [151]. M. van der Zee, A. Sacchetti, M. Cansoy, R. Joosten, M. Teeuwssen, C. Heijmans-Antonissen, et al. IL6/JAK1/STAT3 Signaling Blockade in Endometrial Cancer Affects the ALDHhi/CD126+ Stem-like Component and Reduces Tumor Burden. *Cancer Res*. 75 (2015):3608-3622.
- [152]. A.R. Green, V.L. Green, M.C. White, V. Speirs. Expression of cytokine messenger RNA in normal and neoplastic human breast tissue: identification of interleukin-8 as a potential regulatory factor in breast tumours. *Int J Cancer*. 72 (1997):937-941.

- [153]. A. Freund, C. Chauveau, J.P. Brouillet, A. Lucas, M. Lacroix, A. Licznar, et al. IL-8 expression and its possible relationship with estrogen-receptor-negative status of breast cancer cells. *Oncogene*. 22 (2003):256-265.
- [154]. R.I. Fernando, M.D. Castillo, M. Litzinger, D.H. Hamilton, C. Palena. IL-8 signaling plays a critical role in the epithelial-mesenchymal transition of human carcinoma cells. *Cancer Res*. 71 (2011):5296-5306.
- [155]. J.D. Adams, Jr., C. Garcia. Women's health among the Chumash. *Evid Based Complement Alternat Med*. 3 (2006):125-131.
- [156]. S. Estrada-Soto, A. Sanchez-Recillas, G. Navarrete-Vazquez, P. Castillo-Espana, R. Villalobos-Molina, M. Ibarra-Barajas. Relaxant effects of *Artemisia ludoviciana* on isolated rat smooth muscle tissues. *J Ethnopharmacol*. 139 (2012):513-518.
- [157]. H.K. Ju, H.W. Lee, K.S. Chung, J.H. Choi, J.G. Cho, N.I. Baek, et al. Standardized flavonoid-rich fraction of *Artemisia princeps* Pampanini cv. Sajabal induces apoptosis via mitochondrial pathway in human cervical cancer HeLa cells. *J Ethnopharmacol*. 141 (2012):460-468.
- [158]. A.O. Maria, M. Repetto, S. Llesuy, O. Giordano, J. Guzman, E. Guerreiro. Antioxidant activity of *Artemisia douglasiana* besser extract and dehydroleucodine. *Phytother Res*. 14 (2000):558-560.

- [159]. C. Yun, Y. Jung, W. Chun, B. Yang, J. Ryu, C. Lim, et al. Anti-Inflammatory Effects of Artemisia Leaf Extract in Mice with Contact Dermatitis In Vitro and In Vivo. *Mediators Inflamm.* 2016 (2016):8027537.
- [160]. S.B. Kwak, S. Koppula, E.J. In, X. Sun, Y.K. Kim, M.K. Kim, et al. Artemisia Extract Suppresses NLRP3 and AIM2 Inflammasome Activation by Inhibition of ASC Phosphorylation. *Mediators Inflamm.* 2018 (2018):6054069.
- [161]. S.W. Min, N.J. Kim, N.I. Baek, D.H. Kim. Inhibitory effect of eupatilin and jaceosidin isolated from *Artemisia princeps* on carrageenan-induced inflammation in mice. *J Ethnopharmacol.* 125 (2009):497-500.
- [162]. E.J. Choi, G.H. Kim. Antioxidant and anticancer activity of *Artemisia princeps* var. *orientalis* extract in HepG2 and Hep3B hepatocellular carcinoma cells. *Chin J Cancer Res.* 25 (2013):536-543.
- [163]. A. Hirano, M. Goto, T. Mitsui, A. Hashimoto-Hachiya, G. Tsuji, M. Furue. Antioxidant *Artemisia princeps* Extract Enhances the Expression of Filaggrin and Loricrin via the AHR/OVOL1 Pathway. *Int J Mol Sci.* 18 (2017).
- [164]. K.E. Hwang, Y.S. Choi, S.M. Choi, H.W. Kim, J.H. Choi, M.A. Lee, et al. Antioxidant action of ganghwayakssuk (*Artemisia princeps* Pamp.) in combination with ascorbic acid to increase the shelf life in raw and deep fried chicken nuggets. *Meat Sci.* 95 (2013):593-602.

- [165]. K.D. Yoon, Y.W. Chin, M.H. Yang, J. Kim. Separation of anti-ulcer flavonoids from Artemisia extracts by high-speed countercurrent chromatography. Food Chem. 129 (2011):679-683.
- [166]. J.H. Kim, S.H. Jung, Y.I. Yang, J.H. Ahn, J.G. Cho, K.T. Lee, et al. Artemisia leaf extract induces apoptosis in human endometriotic cells through regulation of the p38 and NFkappaB pathways. J Ethnopharmacol. 145 (2013):767-775.
- [167]. J.H. Cho, J.G. Lee, Y.I. Yang, J.H. Kim, J.H. Ahn, N.I. Baek, et al. Eupatilin, a dietary flavonoid, induces G2/M cell cycle arrest in human endometrial cancer cells. Food Chem Toxicol. 49 (2011):1737-1744.
- [168]. K.S. Chung, H.E. Choi, J.S. Shin, E.J. Cho, Y.W. Cho, J.H. Choi, et al. Chemopreventive effects of standardized ethanol extract from the aerial parts of Artemisia princeps Pampanini cv. Sajabal via NF-kappaB inactivation on colitis-associated colon tumorigenesis in mice. Food Chem Toxicol. 75 (2015):14-23.
- [169]. N. Yamamoto, Y. Kanemoto, M. Ueda, K. Kawasaki, I. Fukuda, H. Ashida. Anti-obesity and anti-diabetic effects of ethanol extract of Artemisia princeps in C57BL/6 mice fed a high-fat diet. Food Funct. 2 (2011):45-52.
- [170]. U.J. Jung, N.I. Baek, H.G. Chung, M.H. Bang, J.S. Yoo, T.S. Jeong, et al. The anti-diabetic effects of ethanol extract from two variants of Artemisia princeps Pampanini in C57BL/KsJ-db/db mice. Food Chem Toxicol. 45 (2007):2022-2029.

- [171]. R. Liu, H.S. Choi, S.L. Kim, J.H. Kim, B.S. Yun, D.S. Lee. 6-Methoxymellein Isolated from Carrot (*Daucus carota* L.) Targets Breast Cancer Stem Cells by Regulating NF-kappaB Signaling. *Molecules*. 25 (2020).
- [172]. M. Rokavec, M.G. Oner, H. Li, R. Jackstadt, L. Jiang, D. Lodygin, et al. IL-6R/STAT3/miR-34a feedback loop promotes EMT-mediated colorectal cancer invasion and metastasis. *J Clin Invest*. 124 (2014):1853-1867.
- [173]. S. Kitajima, A. Yoshida, S. Kohno, F. Li, S. Suzuki, N. Nagatani, et al. The RB-IL-6 axis controls self-renewal and endocrine therapy resistance by fine-tuning mitochondrial activity. *Oncogene*. 36 (2017):5145-5157.
- [174]. H.H. Al-Khalaf, H. Ghebeh, R. Inass, A. Aboussekhra. Senescent Breast Luminal Cells Promote Carcinogenesis through Interleukin-8-Dependent Activation of Stromal Fibroblasts. *Mol Cell Biol*. 39 (2019).
- [175]. M. Zhu, X. Liu, Y. Wang, L. Chen, L. Wang, X. Qin, et al. YAP via interacting with STAT3 regulates VEGF-induced angiogenesis in human retinal microvascular endothelial cells. *Exp Cell Res*. 373 (2018):155-163.
- [176]. K. Taniguchi, T. Moroishi, P.R. de Jong, M. Krawczyk, B.M. Grebbin, H. Luo, et al. YAP-IL-6ST autoregulatory loop activated on APC loss controls colonic tumorigenesis. *Proc Natl Acad Sci U S A*. 114 (2017):1643-1648.

- [177]. I. Chaib, N. Karachaliou, S. Pilotto, J. Codony Servat, X. Cai, X. Li, et al. Co-activation of STAT3 and YES-Associated Protein 1 (YAP1) Pathway in EGFR-Mutant NSCLC. *J Natl Cancer Inst.* 109 (2017).
- [178]. M. Shibata, A. Ooki, Y. Inokawa, P. Sadhukhan, M.T. Ugurlu, E. Izumchenko, et al. Concurrent Targeting of Potential Cancer Stem Cells Regulating Pathways Sensitizes Lung Adenocarcinoma to Standard Chemotherapy. *Mol Cancer Ther.* 19 (2020):2175-2185.
- [179]. M.J. Abad, L.M. Bedoya, L. Apaza, P. Bermejo. The artemisia L. Genus: a review of bioactive essential oils. *Molecules.* 17 (2012):2542-2566.
- [180]. J.W. Kim, H.G. Choi, J.H. Song, K.S. Kang, S.H. Shim. Bioactive secondary metabolites from an endophytic fungus *Phoma* sp. PF2 derived from *Artemisia princeps* Pamp. *J Antibiot (Tokyo).* 72 (2019):174-177.
- [181]. F. Karadeniz, J.H. Oh, J.I. Lee, H. Kim, Y. Seo, C.S. Kong. 6-Acetyl-2,2-Dimethylchroman-4-One Isolated from *Artemisia princeps* Suppresses Adipogenic Differentiation of Human Bone Marrow-Derived Mesenchymal Stromal Cells via Activation of AMPK. *J Med Food.* 23 (2020):250-257.
- [182]. J.G. Lee, J.H. Kim, J.H. Ahn, K.T. Lee, N.I. Baek, J.H. Choi. Jaceosidin, isolated from dietary mugwort (*Artemisia princeps*), induces G2/M cell cycle arrest by inactivating cdc25C-cdc2 via ATM-Chk1/2 activation. *Food Chem Toxicol.* 55 (2013):214-221.

- [183]. M.A. Jeong, K.W. Lee, D.Y. Yoon, H.J. Lee. Jaceosidin, a pharmacologically active flavone derived from *Artemisia argyi*, inhibits phorbol-ester-induced upregulation of COX-2 and MMP-9 by blocking phosphorylation of ERK-1 and -2 in cultured human mammary epithelial cells. *Ann N Y Acad Sci.* 1095 (2007):458-466.
- [184]. D.H. Kim, H.K. Na, T.Y. Oh, W.B. Kim, Y.J. Surh. Eupatilin, a pharmacologically active flavone derived from *Artemisia* plants, induces cell cycle arrest in ras-transformed human mammary epithelial cells. *Biochem Pharmacol.* 68 (2004):1081-1087.
- [185]. E.J. Choi, S. Lee, J.R. Chae, H.S. Lee, C.D. Jun, S.H. Kim. Eupatilin inhibits lipopolysaccharide-induced expression of inflammatory mediators in macrophages. *Life Sci.* 88 (2011):1121-1126.
- [186]. J.Y. Lee, H. Bae, C. Yang, S. Park, B.S. Youn, H.S. Kim, et al. Eupatilin Promotes Cell Death by Calcium Influx through ER-Mitochondria Axis with SERPINB11 Inhibition in Epithelial Ovarian Cancer. *Cancers (Basel).* 12 (2020).
- [187]. A.K. Croker, D. Goodale, J. Chu, C. Postenka, B.D. Hedley, D.A. Hess, et al. High aldehyde dehydrogenase and expression of cancer stem cell markers selects for breast cancer cells with enhanced malignant and metastatic ability. *J Cell Mol Med.* 13 (2009):2236-2252.
- [188]. H. Nakshatri. Radiation resistance in breast cancer: are CD44+/CD24-/proteasome low/PKH26+ cells to blame? *Breast Cancer Res.* 12 (2010):105.

- [189]. Z. Wu, B. Zou, X. Zhang, X. Peng. Eupatilin regulates proliferation and cell cycle of cervical cancer by regulating hedgehog signalling pathway. *Cell Biochem Funct.* 38 (2020):428-435.
- [190]. D. Kesanakurti, C. Chetty, D. Rajasekhar Maddirela, M. Gujrati, J.S. Rao. Essential role of cooperative NF-kappaB and Stat3 recruitment to ICAM-1 intronic consensus elements in the regulation of radiation-induced invasion and migration in glioma. *Oncogene.* 32 (2013):5144-5155.
- [191]. N. Uddin, R.K. Kim, K.C. Yoo, Y.H. Kim, Y.H. Cui, I.G. Kim, et al. Persistent activation of STAT3 by PIM2-driven positive feedback loop for epithelial-mesenchymal transition in breast cancer. *Cancer Sci.* 106 (2015):718-725.

SUPPLEMENTARY FIGURES

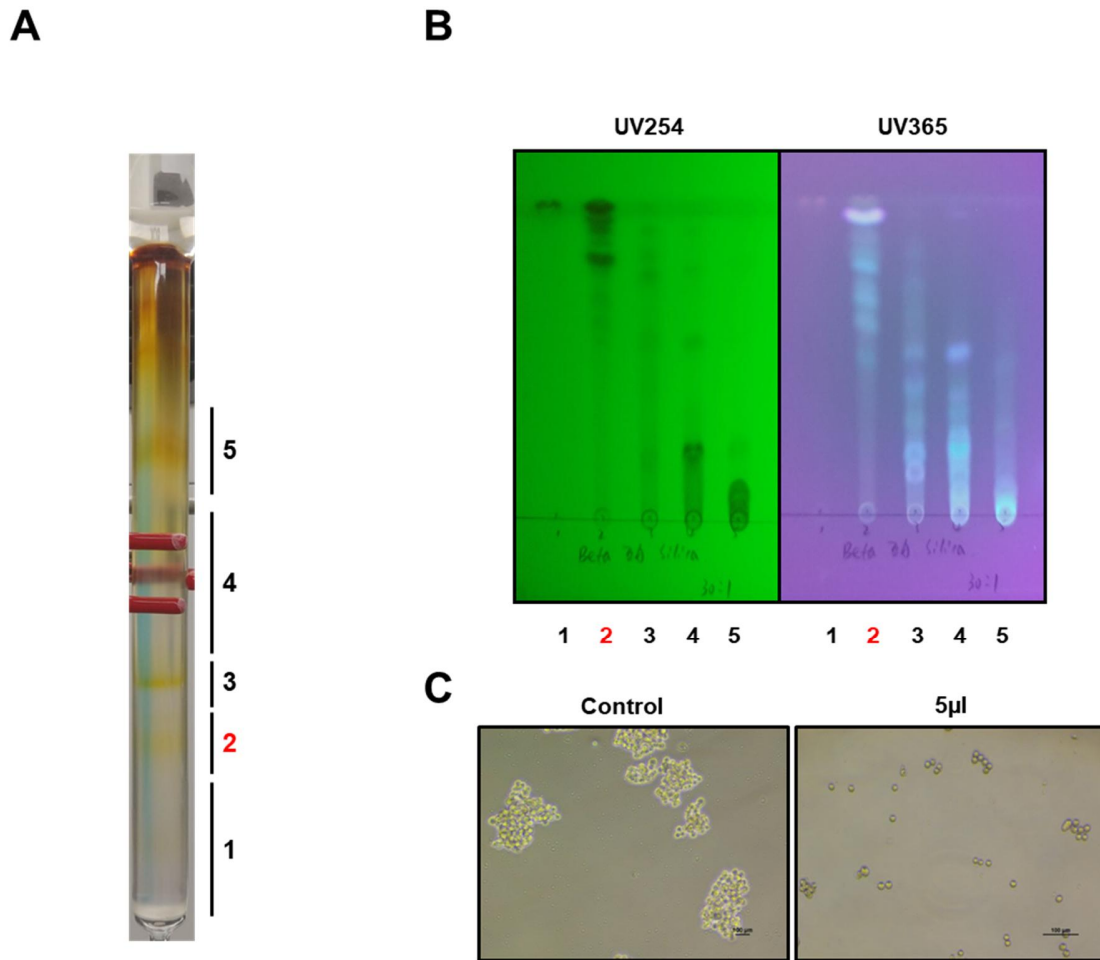


Figure S2-1. The purification procedure of a mammosphere formation inhibitor derived from beet using silica gel column chromatography. (A) The sample was isolated by silica gel chromatography with a solvent mixture [CHCl_3 : MeOH (10:1)]. (B) TLC plate analysis of the purified sample (CHCl_3 : MeOH = 30:1). Active fraction: #2. (C) Mammosphere formation assay using the purified fraction #2.

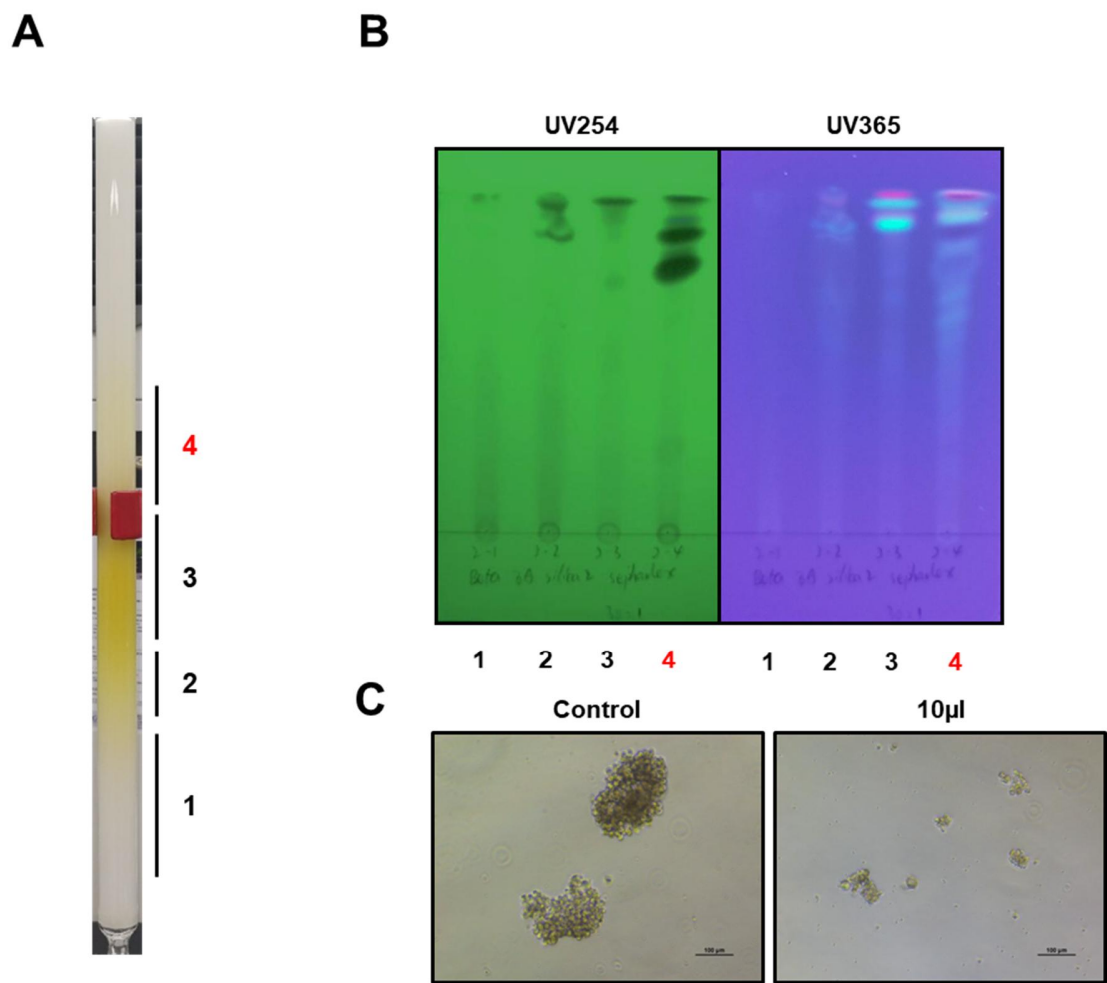


Figure S2-2. The purification procedure of a mammosphere formation inhibitor derived from beet using Sephadex LH-20 column chromatography. (A) The sample was isolated by Sephadex LH-20 chromatography with MeOH. (B) TLC plate analysis of the purified sample (CHCl₃ : MeOH = 30:1). Active fraction: #4. (C) Mammosphere formation assay using the purified fraction #4.

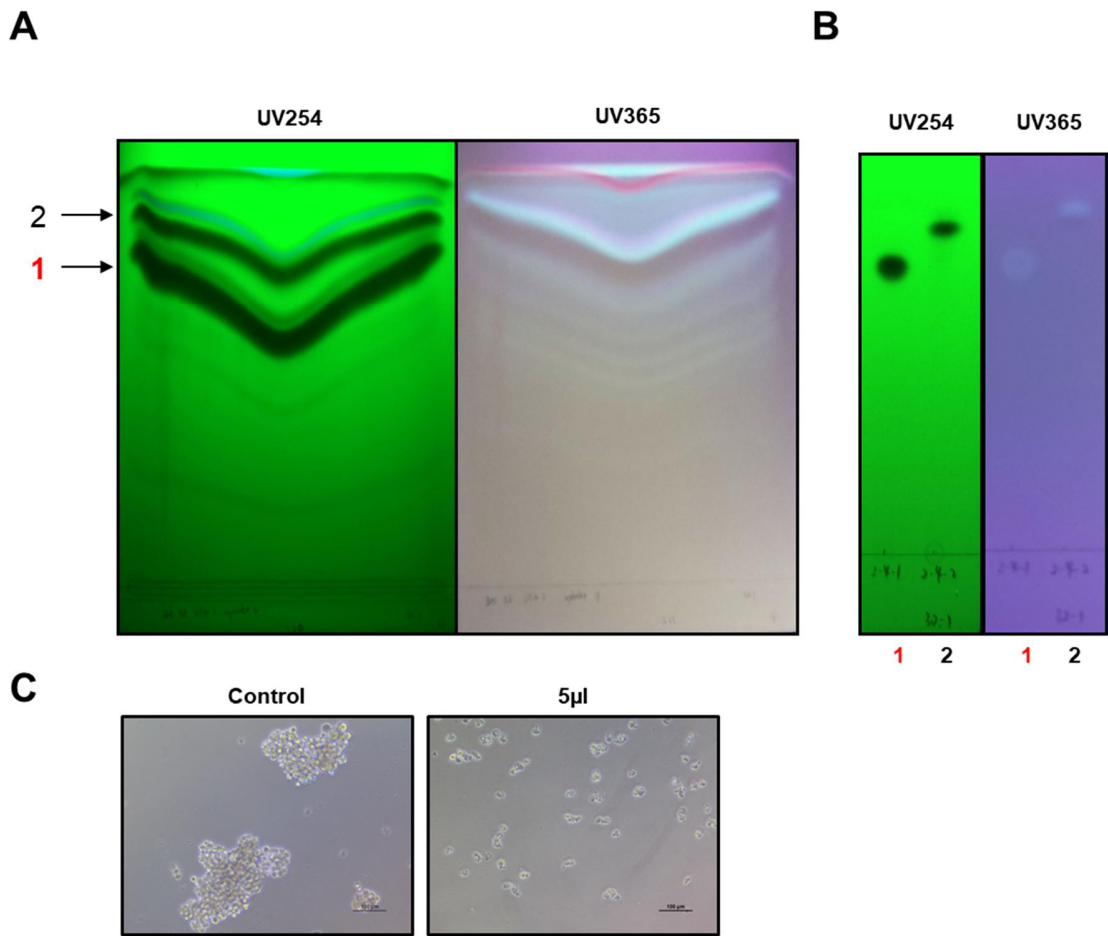


Figure S2-3. The purification procedure of a mammosphere formation inhibitor derived from beet using preparative thin layer chromatography with CHCl_3 :MeOH (30:1). (A) Preparatory TLC chromatography containing fractions 1 and 2. (B) TLC plate analysis of the prepared TLC bands after the samples were scraped and purified (fractions 1 and 2, CHCl_3 : MeOH = 30:1). Active fraction: #1. (C) Mammosphere formation assay using the purified fraction #1.

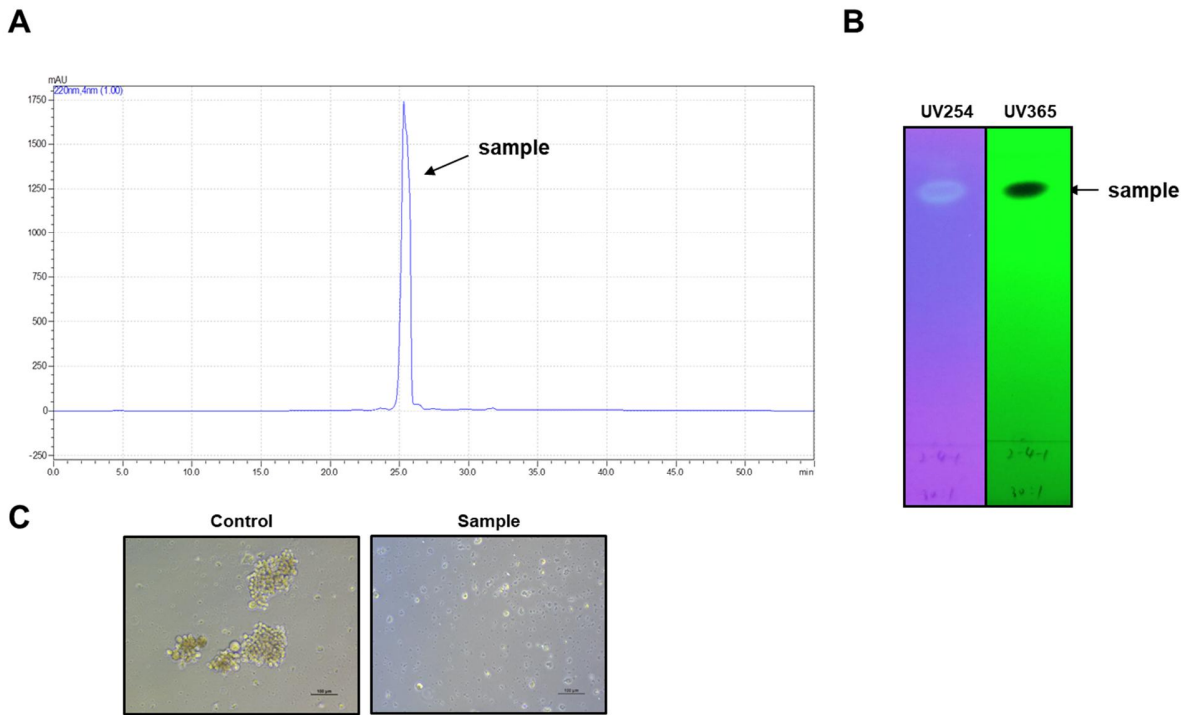


Figure S2-4. Purification procedure of a mammosphere formation inhibitor derived from beet using HPLC. (A) Assessment of the major fractions using HPLC at two wavelengths. Samples were collected based on the 254 and 220 nm wavelengths. (B) TLC plate analysis of the purified sample (CHCl_3 : MeOH = 30:1). (C) Mammosphere formation assay using the purified sample.

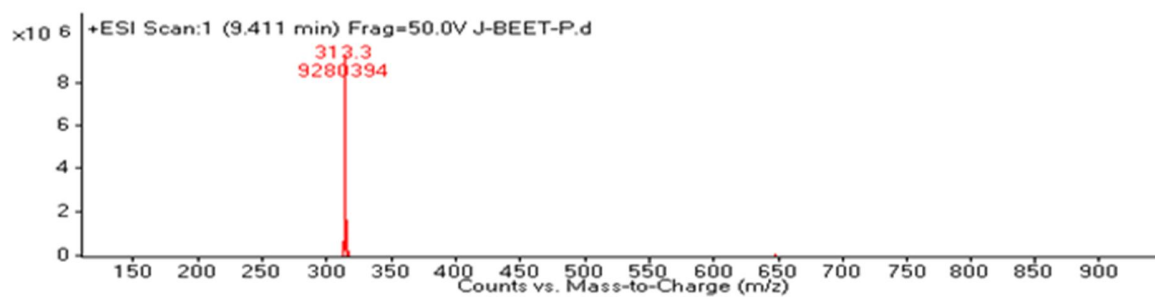


Figure S2-5. ESI-mass spectrum in positive mode of the purified sample

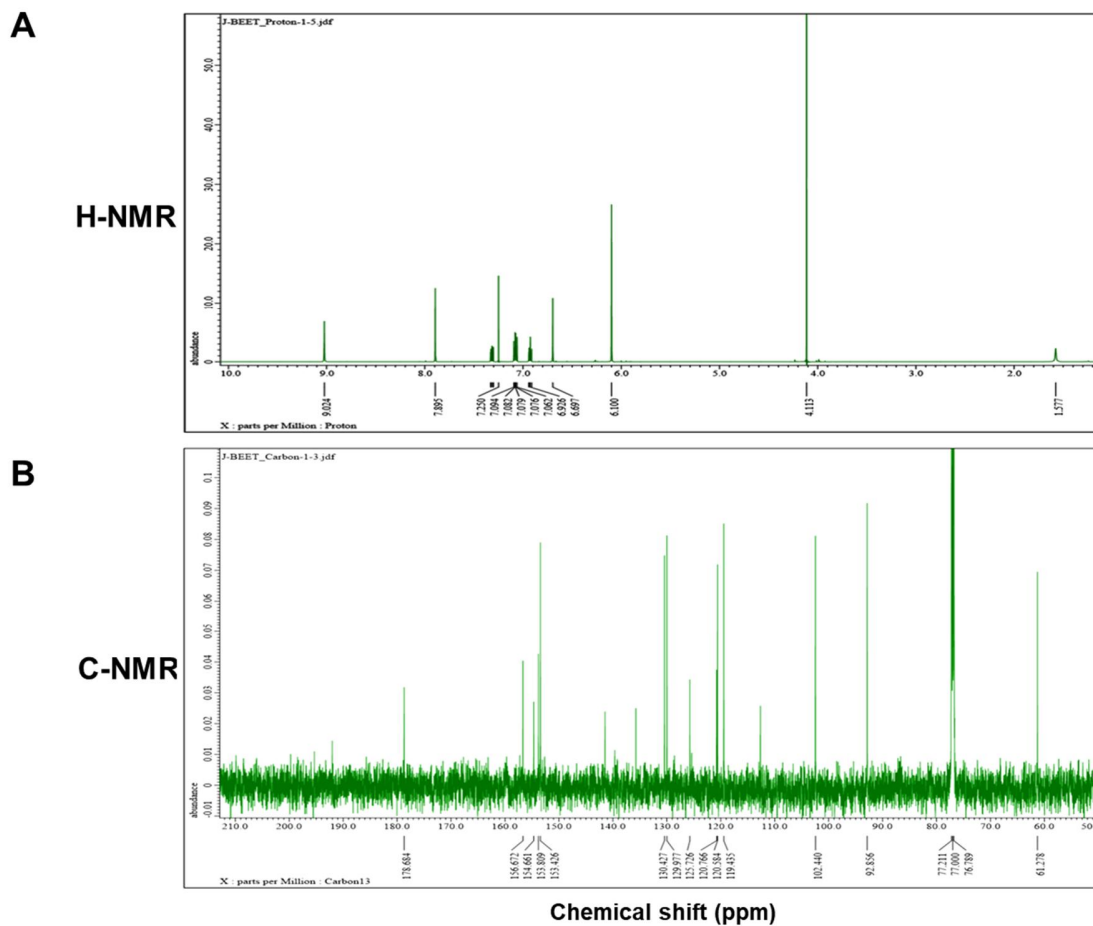


Figure S2-6. ^1H NMR and ^{13}C NMR spectra of purified sample

HMQC

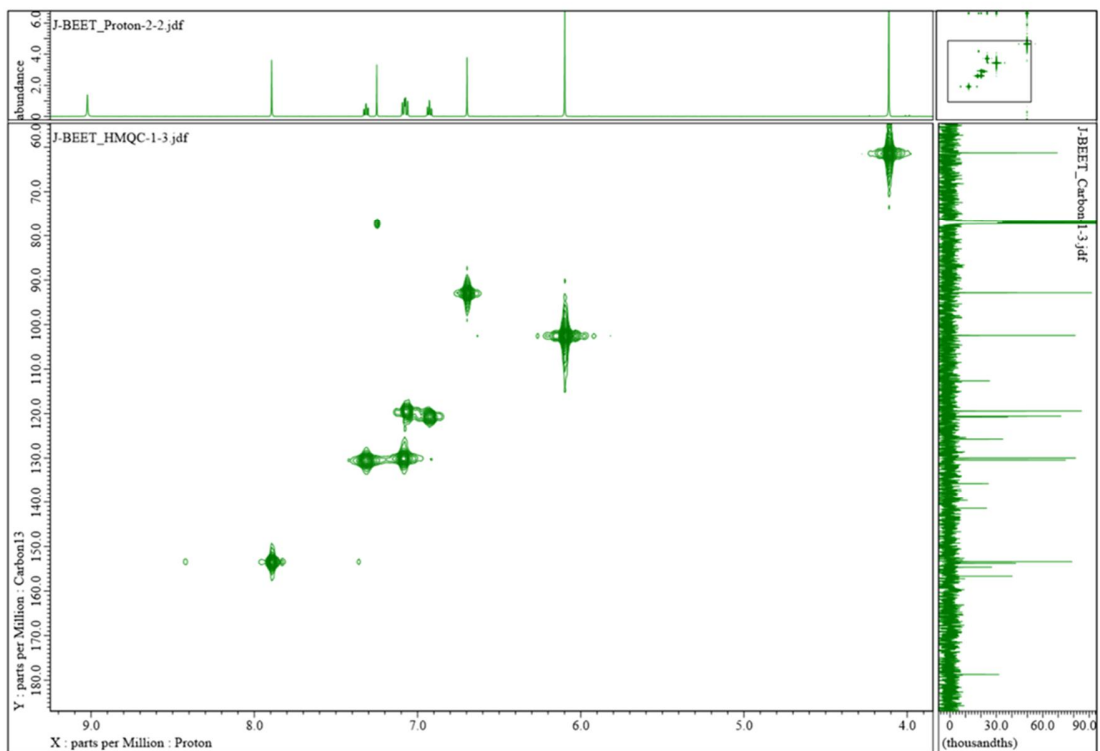


Figure S2-7. HMQC spectrum of the purified sample.

COSY

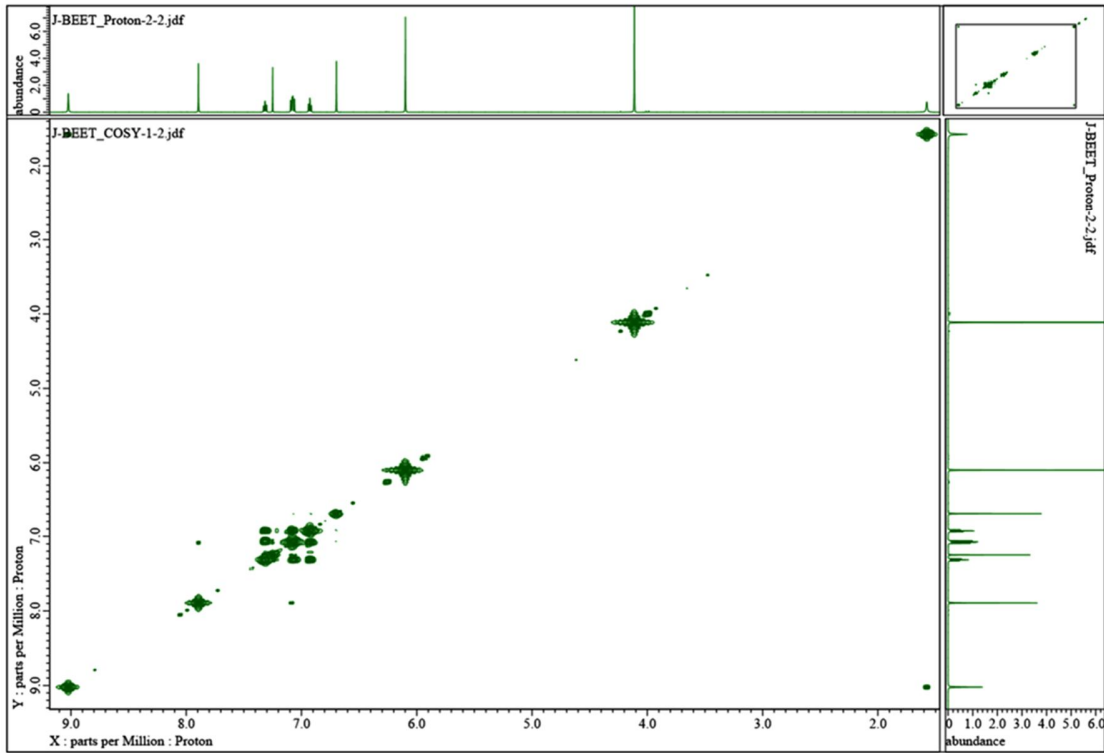


Figure S2-8. ^1H - ^1H COSY spectrum of the purified sample.

HMBC

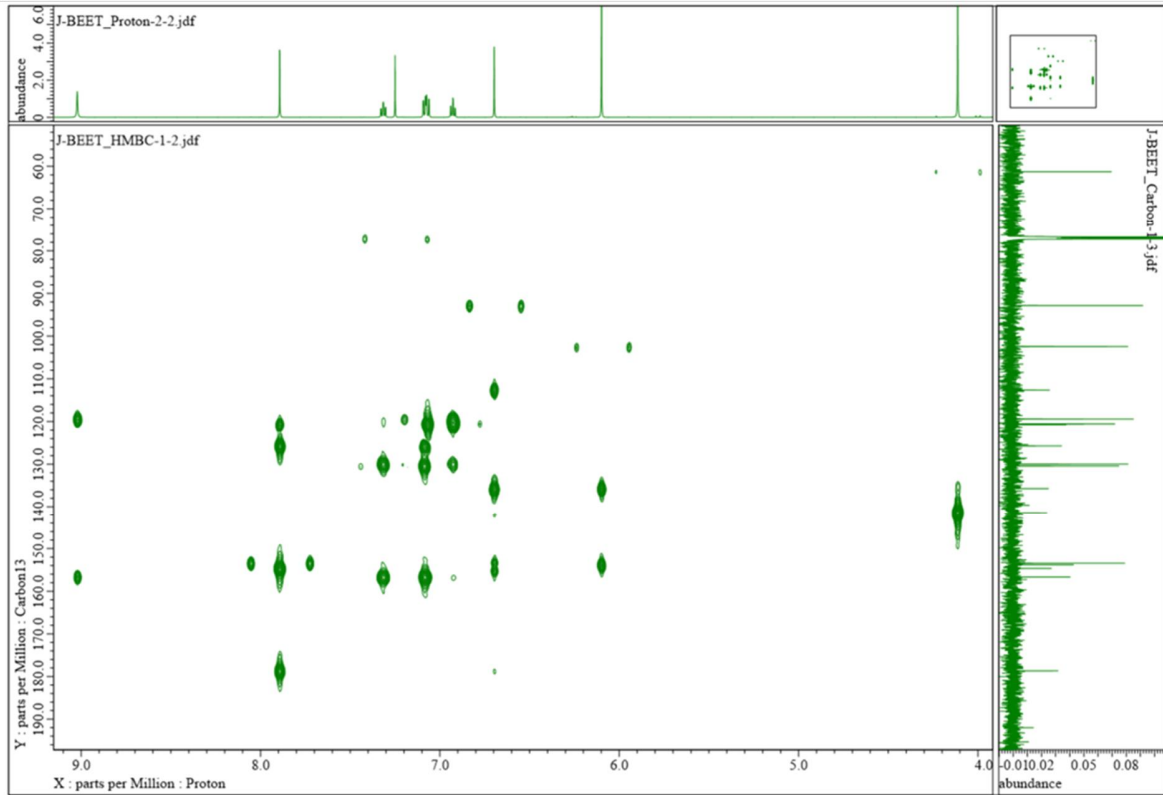
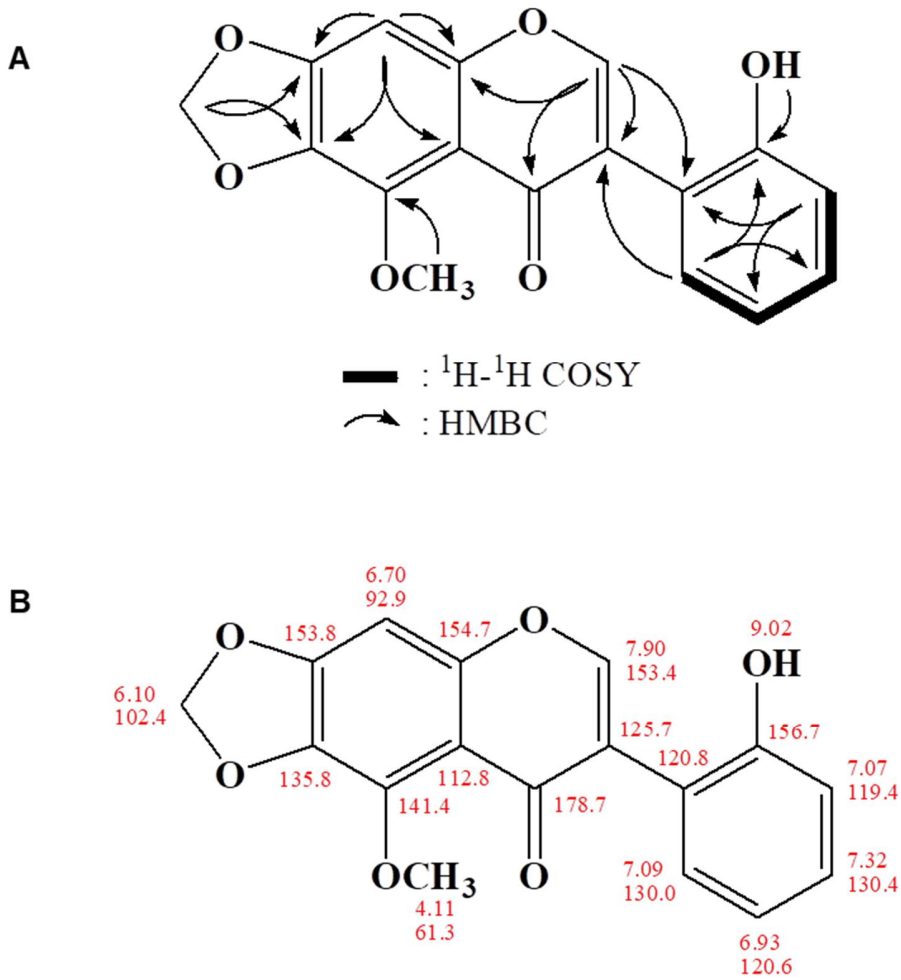


Figure S2-9. HMBC spectrum of the purified sample.



Betavulgarin: $\text{C}_{17}\text{H}_{12}\text{O}_6$, Molecular weight: 312

Figure S2-10. Two-dimensional NMR data (A) and ^1H and ^{13}C peaks assignments (B) of the purified sample

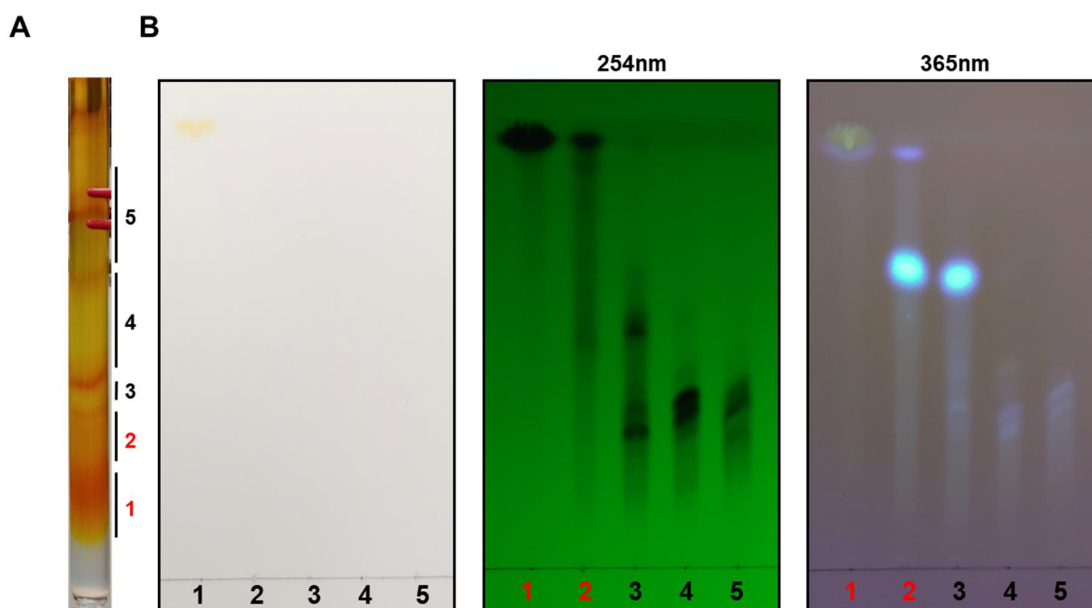


Figure S3-1. The purification procedure of a mammosphere formation inhibitor derived from carrot using silica gel column chromatography. (A) The sample was isolated by silica gel chromatography with a solvent mixture [CHCl_3 : MeOH (10:1)]. (B) TLC plate analysis of the purified sample (CHCl_3 : MeOH = 10:1). Active fraction: #1 and #2. Mix #1 and #2.

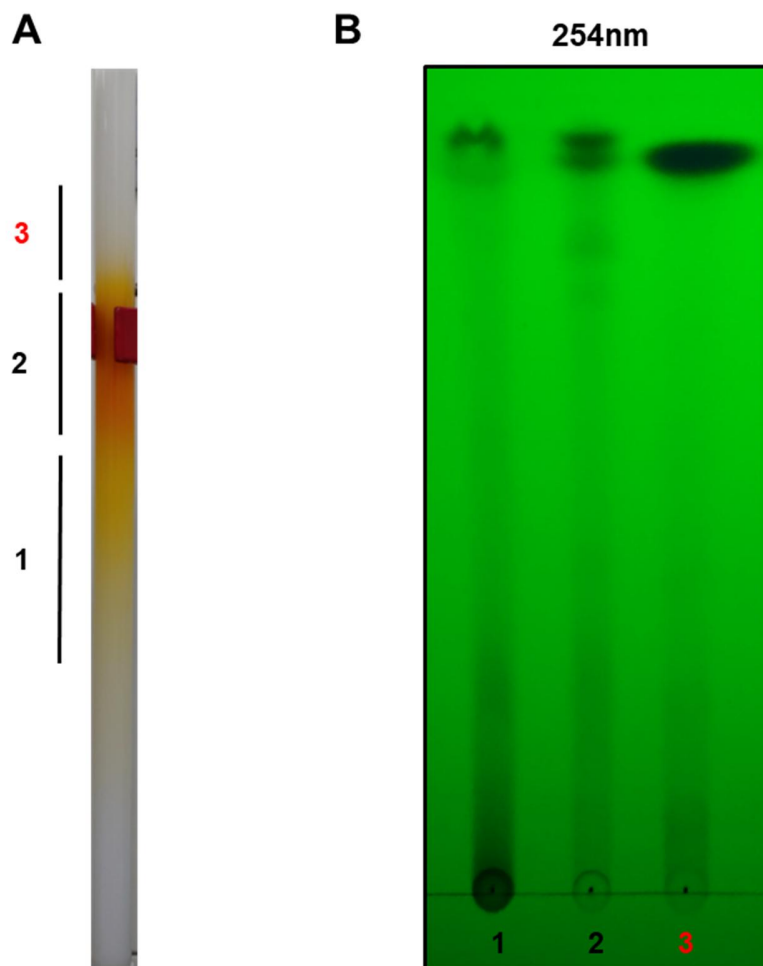


Figure S3-2. The purification procedure of a mammosphere formation inhibitor derived from carrot using Sephadex LH-20 column chromatography. (A) The sample was isolated by Sephadex LH-20 chromatography with MeOH. (B) TLC plate analysis of the purified sample (CHCl_3 : MeOH = 100:1). Active fraction: #3.

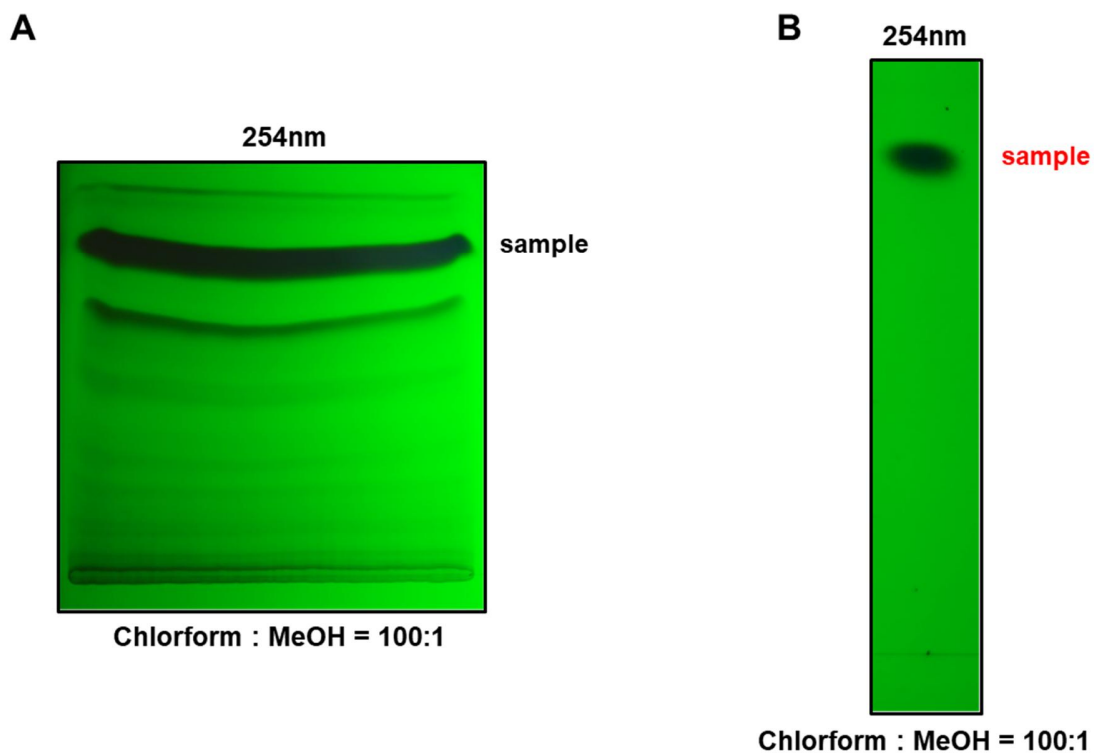


Figure S3-3. The purification procedure of a mammosphere formation inhibitor derived from carrot using preparative thin layer chromatography with CHCl_3 : MeOH (100:1). (A) Preparatory TLC chromatography. (B) TLC plate analysis of the prepared TLC band after the samples were scraped and purified (CHCl_3 : MeOH = 100:1).

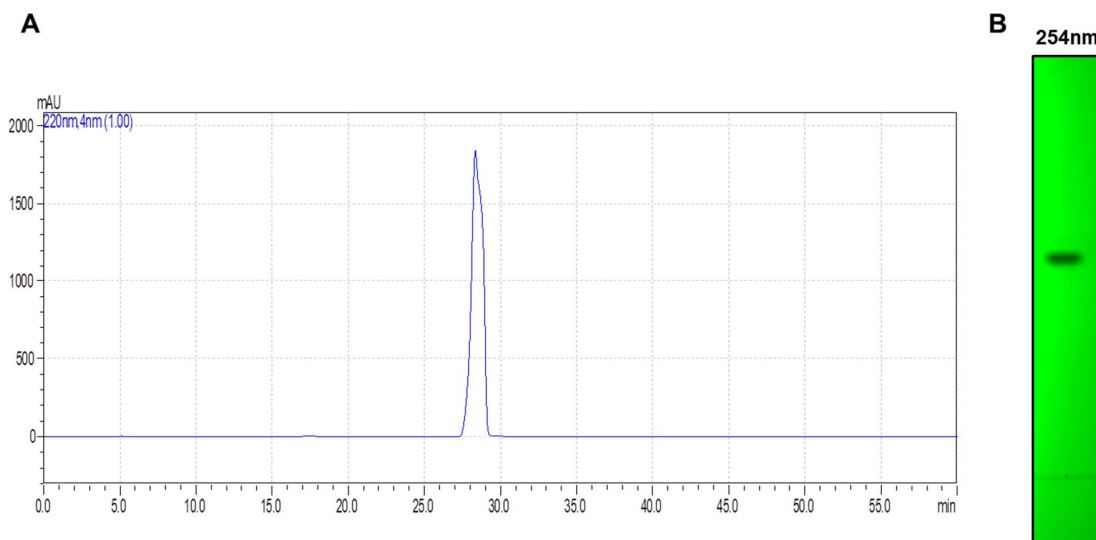


Figure S3-4. Purification procedure of a mammosphere formation inhibitor derived from carrot using HPLC. (A) Assessment of the major fractions using HPLC at one wavelength. Samples were collected based on the 220 nm wavelength. (B) TLC plate analysis of the purified sample (CHCl₃ : MeOH = 100:1).

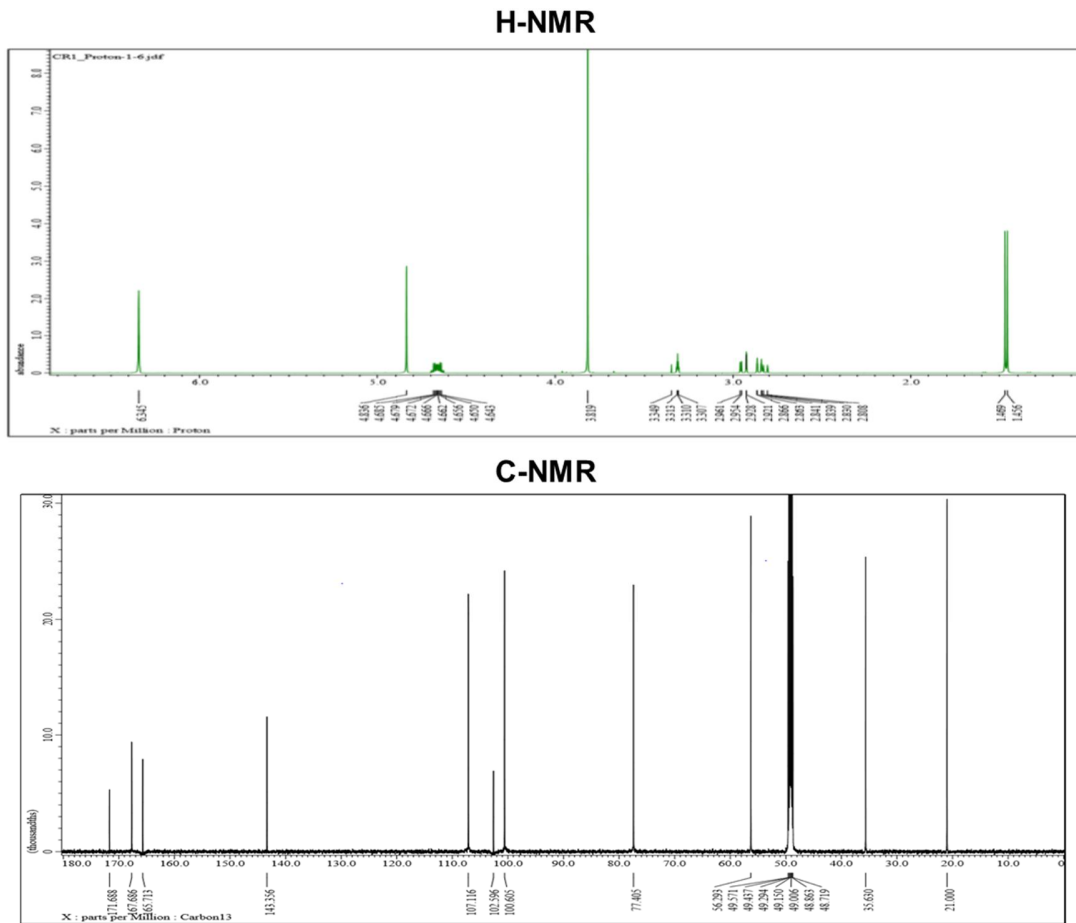


Figure S3-5. ^1H NMR and ^{13}C NMR spectra of purified sample.

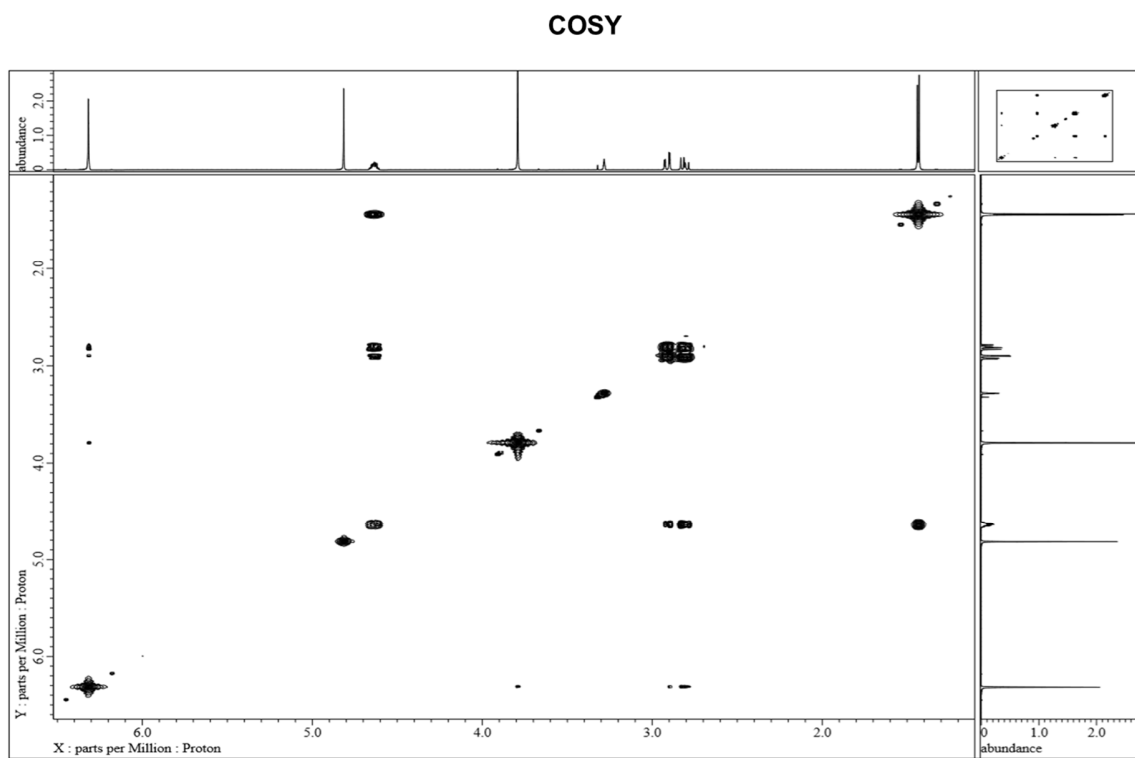


Figure S3-6. COSY 2D-NMR spectra of the purified sample.

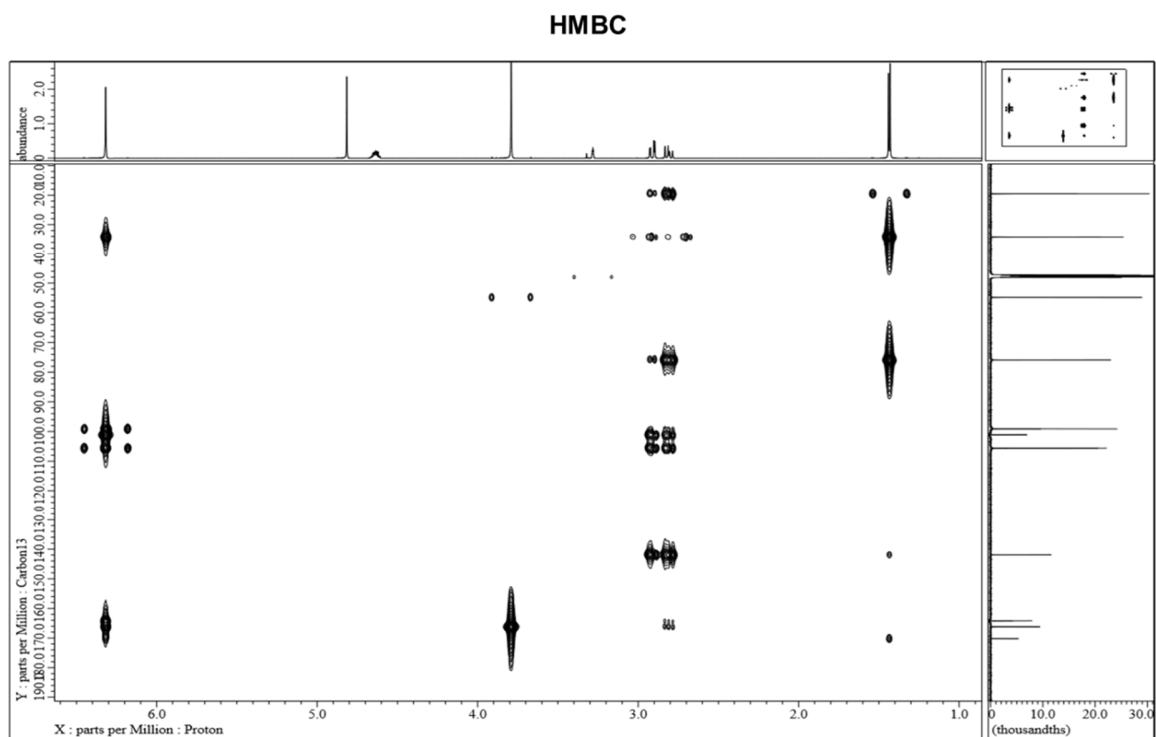


Figure S3-7. HMBC 2D-NMR spectra of the purified sample.

HMQC

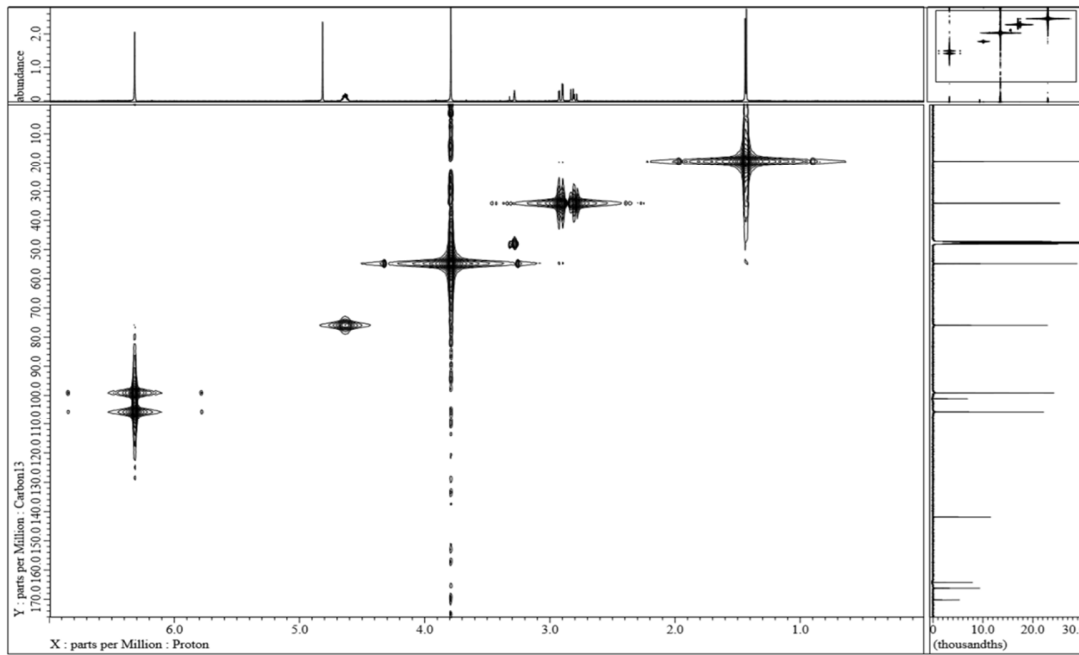


Figure S3-8. HMQC 2D-NMR spectra of the purified sample.

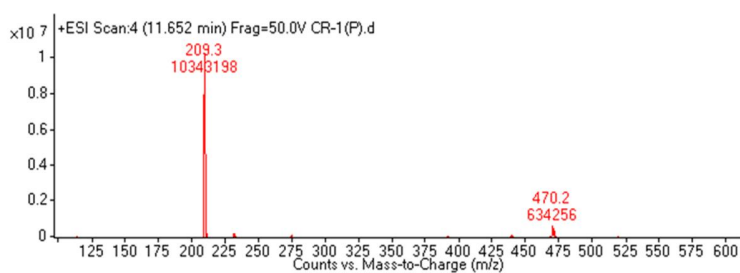
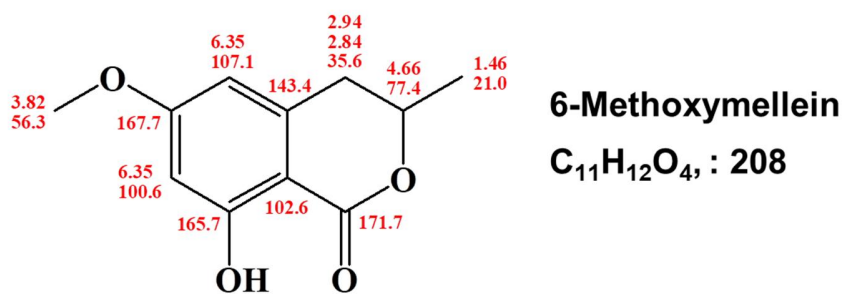
A**B**

Figure S3-9. ESI mass spectrometry (A) and two-dimensional NMR data an ¹H and ¹³C peaks assignments (B) of the purified sample.

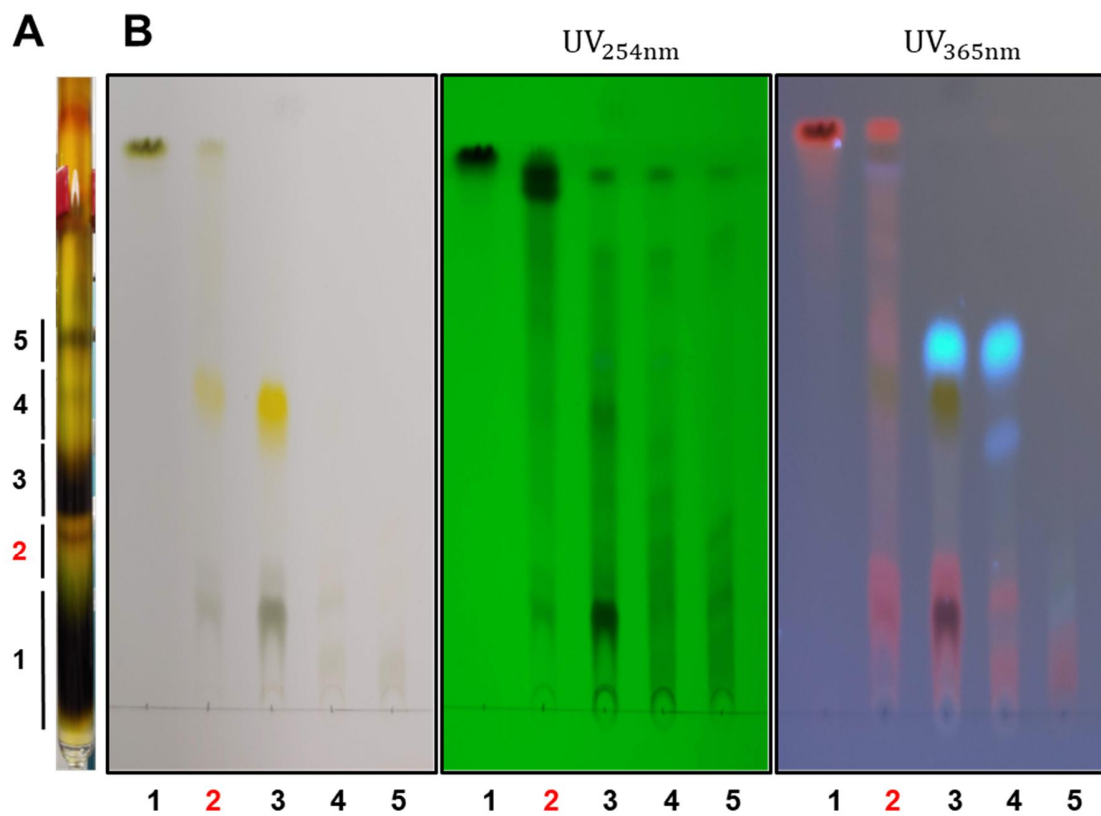


Figure S4-1. The purification procedure of a mammosphere formation inhibitor derived from *Artemisia princeps* using silica gel column chromatography. (A) The sample was isolated by silica gel chromatography with a solvent mixture [CHCl_3 : MeOH (10:1)]. (B) TLC plate analysis of the purified sample CHCl_3 : MeOH = 10:1). Active fraction: #2.

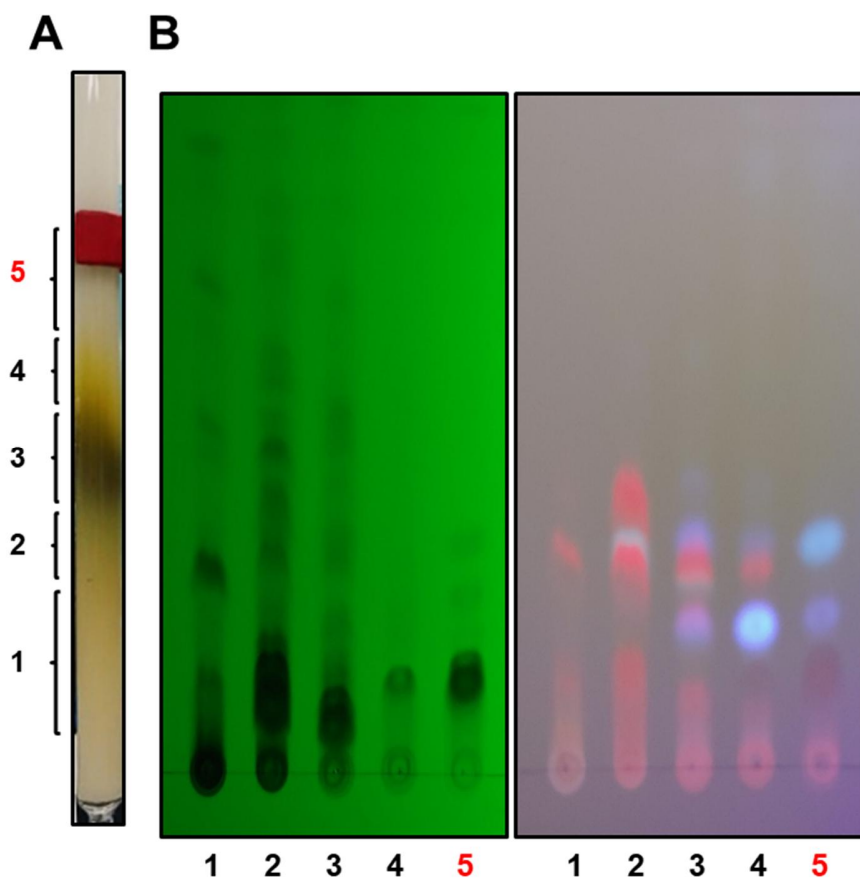


Figure S4-2. The purification procedure of a mammosphere formation inhibitor derived from *Artemisia princeps* using Sephadex LH-20 column chromatography. (A) The sample was isolated by silica gel chromatography with MeOH. (B) TLC plate analysis of the purified sample (CHCl_3 : MeOH = 100:1). Active fraction: #5.

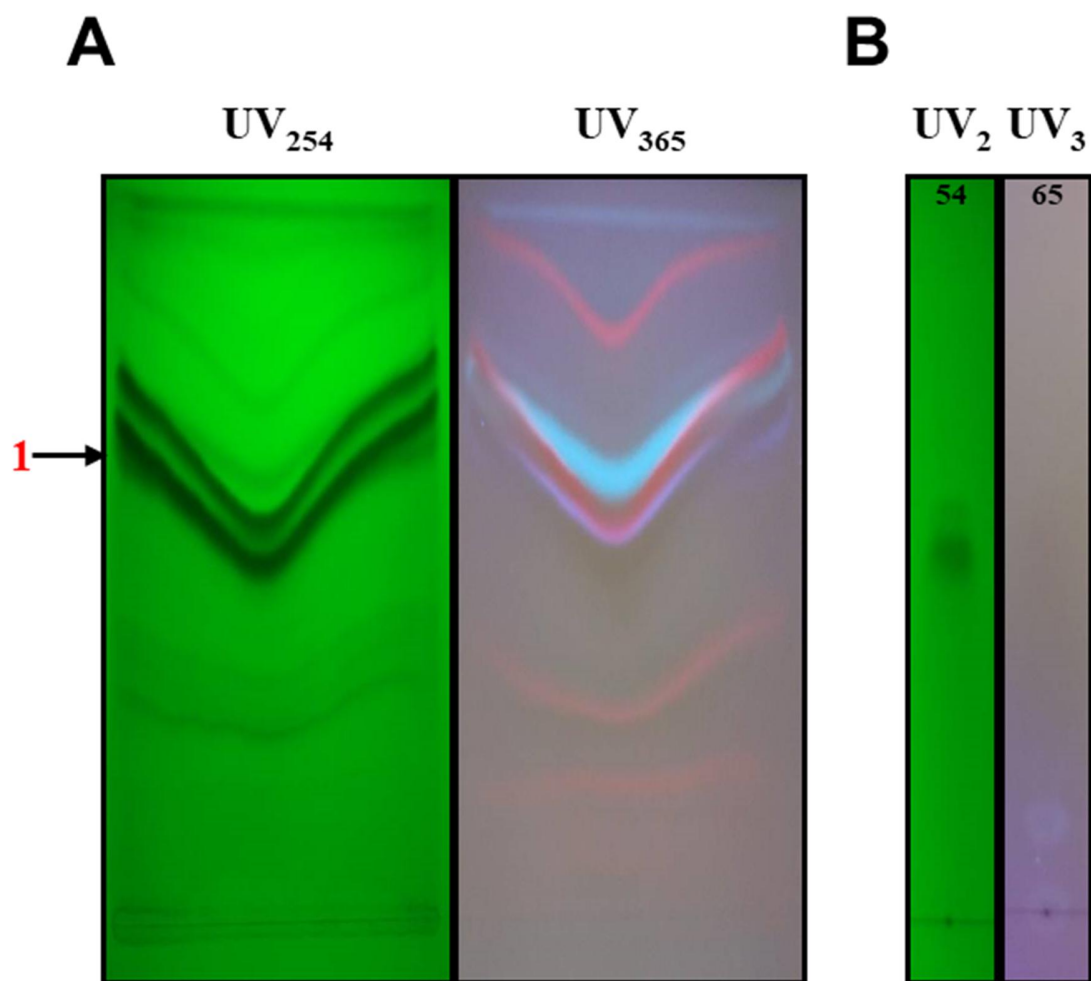


Figure S4-3. The purification procedure of a mammosphere formation inhibitor derived from *Artemisia princeps* using preparative thin layer chromatography with CHCl_3 : MeOH (30:1). (A) Preparatory TLC chromatography. (B) TLC plate analysis of the prepared TLC bands after the samples were scraped and purified (CHCl_3 : MeOH = 30:1).

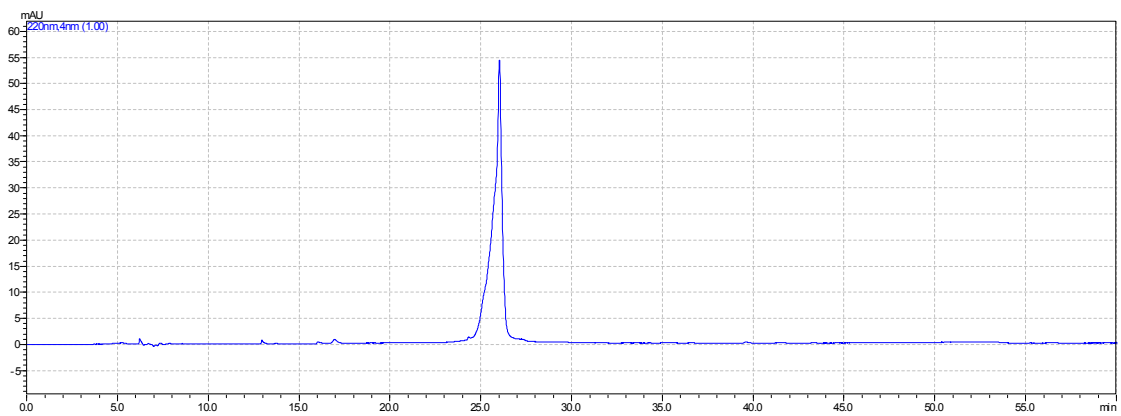


Figure S4-4. Purification procedure of a mammosphere formation inhibitor derived from *Artemisia princeps* using HPLC.

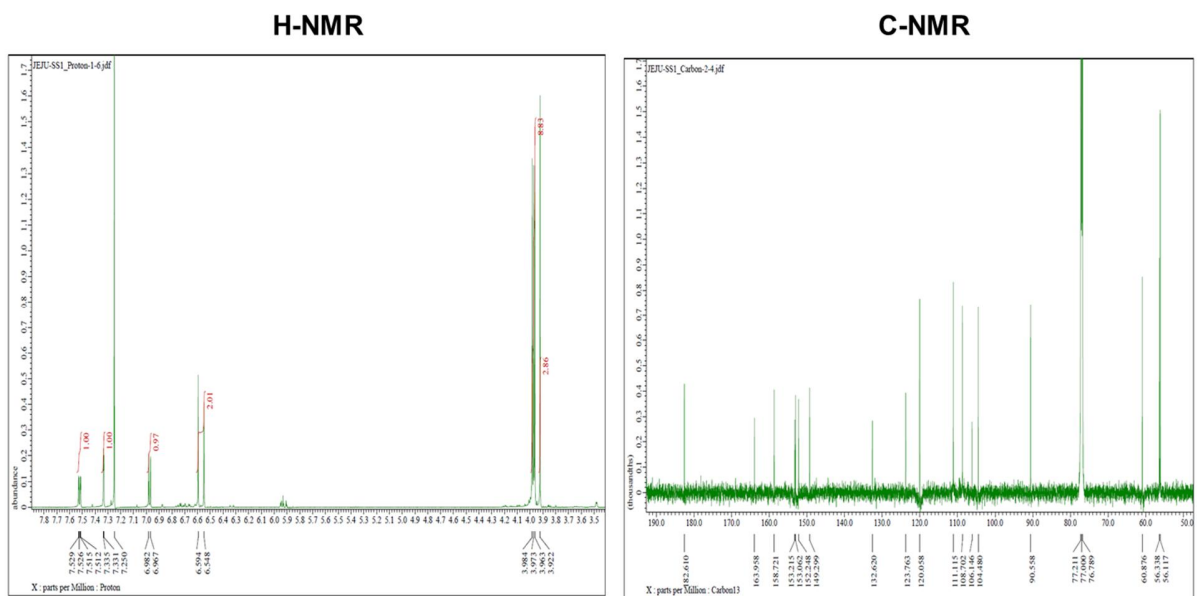


Figure S4-5. ^1H NMR and ^{13}C NMR spectra of purified sample

HMBC

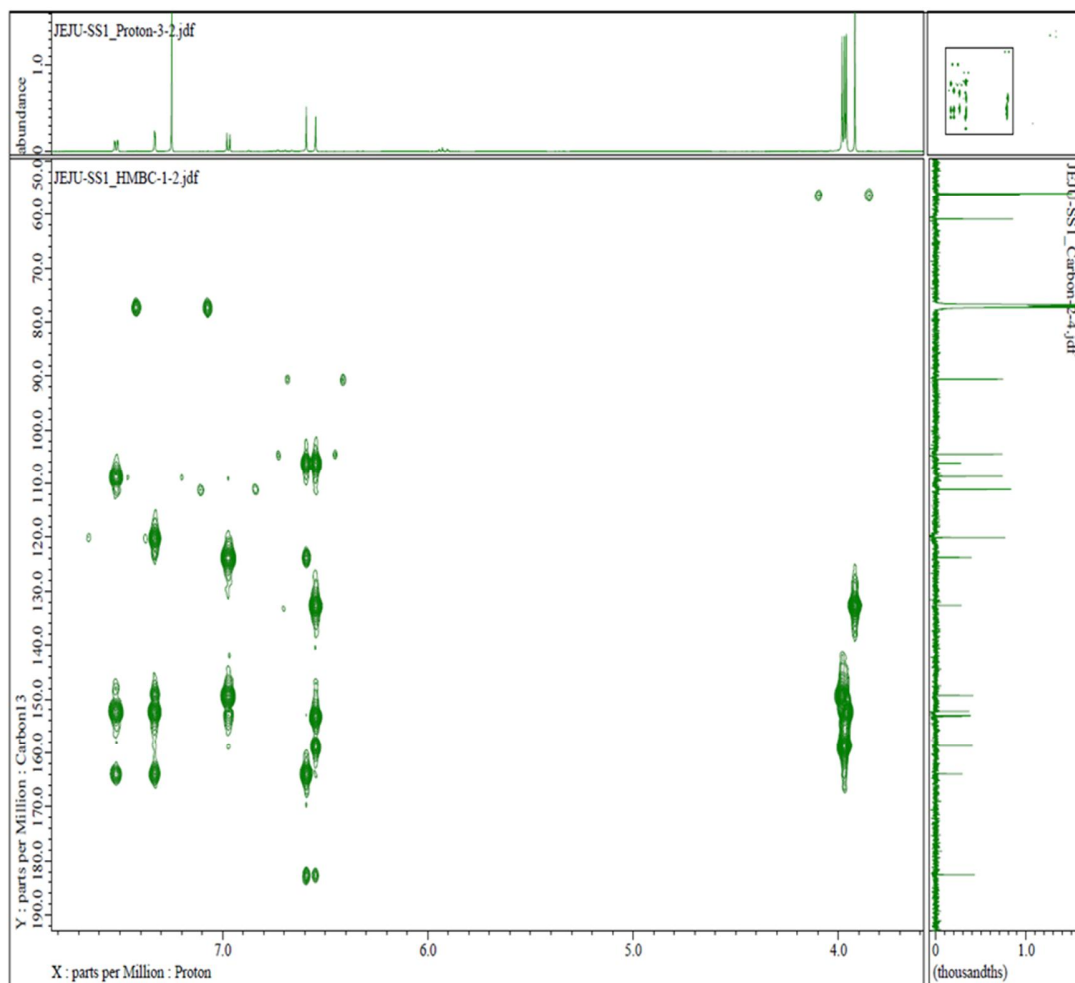


Figure S4-6. COSY 2D-NMR spectra of the purified sample.

HMQC

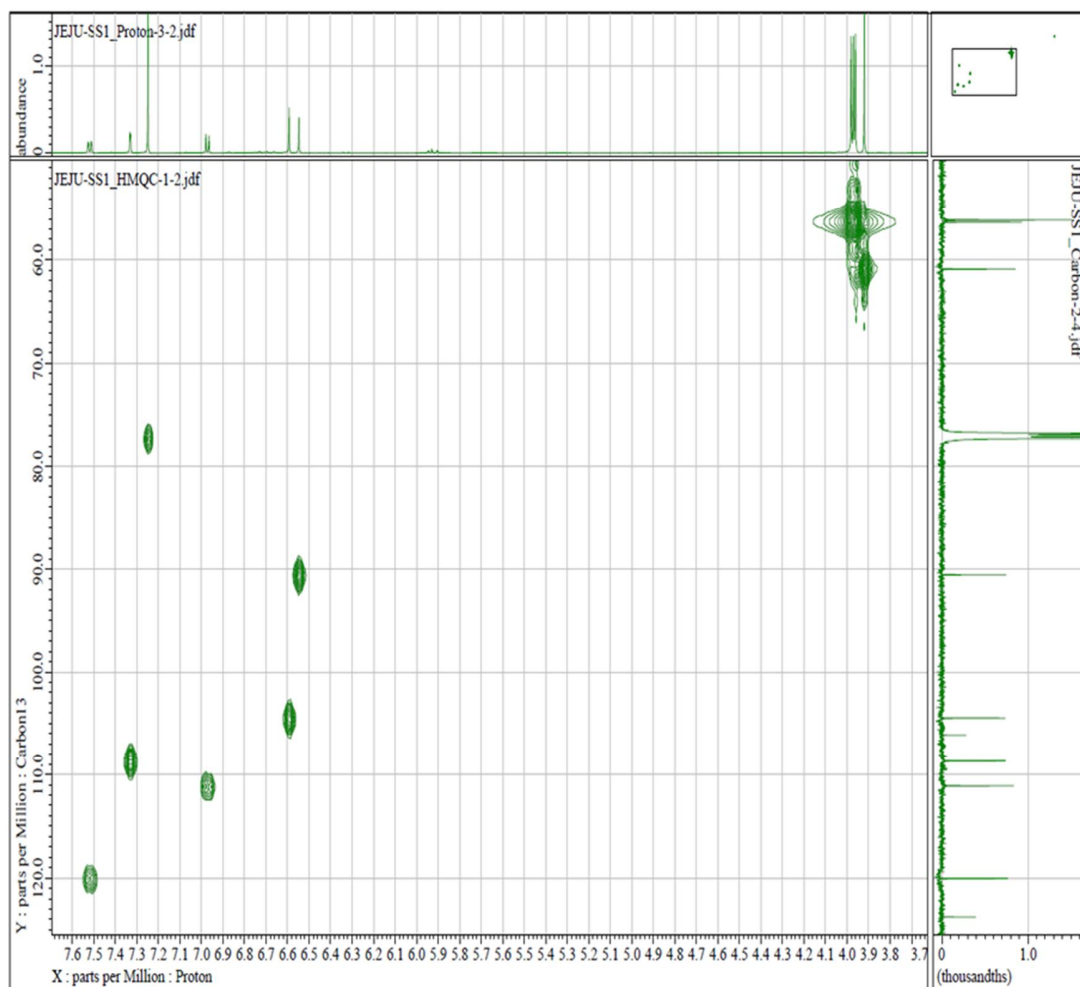
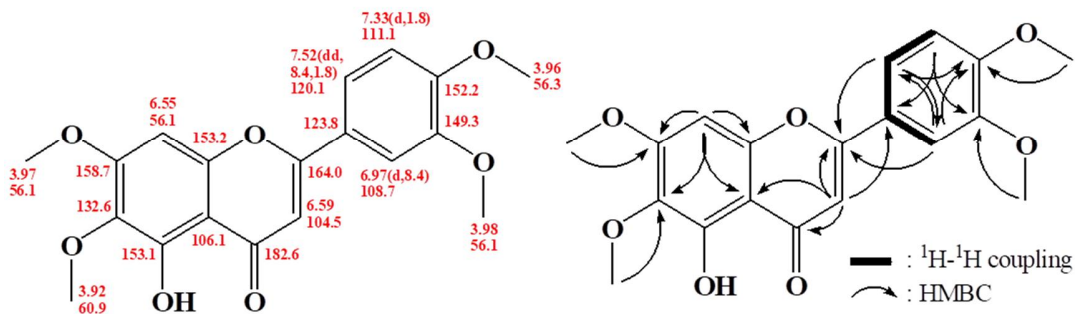
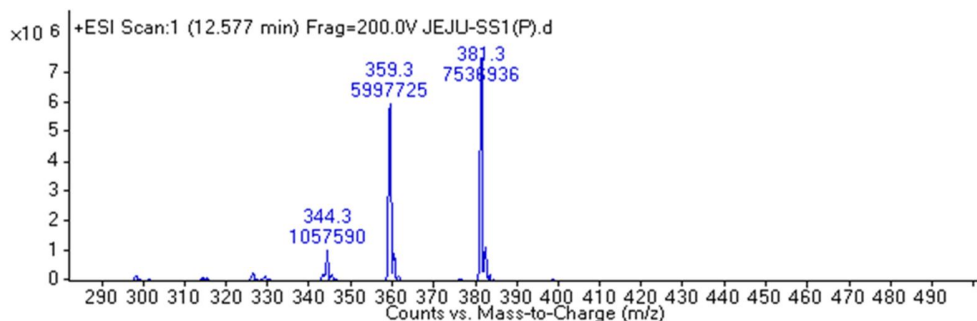


Figure S4-7. HMBC 2D-NMR spectra of the purified sample.



5-Hydroxy-3', 4', 6, 7-tetramethoxyflavone (C₁₉H₁₈O₇; 358)

Figure S4-8. LC-MASS of the purified sample.

LIST OF TABLE

Genes	Primers
Nanog	Forward: 5'-ATGCCTCACACGGAGACTGT-3' Reverse: 5'-AAGTGGGTTGTTTGCCTTTG-3'
Sox2	Forward: 5'-TTGCTGCCTCTTTAAGACTAGGA-3' Reverse: 5'-CTGGGGCTCAAACCTTCTCTC-3'
Oct4	Forward: 5'-AGCAAAACCCGGAGGAGT-3' Reverse: 5'-CCACATCGGCCTGTGTATATC-3'
C-myc	Forward : 5'-CCTGGTGCTCCATGAGGAGAC-3' Reverse : 5'-CAGACTCTGACCTTTTGCCAGG-3'
β-actin	Forward: 5'-TGTTACCAACTGGGACGACA-3' Reverse: 5'-GGGGTGTGAAGGTCTCAA-3

Table 1. Specific Real-time RT-qPCR primer sequences containing *Nanog*, *Sox2*, *Oct4*, *C-myc* and *β-actin* genes

LIST OF PUBLICATION INCLUDED IN THE THESIS

I

1. **Ren Liu**, Hack Sun Choi, Xing Zhen, Su-Lim Kim, Ji-Hyang Kim, Yu-Chan Ko, Bong-Sik Yun, and Dong-Sun Lee. Betavulgarin Isolated from Sugar Beet (*Beta vulgaris*) Suppresses Breast Cancer Stem Cells through Stat3 Signaling. *Molecules*. 2020 Jun 30;25 (13):2999. **IF: 3.267**
2. **Ren Liu**, Hack Sun Choi, Su-Lim Kim, Ji-Hyang Kim, Bong-Sik Yun, and Dong-Sun Lee. 6-Methoxymellein Isolated from Carrot (*Daucus carota L.*) Targets Breast Cancer Stem Cells by Regulating NF- κ B Signaling. *Molecules* . 2020 Sep 23;25(19):4374. **IF: 3.267**
3. **Ren Liu**, Hack Sun Choi, Yu-Chan Ko, Bong-Sik Yun and Dong-Sun Lee. 5-Desmethylinensetin isolated from Artemisia princeps suppresses the stemness of breast cancer cells via Stat3/IL-6 and Stat3/YAP1 signaling. *Life sciences*. **Accepted. IF: 3.647**

II

1. Xing Zhen, Hack Sun Choi, Ji-Hyang Kim, Su-Lim Kim, **Ren Liu**, Bong-Sik Yun, and Dong-Sun Lee. Machilin D, a Lignin Derived from Saururus chinensis, Suppresses Breast Cancer Stem Cells and Inhibits NF- κ B Signaling. *Biomolecules*. 2020 Feb 5;10(2):245. **IF: 4.082**
2. Xing Zhen, Hack Sun Choi, Ji-Hyang Kim, Su-Lim Kim, **Ren Liu**, Yu-Chan Ko , Bong-Sik Yun, Dong-Sun Lee. Caudatin Isolated from Cynanchum auriculatum Inhibits Breast Cancer Stem Cell Formation via a GR/YAP Signaling. *Biomolecules* . 2020 Jun 18;10 (6):925. **IF: 4.082**

3. Yu-Chan Ko, Hack Sun Choi, **Ren Liu**, Ji-Hyang Kim, Su-Lim Kim, Bong-Sik Yun, Dong-Sun Lee. Inhibitory Effects of Tangeretin, A Citrus Peel-Derived Flavonoid, on Breast Cancer Stem Cell Formation through Suppression of Stat3 Signaling. *Molecules*. 2020 Jun ;25(11):2599. **IF: 3.267**
4. XING ZHEN, HU-NAN SUN, **REN LIU**, HACK SUN CHOI, and DONG-SUN LEE. Non-thermal Plasma-activated Medium Induces Apoptosis of Aspc1 Cells Through the ROS-dependent Autophagy Pathway. *In Vivo*. Jan-Feb 2020;34(1):143-153. **IF: 1.541**
5. HYE BIN KOH, HU-NAN SUN, ZHEN XING, **REN LIU**, NISANSALA CHANDIMALI, TAEHO KWON, and DONG-SUN LEE. Wogonin Influences Osteosarcoma Stem Cell Stemness Through ROS-dependent Signaling. *In Vivo* . May-Jun 2020;34(3):1077-1084. **IF: 1.541**
6. Nisansala Chandimali , Hu-Nan Sun , Ling-Zu Kong , Xing Zhen , **Ren Liu** , Taeho Kwon , Dong-Sun Lee. Shikonin-induced Apoptosis of Colon Cancer Cells Is Reduced by Peroxiredoxin V Expression. *Anticancer Res*. 2019 Nov;39(11):6115-6123. **IF: 1.994**

Acknowledgment

I would like to express my deep and sincere gratitude to my research supervisor, professor Dong-Son Lee, for giving me the opportunity to do research and providing invaluable guidance throughout this research. His dynamism, vision, sincerity and motivation have deeply inspired me. He has taught me the methodology to carry out the research and to present the research works as clearly as possible. It was a great privilege and honor to work and study under his guidance. I am extremely grateful for what he has offered me. I would also like to thank him for his friendship, empathy, and great sense of humor. I am extending my heartfelt thanks to Hack-Sun Choi, for the guidance throughout research, and for his acceptance and patience during the discussion I had with him on research work and thesis preparation.

I am extremely grateful to my parents for their love, prayers, caring and sacrifices for educating and preparing me for my future. I am very much thankful to my wife and my daughters for their love, understanding, prayers and continuing support to complete this research work.

I would like to say thanks to my friends and research colleagues, Ji-Hyang Kim, Su-Lim Kim, Zhen Xing and Yo-Chan Ko for their helps throughout my experiments.

Finally, my thanks go to all the people who have supported me to complete the research work directly or indirectly.